# BLENDS IN TWO DIMENSIONS: MIXTURES OF LIQUID CRYSTALLINE POLYMERS AT THE AIR-WATER INTERFACE

By

ANGELA F. THIBODEAUX

A DISSERTATION PRESENTED TO THE GRADUATE SCHOOL OF
THE UNIVERSITY OF FLORIDA IN PARTIAL FULFILLMENT
OF THE REQUIREMENTS FOR THE DEGREE OF
DOCTOR OF PHILOSOPHY

UNIVERSITY OF FLORIDA

1993

# ACKNOWLEDGMENTS

I would like to acknowledge my husband Dr. Jim Konzelman, without whose help I may not have made it to the defense date. Thanks for your patience and support. Also, to everyone who has come and gone from the UF's "Polymer Floor" over the past five years; thanks for the friendship and camaraderie that got me through the tough times. I also owe thanks to my parents, Lorraine and Darwin Thibodeaux, for their support and encouragement during my graduate work.

The best thing about graduate school was the wonderful people I met. The worst thing was watching these people leave year after year. I'll never forget these years or the people that made it special.

# TABLE OF CONTENTS

page

ACKNOWLEDGMENTS .... ii

ABSTRACT .... vi

CHAPTERS

1 INTRODUCTION .... 1
  Langmuir-Blodgett Films .... 1
    History/Background .... 1
    Modern Contributors .... 3
    Basic Concepts .... 5
    Spreading of a Liquid at an Interface .... 5
    General Apparatus and Procedure .... 7
    Deposition of Monolayer Films onto Solid Substrates .... 10
    Polymer Monolayers and Multilayers .... 16
    Blend Monolayers .... 19
  Liquid Crystals and Side Chain Liquid Crystalline Polymers .... 21
    Polymer Liquid Crystals .... 24
    Ferroelectric Liquid Crystals .... 25
    Monolayers and Multilayers of Liquid Crystalline Materials .... 28
  Applications of Langmuir Blodgett Films .... 30
  Analytical Techniques .... 34
    Brewster Angle Microscopy (BAM) .... 34
    Small Angle X-ray Scattering (SAXS) .... 36
  Summary .... 39

2 EXPERIMENTAL .... 41

  Materials .... 41
    Poly(4-tetraetyleneoxide-4'-methoxybiphenyl methacrylate) (PM4) .... 41
    Poly(octadecylmethacrylate) (PODMA) .... 41

page

(R)-4'-(1-ethoxycarbonyl-1-ethoxy)phenyl-4-[4-(9-decenyl-oxy)-phenyl]benzoate (10PPB2)........42
10PPB2-CO........44
Monolayers........44
General Procedure and Equipment........44
Brewster Angle Microscopy........46
Multilayers........47
General Procedure and Equipment........47
X-Ray Measurements........49
Differential Scanning Calorimetry........50
Thermal Stability Microscope Study of Multilayers........51

3 BLENDS OF A FERROELECTRIC SIDE CHAIN LIQUID CRYSTALLINE COPOLYMER WITH CORRESPONDING MESOGENIC MONOMER: MIXTURES FOR PRODUCING A MORE LATERALLY CONDENSED MONOLAYER........53

Introduction........53
Monolayers and Multilayers of the Pure Copolymer........56
Monolayer Film behavior of 10PPB2-CO........56
Deposition Behavior of 10PPB2-CO........57
Small Angle X-ray Analysis........63
Monolayers and Multilayers of Copolymer/Mesogen Blends........68
Bulk Properties of the Pure Components........69
Monolayer Film Behavior of the Pure Components........70
Monolayer Film Behavior of the Blends........73
Thermodynamics of Mixing in the Monolayer Blends........80
Brewster Angle Microscopy (BAM)........87
Deposition of Blend Monolayers of 10PPB2/10PPB2-CO........100
X-ray of Blend Multilayers........102
Summary........111

page

4 BLENDS OF A SIDE-CHAIN LIQUID CRYSTALLINE POLYMER WITH POLY(OCTADECYL METHACRYLATE) AT THE AIR-WATER INTERFACE MIXTURES FOR PRODUCING A MORE FLUID AND STABLE MONOLAYER ....................................... 116

Introduction ....................................... 116
Monolayers and Multilayers of the Pure LC Polymer ....................................... 119
Bulk Properties of PM4 ....................................... 119
Monolayer Properties of PM4 ....................................... 120
Deposition of PM4 monolayers ....................................... 125
Monolayers and Multilayers of PM4/PODMA Blends ....................................... 126
PODMA Monolayer Behavior ....................................... 126
Monolayer Film Behavior of the Blends ....................................... 129
Thermodynamics of Mixing in the Monolayer Blends ....................................... 141
Other Monolayer Blend Examples ....................................... 146
Bulk Thermal Behavior of PM4/PODMA Blends ....................................... 149
Deposition of PM4/PODMA Blend Monolayers ....................................... 152
X-ray of Blend Multilayers ....................................... 153
Summary ....................................... 159

5 CONTRAST OF THE TWO BLEND MONOLAYER SYSTEMS ....................................... 162
Bulk and Monolayer Behavior of the Liquid Crystalline Polymers ....................................... 162
Monolayer Behavior and Structure of the Blend Systems ....................................... 165
Multilayer Structure of the Polymers and Blends ....................................... 167
A Final Word ....................................... 170

REFERENCES ....................................... 171

BIOGRAPHICAL SKETCH ....................................... 181

Abstract of Dissertation Presented to the Graduate School
of the University of Florida in Partial Fulfillment of the
Requirements for the Degree of Doctor of Philosophy

# BLENDS IN TWO DIMENSIONS: MIXTURES OF LIQUID CRYSTALLINE POLYMERS AT THE AIR-WATER INTERFACE

By
Angela F. Thibodeaux

December 1993

Chairman: Professor Randolph S. Duran
Major Department: Chemistry

Side chain liquid crystalline polymers and mixtures with other materials were investigated as monolayer and multilayer films. Miscibility of the blend monolayers was determined by analysis of the surface pressure-mean molecular area isotherms at various mixture compositions. The morphology of some blend monolayers was investigated using Brewster angle microscopy. Additionally, the monolayer films were transferred to solid plates as multilayers; and the layer structure probed with small angle X-ray diffraction.

The first side chain liquid crystalline polymer ((R)-4'-(1-ethoxycarbonyl-1-ethoxy)phenyl-4-[4-(9-decenyloxy)-phenyl]benzoate) studied exists in a liquid crystalline Sc* phase at room temperature. The polymer was found to form highly reversible and stable monolayer films at the air-water interface, and deposited onto hydrophobic substrates in a x-type deposition. However, the monolayers rearrange after transfer, independent of the deposition method used. To increase lateral mesogen density, mixed monolayers of the polymer with the corresponding mesogenic monomer were produced. The results from isothermal analysis indicate that the blends are miscible over all concentrations investigated. Additionally, Brewster angle microscopy allowed the visualization of orientational order in the monomer and blend monolayers. Mixed monolayers were also transferred to solid substrates and investigated with small angle X-ray diffraction to elucidate layer order and structure.

The second side chain liquid crystalline polymer (poly(4-tetraetyleneoxide-4'-methoxybiphenyl methacrylate)) studied exists in an ordered LC smectic E phase above 38°C. The monolayer films were accordingly less fluid and stable, relative to the previous LC polymer. To improve the monolayer stability, mixtures were made with another film forming polymer, poly(octadecylmethacrylate). Excess area analysis of the isotherms indicated that the mixtures were miscible over most concentrations studied. However, $\Delta G_{mix}^{xs}$ values indicated that the mixing process was not energetically favorable. Based on isothermal data, miscibility analysis, and comparable mixture data it was theorized that the mixing occurs between the PMMA backbones of both polymers, while the side chains orient away from each other.

# CHAPTER 1

# INTRODUCTION

> *Imagine a vast sheet of paper in which . . . figures, instead of remaining fixed in their places, move freely about, on or in the surface, but without the power of rising above or sinking below it, very much like shadows*
>
> - Edwin A. Abbott, 1884, excerpt from "Flatland".[1]

## Langmuir-Blodgett Films

### History/Background

Irving Langmuir, whose name is associated with the technique for producing monomolecular films, is thought to be the first to note the existence of oriented monolayers on water. However, many pioneers in surface science produced significant advances leading up to his breakthrough in the early 1900's. In fact, the calming effect of oil on a stormy ocean surface was noted by Greek seafarers as long ago as 429 A.D.[2]

First documentation of oil monolayers on water was made by Benjamin Franklin around 1770. He performed the famous Clapham pond experiment in which he noted the calming effect of approximately a teaspoon of oil on the pond's surface, and recognized the incredible "spreading" energy of the film.[3]

In 1890, Lord Rayleigh was the first scientist to discuss the change in surface tension of a water surface caused by the addition of small amounts of oil. In addition, he noticed that the surface tension of water with a few drops of oil placed on the surface varied with the surface area of the oil film. He was the first to suspect that these films were of molecular thickness, although he failed to prove this experimentally.[4]

Agnes Pockels is credited with building the first "Langmuir" trough on her kitchen table, and the first to perform what are now referred to as isotherm experiments. From her experimental data, the mean area per molecule in a stearic acid monolayer is calculated at 22 $Å^2$, which is amazingly accurate compared to today's measurements.[5-7] Although the equipment and the typical monolayer characterization experiments (isotherms) used today have changed little from the basic set up designed by Ms. Pockels, she did not recognize the significance of her data. It was not until Irving Langmuir's research in the early 1900's that these oil layers were scientifically proven to be monomolecular in thickness.

Although the basic apparatus was developed and experiments performed by others years earlier, Irving Langmuir is recognized as the founding father of monolayer research. There is no doubt, however, that he furthered the field of monolayer and surface science as none who had gone before him. For his contributions, he was awarded the Nobel Prize for his work on monolayer films in 1932. Langmuir was familiar with the publications of Pockels and Rayleigh, and was amazed that little research was done following their initial experiments. He further developed the experimental equipment and technique developed by Ms. Pockels, and proved what Rayleigh had suspected--that the films on the water surface were one molecule in thickness. Additionally, Langmuir established that the amphiphilic molecules which formed monolayers were oriented with respect to the water surface.[8,9]

Katherine Blodgett was the first woman scientist to be hired by General Electric in 1919, where she began her pioneering research with Dr. Langmuir on monolayer transfer to solid substrates. These built-up multilayers became known as Langmuir-Blodgett films (whereas floating monolayers are more correctly called Langmuir films) due to their contributions in this area. A great deal of Blodgett's later work at GE involved research on LB film optical properties for such applications as anti-reflective coatings and "step gauges" to accurately determining film thickness.[10,11] She also studied and published theories regarding the actual mechanism of deposition, including the overturning of layers during this process.[10,12,13]

## Modern Contributors

Following Langmuir and Blodgett, some of the most significant contributions to the understanding of the fundamental properties and physics of monolayers were made during the period from the late 1920's until shortly after the Second World War. Significant work was published during this period by Harkins,[14-18] Adam,[19-21] Rideal[22-25] and Crisp,[26-28] whose research developed the basic physical and thermodynamic principles of the behavior of films confined to surfaces. After World War II monolayer research continued, but at a significantly lower level.

One of the most read authors and researchers in the field of Langmuir Blodgett films is George L. Gaines, Jr. whose book "Insoluble Monolayers at the Gas-Liquid Interfaces," published in 1967 is still considered mandatory reading for those starting research in the area monomolecular films. Additionally, he extended the thermodynamic treatment of monolayers at surfaces developed by Gibbs to more specific conditions.[29] This treatment is used by researchers today to explain the phenomena of pure and mixed monolayer films. He also published an extensive review on polymer monolayer behavior.[30] Coinciding with the release of Gaines' book, a resurgence in the interest in studying monolayer and multilayer films occurred; spurred by the shrinking dimensions of electronic circuitry and growing interest in biological systems applications.

Since the renewed interest in Langmuir-Blodgett films in the early 1970's, research and publications have increased exponentially. Major names in the area such as Möbius (surface potential measurements),[31] Möhwald (physical properties of monolayer behavior and phase transitions),[32,33] Ringsdorf (liquid crystals, liquid crystalline polymers, and biological membrane models),[34-44] Ulman (updated overview of Langmuir Blodgett research and applications),[45] and Wegner(rigid rod and other polymeric monolayers)[44,46-49,50] are just a few of the scientists who have contributed large bodies of information to the field of monolayer research over the past twenty years.

## Basic Concepts

The Langmuir-Blodgett (LB) technique takes advantage of the properties of certain materials which spread at an air-liquid interface to form monolayers. These materials are most often spread on a water subphase, and the molecules that spread in this case are referred to as amphiphilic. The balance of hydrophobic regions, which tend to remain out of the water phase, and hydrophilic regions, which tend to associate in the water, causes the materials to spread at the interface rather than dissolving or forming a lens on the surface as shown in Figure 1-1.[51]

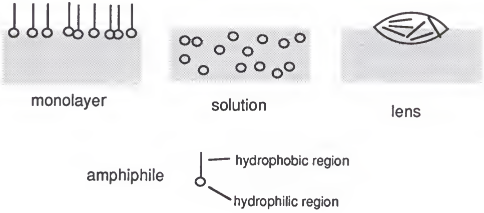

Figure 1-1. Monolayer, solution, and lens formation at a liquid surface.

## Spreading of a Liquid at an Interface

The forces that cause a material to spread on a liquid surface are expressed in the values of surface energy or surface tension, $\gamma$. Surface tension can be described as the interactions between areas in a molecule of different chemical nature with the surroundings.

These interactions tend to cause molecules to be pulled into the bulk liquid and thus minimize the surface area.[2] Thermodynamically, surface tension is defined as follows,

$$\gamma = (\delta G/\delta s)_{T,V,n} \quad (1.1)$$

where G is the free energy, s is the surface area of the liquid, T is the temperature, V is volume of the liquid, and n is the number of moles of liquid.

The combination of the surface energies of a material B placed on liquid A as shown in Figure 1-2, and the energy between the two materials will determine whether B will spread on A.

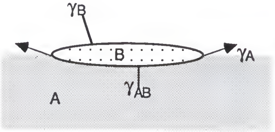

Figure 1-2. The surface tension values at the interfaces which will determine if liquid B will spread on liquid A.

The value referred to as the spreading coefficient, $S_{B/A}$, can be used as an indicator for spreading and is given below.

$$S_{B/A} = \gamma_A - \gamma_B - \gamma_{AB} \quad (1.2)$$

In the case of a positive value of $S_{B/A}$, B may spread on A. However, as A and B become mutually saturated with time, the $\gamma$ values will change and the spreading coefficient can become negative. This equation represents two major balancing forces involved at the interface in order for spreading to occur. These forces are the work of adhesion and work of cohesion, and are related to the spreading coefficient as shown below.

$$\omega_{AB} = \gamma_A + \gamma_B - \gamma_{AB} \quad \text{(work of adhesion)} \quad (1.3)$$

$$\omega_{BB} = 2\gamma_B \quad \text{(work of cohesion)} \quad (1.4)$$

$$S_{B/A} = \omega_{AB} - \omega_{BB} \quad (1.5)$$

Thus, if the molecules in B tend to adhere to surface A rather than cohere to themselves, B will spread on A.

Surface pressure, $\Pi$, of a surface active film on a liquid surface can also be determined from surface tension as related in Equation 1.6,

$$\Pi = \gamma_o - \gamma \quad (1.6)$$

where $\gamma_o$ is the surface tension of the pure clean subphase and $\gamma$ is the surface tension of the subphase plus monolayer film at a given temperature. The plot of $\Pi$ versus mean molecular area at constant temperature is referred to as an isotherm, and is the primary means of characterizing monolayer films. Monolayer isotherms can be considered two-dimensional analogs of bulk pressure/volume isotherms, and yield similar information about the films such as phase transitions and compressibility.[51]

## General Apparatus and Procedure

The Langmuir-Blodgett method involves spreading such amphiphilic substances from a dilute solution of volatile solvent onto a water subphase. The molecules are confined to the subphase surface in a shallow well referred to as a trough (Figure 1-3), which is made of, or coated with, inert material (usually Teflon®). Additionally, the film forming molecules are confined at one or both ends of the trough by movable barriers. Barrier material can be hydrophilic or hydrophobic, depending on the subphase used. The hydrophobic barriers cause a large convex meniscus at the film-water-barrier junction which may allow some film to slip below the barrier during compression. Therefore, in the case of pure water, hydrophilic barriers are advantageous in preventing film leakage.

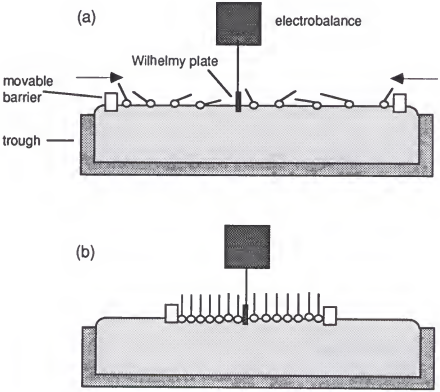

Figure 1-3. Langmuir-Blodgett trough. Monolayer experiment (a) before compression and (b) after compression.

After spreading, the molecules should be far enough apart in order to minimize interactions. From this state the monolayer is compressed by the movable barriers to a more condensed, oriented monolayer film as shown in Figure 1-3(b). During the compression, the monolayer film's physical properties can be measured. The most common method of characterizing monolayers is the measurement of surface pressure ($\Pi$) versus mean molecular area per molecule, or in the case of polymers, per limiting area repeat unit. The surface pressure is measured one of two ways - directly, with a Langmuir balance which measures the force exerted on a floating barrier by the film; or indirectly, with a Wilhelmy balance, that measures changes in surface tension which are subsequently converted to surface pressure using equation (1.6). As mentioned above, compression can be affected from one or both ends depending on the experimental setup. Compression from both ends is useful with viscous materials such as polymers, where shear forces around the Wilhelmy plate can cause error in the measured pressure values.[2,45,52]

Although some research groups have designed and built their own Langmuir trough and balance systems for specialized experiments, a number of excellent commercial systems are available. An example of the KSV Instruments, Ltd. LB5000 computer controlled trough, similar to the one used in the research presented herein, is shown in Figure 1-4.

The system consists of a main frame which can hold several measuring devices above the trough and houses the barrier drive. Devices and barriers are controlled through the main frame by an IBM compatible computer and driven by a KSV package software program. The advantages of the KSV trough system is the modular design, which allows versatility in experimental setup. Different measuring devices such as surface potential, surface pressure and UV absorbence can be attached to elevators along the main frame. Also different troughs can be used or removed from the set up, since the measuring devices and barrier drives are not integrated into the trough.

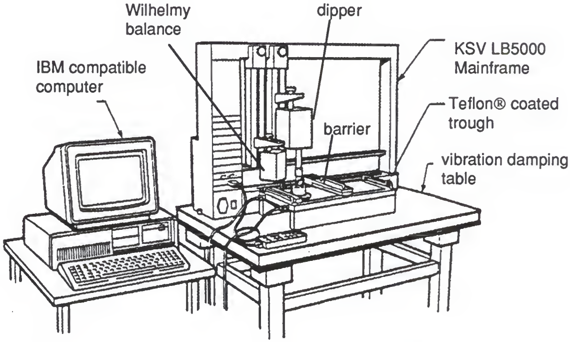

Figure 1-4. KSV LB5000 computer-controlled Langmuir-Blodgett film balance and trough system.

## Deposition of Monolayer Films onto Solid Substrates

Often the ultimate goal in producing monolayer films at an air-liquid interface is to transfer the highly ordered close-packed films to a solid substrate. This transfer and build up can be accomplished by vertical deposition as developed by Katherine Blodgett in the 1930's (Figure 1-5).[10,12]

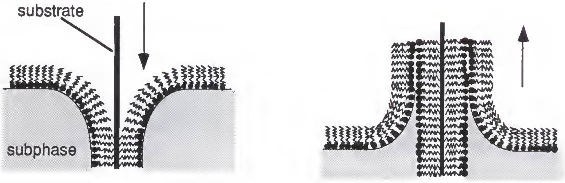

Figure 1-5. Conventional vertical deposition of a monolayer onto a hydrophobic substrate. Arrow indicates direction of substrate movement.

Monolayers can be transferred onto various types of solid plates depending on the surface treatment of the material. Films usually transfer to hydrophilic surfaces such as clean glass, quartz, or Si wafers; or hydrophobic surfaces produced by treating the previously mentioned materials with alkylchlorosilanes.[53] Monolayer transfer depends on the adhesive forces between the monolayer surface and substrate being facilitated when the above are greater than the attractive forces between monolayer and subphase. Some factors that can influence the transfer process are the nature of the substrate surface, subphase polarity, temperature, deposition speed and delay time above the liquid surface.

Actual transfer involves compressing the monolayer film to a stable pressure below collapse, and maintaining this pressure by computer control of the movable barrier throughout deposition. Monolayer stability is determined in an experiment prior to dipping by compressing to a target pressure, holding the pressure constant, and monitoring the change in mean molecular area with time. A pressure suitable for dipping is one that results in little or no change in mean molecular area after a reasonable relaxation period (5-20 minutes depending on the viscosity of the monolayer material). Once a stable pressure is determined the film is held at constant pressure with the movable barriers. A relaxation or stabilization time is usually required to allow the monolayer to equilibrate before deposition begins. Once the monolayer is stable the dipper arm brings the substrate down and up through the film at a controlled rate as shown in Figure 1-5.

Deposition data is collected during transfer in the form of transfer ratios. This value is defined as the area change of the monolayer at the water surface calculated by the barrier movement, divided by the area of substrate that actually passes through the monolayer. Any area change at the film surface (while maintaining a constant pressure during deposition) is assumed to result from monolayer transfer onto the surface of the substrate. Complete transfer would yield transfer ratios of 1.0. Transfer may occur on both the downstroke and upstroke as shown in Figure 1-5 to produce multilayers with an overall bilayer organization which are referred to as y-type films. Some materials transfer preferentially during either upstroke or downstroke and can produce non-centrosymmetric multilayers, which are referred to as x-type and z-type films

(Figure 1-6). The nature of the substrate surface usually defines the difference in x-type and z-type film formation.[2,45,52]

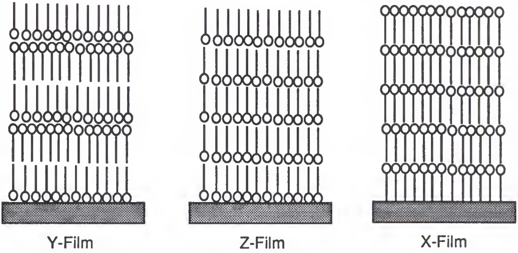

Figure 1-6. Multilayer film types.

Although the vertical monolayer deposition developed by Blodgett and Langmuir is most commonly used, alternative transfer methods exist. One such method developed by Langmuir and Schaefer in 1938 is referred to as Schaefer's method and involves transferring the monolayer film to a horizontally positioned plate, and then lifting the film off the subphase.[54] This method has advantages over vertical transfer, since it involves little or no deformation of the film during the transfer process as is caused during conventional deposition. Because of this, viscous and solid-like films which can't be deposited by the vertical method can often be transferred using Schaefer's method. Since there are no commercially available automated dipping apparatus for horizontal deposition at this time, it is not as convenient a method as vertical transfer. However, according to Ulman this may not be true for long.[45]

Deposition of monolayer films using an alternate trough and deposition apparatus. More intricate multilayer architectures may be built up with a specialized trough called an alternate deposition trough. The first design for a two-compartment trough for producing alternating layer structures was published by Puterman et. al. in 1964.[55] The generic design that has developed since then,

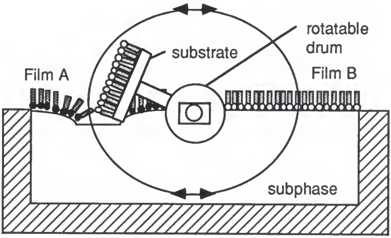

cross section, side view

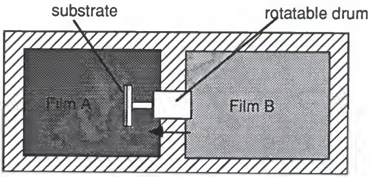

top view

Figure 1-7. Alternate deposition trough design using a rotating drum to transfer substrate from one trough compartment to another.

usually involves a two compartment trough with a common subphase area. A roller mechanism in between the two compartments is used to transfer the substrate from one film to the other and is schematically represented in Figure 1-7.[56] The disadvantage to this particular design is the absence of a separate confined subphase area containing no film, and through which the substrate can pass. This third compartment was incorporated into the KSV alternate deposition system design to allow complete flexibility in building up various alternating layer structures.

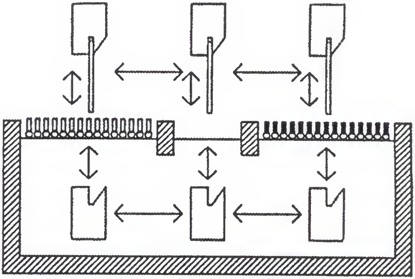

Figure 1-8.KSV alternate trough and dipping arm design. Schematic shows the possible routes a substrate can take through two films and a central area without film.

The KSV LB5000 alternate trough used in this research, contains two confined surface areas where up to two different monolayer films can be spread and compressed, and a central clean surface area where no film is spread. A deep dipping well is common to all three areas. A specialized dipper arm with two computer controlled clips and a turning motor allow the substrate to be taken up or down through any of the three regions in any conceivable sequence as shown in Figure 1-8. Various complicated superstructures can be made with one or two film forming compounds utilizing this method.[52]

## Polymer Monolayers and Multilayers

The majority of research conducted in the field of Langmuir-Blodgett monolayer and multilayer films to date has focused on low molecular weight amphiphiles. However, a shift in interest to polymeric analogs of the low molecular weight monolayer materials and novel polymeric systems for LB systems has occurred over the last few decades. It was discovered that multilayer films of the smaller molecules were not thermally and mechanically stable enough to be feasible candidates for industrial applications. In fact, most LB multilayer films of low molecular weight materials decompose at temperatures below 100°C. The significant solubility of low molecular weight amphiphiles is also a problem, since these materials dissolve in most commonly used solvents. To overcome these drawbacks, researchers turned to polymers as monolayer forming subjects.[30,44,52]

The first documentation of polymeric monolayers was made by Katz and Samwel in 1928, who looked at isotherms of poly(vinyl acetate) and poly(methyl acrylate).[57] A review on polymer Langmuir films was first published in 1946 by Crisp,[26] who attempted to categorize the monolayers based on viscosity and isothermal reversibility. Gaines included a section on polymeric spreading materials in his manuscript of 1967[2] and in 1991 published an extensive overview of polymer monolayer behavior up to the present time.[30]

Initially, simple polymer systems, such as polyacrylates[57-59] and polymethacrylates,[2,60] poly(vinyl acetate),[57,61] poly(vinyl fluoride),[62] poly(vinylidene fluoride),[62] and poly(dimethylsiloxane),[63,64] were investigated at the air-water interface. These systems form stable monolayer films on pure water; however, transfer to solid substrates, results in inhomogeneous films containing numerous defects. Although simple polymers remain of interest in basic scientific research, usually to further compare the monolayer behavior of these systems to the well documented three dimensional behavior, more novel polymer systems currently dominate LB research efforts.

Since simple polymer chains do not form an organized multilayer structure when transferred, it was argued that the usually symmetrical structure of the monomeric units fail to strongly orient the molecules with respect to the air-water interface. One solution to this was to use amphiphiles, previously shown to orient at water surfaces, and link them together in a polymeric form. Some researchers spread amphiphiles with polymerizable groups on the water surface, and then polymerized the monomers on the trough,[38,39,65-67] or after transfer to a solid substrate.[40,68-71] Due to shrinkage and movement during the polymerization, structural problems arose in the films produced by irradiating photopolymerizable monomeric monolayers in a multilayer film.[71] Polymerization research at the air-water interface continues[72-74] and polymerization of transferred LB layers can be successful when appropriate materials are used.[75] However, spreading of preformed polymers is the most expedient way of producing polymer monolayers and multilayers free from structural defects.

Subsequently, researchers in the LB field have synthesized numerous orientable groups and have attached them as side chains or incorporated them into the backbones. Polymers studied usually fall into one of three categories: i) amphiphilic polymers, such as polymers of fatty acids, poly(octadecyl methacrylate),[48,49,76,77] poly (octadecyl acrylate),[76,77] and poly(vinyl stearate)[68] ii) liquid crystalline polymers, stiff polar molecules attached via a flexible spacer to a common polymer backbone or incorporated into the main chain of a flexible polymer,[78-82] and iii) rod-like polymers,[46,49,50] such as poly (alkyl glutamates), which are comprised of a stiff mesogenic polymer backbone with flexible, hydrophilic or hydrophobic side chains. Polymers from all of these groups have been shown to form stable monolayers, transfer to solid substrates, and in some materials form well ordered multilayer structures.

Although polymer monolayers show similar properties to low molecular weight amphiphiles as far as isotherms and deposition, there exist some vital differences. Polymers are known to aggregate in bulk and even in solutions, and this behavior is seen at the air-water interface as well. Polymer monolayers, virtually always being mixtures of different molecular weight chains, show no sharp phase transitions as seen in smaller monolayer forming substances of monodisperse molecular weight. While low molecular weight materials reach equilibrium quickly, many polymer monolayers require detectable relaxation times and show shear viscosity quite dissimilar to smaller molecules. Even when spread from very dilute solutions, it is hard to imagine that in high molecular weight polymer solution spread at an interface, there are no entanglements and overlaying of chains. Based on this, it is improbable that any high polymer forms a true "monolayer" film, containing regions without two or more molecules stacked. Yet, highly ordered and fluid polymeric monolayer films have been documented, as well as well defined layer order in transferred multilayers of preformed polymers.[26,30,44,45,52,76,77]

The polymers of interest in this research involve liquid crystals and liquid crystalline polymers which will be discussed in a following section of this introduction.

### Blend Monolayers

For decades scientists and formulators have found that it is often easier to manipulate the properties of a polymer by mixing with another polymer or additive; rather than trying to synthesize a new molecule with the exact desired properties. Mixed monolayers have also been studied for similar reasons and have been documented in the literature since the advent of Langmuir-Blodgett film research. The first Langmuir-Blodgett monolayer mixed films were reported in the literature in early 1920's[83,84]. Ries and coworkers published results of monolayer behavior from the blends of fatty acids with polymers in 1961;[85] and Gaines' manuscript[2] devotes a whole chapter to thermodynamics and a general discussion of blend monolayers. More recently, Gabrielli et al. have rigorously investigated the physical and thermodynamic properties of various combinations of polymers and low molecular weight materials as monolayer blends.[86-88]

Researchers have mixed two or more components in monolayers to produce stable films with a component which normally does not form monolayers; to improve film properties of a monolayer forming material; to study intermolecular interactions between different molecules; to alter transferred multilayer properties, and to mimic biological systems which always possess multiple components. Mixtures of liquid crystalline monolayer substances have been made in order to adjust the LC properties and study the effect on the mesogenic interactions at the water surface. Additionally miscible blends of liquid crystals and liquid crystalline polymers have been produced and transferred as self reinforcing blends due to enhanced intermolecular interaction.[89] Blends of ferroelectric side chain LC polymers with mesogenic monomers have been studied in the bulk and as monolayer films[80,90,91] as a method of fine tuning ferroelectric response in the polymers. Details of liquid crystalline behavior is discussed in the following section.

The most important feature of monolayer mixtures to be determined is miscibility. If phase separation occurs, the film will behave with the average properties of the two independent films (or, as in the case of collapse, the less stable component dominates) and no benefit is obtained from mixing. There are numerous methods to determine blend monolayer miscibility based on simple thermodynamic relations, which will be addressed at the point of discussion in Chapters 3 and 4.

## Liquid Crystals and Side Chain Liquid Crystalline Polymers

Liquid crystals are materials that under specific conditions (of temperature or of concentration in solution) exhibit long range orientational or positional order between that of an ordered crystalline solid and an isotropic or disordered liquid. A physical state between a solid crystalline phase and isotropic liquid is termed a mesophase. In the past two decades, this intermediate self ordering has been harnessed and applied as electro optic devices and liquid crystalline displays. However, liquid crystalline phenomena have been reported as early as 1888 when mesophases of cholesteryl benzoate were noted by Reinitzer.[92] The term liquid crystal was coined by Lehmann as early as 1890.[93] Polymeric or high molecular weight liquid crystalline (LC) materials were first studied in 1937 by Bawden and Pirie.[94] Synthetic LC polymers appeared in the literature in the 1950's when Elliot and Ambrose published their findings on poly ($\gamma$ benzyl-L-glutamate).[95] Following these early research efforts, a surge in liquid crystal research began in the early 1970's with the promise of display device applications, and has continued to the present.

Theory and physical aspects of liquid crystals have been thoroughly developed by Onsager and Flory.[96-8] Simplistically, liquid crystalline ordering is a phenomena caused by the shape of the molecules and is a result of packing these shapes in a condensed fluid. Liquid crystals are characterized by large stiff areas with a high aspect ratio (length:width); and it is the stiff region, referred to as the mesogen, which causes ordering. The analogy has been made in the case of rigid rod LCs and low molecular weight mesogens to logs (stiff objects with a high aspect ratio) floating in a river.[44,46,49,50]

Liquid crystalline order can also be induced by molecular phase separation and microphase separation, and the substances exhibiting these phase are termed amphotropic. These molecules do not necessarily have stiff mesogenic regions but extreme amphiphilic nature within the molecules. Some examples of these LC materials are lyotropic soaps and lipids, which orient with respect to solvent molecules in solution. Also block copolymers containing comonomers which phase separate individually, form smectic and other phases dependent upon ratio and size of the polymer blocks. The order demonstrated by the above substances is caused by an attempt to minimize interaction between portions of the molecules or polymers with incompatible chemical nature.[99]

Various categories of mesophase ordering exist in liquid crystalline materials. The three main categories are nematic, cholesteric, and smectic and are depicted in Figure 1-9.

Nematic phases are the least ordered LC mesophase category, and show only average long range orientational order with no positional correlation (Figure 1-9(a)). An analogous phase, termed discotic, arises from shape anisotropy of extremely large disc shaped molecules rather than prolate aspect ratios.

Cholesteric phases, also referred to as chiral nematic, are related to nematic in the lack of long range positional ordering, but in cholesterics, the mesogenic moieties contain chiral centers and preferential ordering occurs locally. The molecular axis directors of molecules which exhibit cholesteric phases progress in a helical manner through the mesophase (See Figure 1-9(b)) and the pitch of the helix is usually temperature dependent.

Smectic liquid crystals are characterized by a layered structure or positional correlation as well as orientational order. There are numerous categories of smectic phases characterized by variations in layer ordering. Two common smectic LC mesophases, Smectic A and Smectic C, are shown in Figure 1-9(c). It is common to represent a smectic phase by a capital letter S followed by a

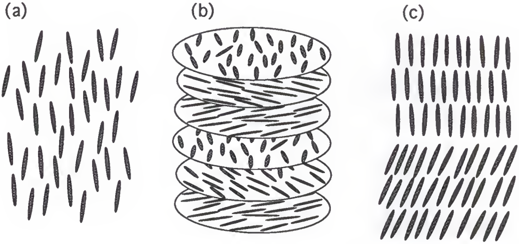

Figure 1-9. The three main categories of liquid crystal mesophases: (a) nematic, (b) cholesteric, and (c) smectic, (top) represents Smectic A phase in which there is little or no tilt of the molecular directors, and (bottom) a Smectic C phase in which the molecules are tilted.

subscript letter corresponding to the appropriate smectic subcategory. For example, a smectic A phase would be referred to as a $S_A$ mesophase.[99]

In addition to the local ordering by self organization, liquid crystal order can be strongly influenced by external fields. Nematic phases can be macroscopically ordered by flow through a small opening, as in the extrusion of high strength fibers.[100] Smectic and nematic phases of mesogens having electric dipoles are macroscopically ordered by electrical fields. This E-field ordering is the basis of LC optoelectric devices such as LCDs, and used in the new flat screen monitor technology. In amphiphilic liquid crystalline molecules, ordering can be modified by the chemical potential gradient that occurs at an interface.[99]

## Polymer Liquid Crystals

Although most commercial LC devices are based on low molecular weight materials, there are some disadvantages in using these smaller molecules, such as containment due to fluidity, and low thermal and mechanical stability of devices and films. Because of these disadvantages, LC mesogens have been incorporated directly into polymer backbones (main chain LC polymers), or attached as a side chain along a polymer backbone (side chain LC polymers). Research began on these new polymers in the mid-1970's, but initial results showed that the mesophases seen in the low molecular weight mesogens were often lost or changed when attached directly to a polymer chain. To overcome the disorder introduced by the polymer backbone in the case of side chain liquid crystalline polymers (LCPs), Finkelmann and Ringsdorf[41,42] showed that separating the mesogen from the backbone attachment site by a flexible spacer helped to decouple the motion of the polymer from that of the LC mesogen. Although the motion of each moiety is not completely independent, it was demonstrated that the ordering of these polymers was directly influenced by the length and nature of the side chain spacer; and if it were completely removed mesophase behavior was often eliminated.[89,99]

## Ferroelectric Liquid Crystals

Certain smectic liquid crystalline materials whose mesogens contain a chiral center exhibit a measurable spontaneous polarization within the layers. Such ordering is denoted in a smectic phase by an asterisk following the smectic symbol, i.e. for a smectic C phase which is the most common of FELC mesophases, the symbol Sc* is used. These materials are referred to as ferroelectric liquid crystals, analogous to ferroelectric crystals in the spontaneous polarization and hysteresis effects exhibited in the relation between dielectric displacement and electric field.[101] However, in smectic ferroelectric LCs the directors of the polarization within the layers progress in a helical manner through the layers as shown in Figure 1-10, and the resulting net polarization of macroscopic material is zero. Therefore, unless the helix is unwound as in an electric field or the thickness of the smectic film is less than the helical pitch, the materials are not true ferroelectrics, and it has been proposed that helielectric may be a more appropriate description for such compounds. Another characteristic of the Sc* phase is that it is a fluid. Thus molecules may locally rotate in a cone defined by their tilt angle with respect to the layer plane, diffuse laterally within a layer, and (with lower probability) diffuse from layer-to-layer. In polymeric FELCs the latter diffusion is considerably less likely, due to confinement of the polymer backbone between smectic planes.[99]

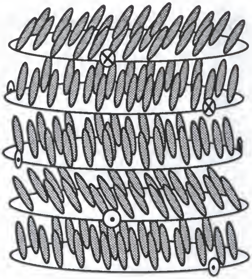

Figure 1-10. The layer structure of a smectic C* phase. Circles with dots indicate the positive direction of the lateral polarization vector, and circles with crosses indicate the negative direction. Tilt directions and polarization vectors progress in a helical fashion through the layers.

Surface-stabilized FELC devices (SSFLCs). In order to take advantage of the local spontaneous polarization phenomena of these helielectric materials, unwinding of the helical ordering of the polarization director through the layers must be achieved. This can be accomplished by placing the molecules in a large electric or magnetic field. Another widely studied approach involves confining the layers between specially treated transparent solid plates which orient the molecules by surface boundary effects and thus, eliminate helix formation. This use of surface stabilization of ferroelectric liquid crystals was first introduced by Clark and Lagerwall in 1980.[102,103] FELC devices created by this method are referred to as surface stabilized ferroelectric liquid crystal (SSFLC) devices and are distinguished by two requirements:

1) The molecular axes of the LC mesogens must be homogeneously aligned in the thin film between the electrodes with the smectic layer, normal parallel to the confining glass plates (referred to as "bookshelf geometry". (See Figure 1-11)

2) The thickness of the LC cell between the plates must be smaller than the helical pitch of the $S_c^*$ phase.

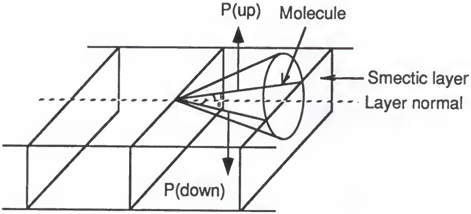

Figure 1-11. Representation of the LC/substrate interface region in a SSFLC device. Surface boundary effects caused by the "bookshelf geometry" of the smectic layers, result in two stable states, P(up) or P(down). The mesogens closest to the substrate surface are restricted to rotate in half of the cone possible in the normal bulk Sc* state.

In Figure 1-11 the conical path traversed by a FELC molecule within the layer structure is shown. It becomes apparent that the molecule at the surface will only have half of this cone in which to rotate. This produces a bistability, resulting from two lower energy positions at the intersections of the half cone with the aligning surface. These two stable states can be switched by reversing a voltage across the SSFLC device cell and will produce an on/off effect depending on the sign of the voltage. It is in this bistable conformation that FELCs have potential as display devices. Another attractive feature of such switching is that it occurs on a much shorter timescale than most conventional LC switching processes.[99]

## Monolayers and Multilayers of Liquid Crystalline Materials

The spreading of a material at an interface generally involves orientation of individual molecules or polymeric units, caused by the different chemical natures of various regions within these substances. As mentioned above, liquid crystalline molecules and polymers are inherently self organizing due to interactions between mesogenic cores and shape induced constraints. Combined with the fact that many liquid crystalline polymers are amphiphilic in nature, it would seem inevitable that these self organizing systems would be investigated as confined to a semi two-dimensional water surface. Consequently, the study of liquid crystalline materials in Langmuir-Blodgett monolayer and multilayer research is extensive and many-faceted.

Langmuir Blodgett films of long alkyl chain fatty acids have been used to orient liquid crystals on a solid surface.[104] Using optical microscopy, it was possible to use the alignment of the overlying LC layer to visualize defects in the underlying LB film.[105] Ringsdorf et al. have synthesized, spread, and transferred a variety of thermotropic liquid crystalline molecules and polymers over the past two decades.[35,41,44] A group of rigid rod main chain LC polymers containing long flexible side chains have been investigated at the air-water interface in the group of Wegner.[46,49,50] These stiff polymers with a high aspect ratio, lay lengthwise on the surface and are oriented during transfer by the forces of vertical deposition and flow processes. Another interesting group of LCs studied at the air-water interface exhibit a discotic phase. It was discovered that these LCs and LCPs orient on their sides at high pressures, to maximize π-π interactions between the mesogenic groups and form columnar phases lying lengthwise on the water surface. A review of discotic LC materials as monolayers and multilayers has been published by Laschevsky et al.[106] Bulk properties of liquid crystals which exhibit a ferroelectric layered phase (usually Sc*) have been a popular topic in the literature and constitute a large number of articles in the journal *Liquid Crystals.* Consequently, since the development of SSFLC devices by Clark and Lagerwall in 1980,[102,103,107] research to produce highly ordered thin films of FELCs has also sparked a great interest in monolayer forming species which organize in this fashion.[80-82,108,109]

Most often the motivation in Langmuir monolayer and LB multilayer research is the production of highly ordered thin films for future molecular electronics, optoelectronic devices, and optical data storage. This is also the case for liquid crystals and liquid crystalline polymers which spread at an air-water interface. The use of LC materials in Langmuir-Blodgett multilayers has also been rationalized as possibly enhancing thermal stability due to the self reinforcing nature of the molecules. In basic scientific research the use of producing monolayers of liquid crystalline materials and studying them at the air-water interface, remains an excellent means of probing the interactions between the self-ordering molecules.

## Applications of Langmuir Blodgett Films

Irving Langmuir, referring to his work on monolayer films in an commemoration speech for the Nobel Prize in 1937, stated

> . . . experiments started perhaps just for the fun of it, or to satisfy scientific curiosity, often lead to unexpected useful results in a field that could not have been predicted.[52]

This statement by Langmuir seems unusually foresighted, considering that the current motivation for research in the field that he pioneered at the turn of the century, is now looking to molecular circuits, monolayer biosensors and mimicking biological systems as potential applications.

In applying the Langmuir-Blodgett monolayer technique as an analytical tool or to produce a monolayer or multilayer device, the motivation is generally to take advantage of two basic features of monolayer films: the monomolecular and uniform thickness and, orientation of the molecules with respect to the water surface. The technique also allows ordered molecules that form monolayers at an air-liquid interface to be studied in an isolated and controlled fashion.

Remarkably, the first attempt to use monolayer films in an applied manner was in 1924, when fatty alcohol films were used to prevent liquid evaporation and retard gas permeation into storage reservoirs.[110] Irving Langmuir and Katherine Blodgett were not to patent their step gauge, anti-reflective coating, or sensor device designs until 1940, and these inventions were never commercially produced by General Electric.[13,111-114] The principles behind the patents, reduction of light reflection by applied fatty acid monolayers on glass, step gauge produced by interference of layers of various thicknesses, and filtration by skeletonized films; however, significantly advanced the understanding of general surface phenomena.

By the time of Gaines' manuscript in 1967[2], little change had been seen in the motivation of Langmuir-Blodgett research since the time of Irving Langmuir and Katherine Blodgett. In fact, in the applications section of Gaines' book, the devices patented and suggested by Blodgett are listed and the only additional application noted are those of ion selective membranes for electrochemical studies[115] and multilayer films as diffraction gratings for soft X-ray sources.[116]

The resurgence in LB research began in the early 1970's with the shrinking size of electronic circuitry and computer data storage media, as well as the advent of liquid crystal display technology. The focus of in LB film research applications has shifted and expanded accordingly. The types of materials studied has gone from simple fatty acids, alcohols, and esters to the most exotic of organic, inorganic, and biological molecules and polymers. LB research has also moved from the idea of using generic monolayers for a specific purpose; to using the LB technique to manipulate or enhance the already known bulk properties of molecules such as in the case of liquid crystalline materials.

The application section of recent overview books such as Ulman's[45] and Roberts'[52] are now extensive. Each cites examples such as mimicking biological membranes, biosensors, piezoelectric devices, pyroelectric devices, conducting films, non linear optical devices, microlithographic resists and numerous other sensor device applications. However, with respect to using the Langmuir-Blodgett technique to study monolayers and multilayers of liquid crystalline materials the applications generally been a) basic research of the self organizing behavior of LC molecules and b) optoelectrical devices and displays and data storage media.

The most useful feature of liquid crystal molecules is that they align themselves in an electric field. If the field is selectively applied to different regions of a thin film of a liquid crystal, regions of contrast will result from the varying regions of different refractive index. This gives these liquid crystal films a type of "on" (electric field applied, anisotropic alignment of the molecular directors, clear or dark) or "off" (electric field removed, isotropic orientation, light or opaque). This is the principle that the low molecular weight display devices are based upon. The main drawback to low molecular weight liquid crystalline materials is that most often utilizable molecules are in liquid form and have to be encased. Consequently the thermal and mechanical stability of these films is poor. Incorporating the liquid crystalline mesogens as side chains along a polymer backbone has been the most common method employed to overcome these drawbacks. However, the polymer matrix adds viscosity to the films and slows the response times of the alignment of the molecules. Fortuitously, this "problem" produces a different potential application for liquid crystalline materials. The long response time, if amplified, can be otherwise viewed as memory and these materials have promise as erasable optical data storage media. Applying the Langmuir-Blodgett method for fabrication of such optical devices and storage media presents the advantage of producing ultrathin films with a highly ordered layer structure and a possible method for manipulating the self organizing tendencies of the liquid crystalline molecules. These features are advantageous because, to decrease the size of storage media or increase the quality of display devices, an increase in optical resolution and contrast is required. Both of these characteristics are dependent upon film thickness and degree of ordering of the molecules within the film.[99]

Finally, ferroelectric liquid crystalline materials are enjoying a great deal of popularity as the most promising LC compounds to result in commercial displays. The bistability of the surface stabilized films incorporated into displays offers exceedingly fast response times. Also some siloxane based FELC polymers and copolymers exhibit competitive response times with many low molecular weight materials with added mechanical and thermal stability offered by the polymer backbone.[117] The Langmuir-

Blodgett technique is the most controlled method to produce the uniform, homogeneous and ultrathin films necessary for maximum efficiency from a surface stabilized configuration. This method will additionally produce a more ordered and defect free thin film which would further enhance the bistable response.

## Analytical Techniques

### Brewster Angle Microscopy (BAM)

Although the analyses of surface pressure vs. area isotherms give some general information of the overall monolayer film behavior, these methods generally cannot provide insight into the local morphology such as domain and aggregate formation in two phase systems, and defect topology and tilt variations in liquid crystals. Visualizing some of these features of films during compression has been possible in recent years with the use of fluorescent microscopy.[33,34,36] However, this method requires, in the case of non-fluorescing materials, the presence of a probe molecule in concentrations as high as 1 mol%. The difficulty in finding a compatible fluorescent marker molecule and the tendency of such probes to disturb their local environments limit the applications of this method.

Brewster angle microscopy (BAM), a method recently developed simultaneously in France[118] and Germany,[119] allows direct visualization of monolayer morphology without the complication of added probe molecules since contrast is dependent upon differences in the refractive indexes of the pure components rather than on emission by excitation of added chromophores. As the accessibility of these instruments increases, BAM measurements may prove to be a more general method to study blends and monolayer morphology.

Brewster angle microscopy is based a simple principle of optics. When p-polarized light is directed at an interface of two materials, as shown in Figure 1-12, with refractive indices $n_1$ and $n_2$, where $n_1 > n_2$, reflected light intensity is zero at the Brewster angle $\alpha$, defined as,

$$\tan(\alpha) = n_2/n_1. \qquad (1.7)$$

When a film possessing a refractive index, $n_{film}$, different from that of $n_2$, is introduced to the surface, light is reflected.

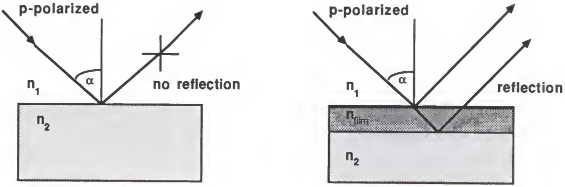

Figure 1-12. Principle of the Brewster angle.

The Brewster angle microscope (BAM) images light reflected from an interface. Such changes in the refractive index at the interface caused by differences in density, orientation and aggregation in pure films and phase separation in mixed films are seen as intensity changes in the BAM image. An advantage of this technique is that contrast is obtained without addition of foreign molecules. Therefore, the concern for miscibility of a fluorescent probe and it's possible effect on monolayer behavior is eliminated.

## Small Angle X-ray Scattering (SAXS)

X-ray diffraction at small angles (corresponding to large periodic distances) has been used frequently in the analysis of transferred multilayers to prove the existence of the transferred LB multilayer structure, as well as, probe the layer ordering in these films.

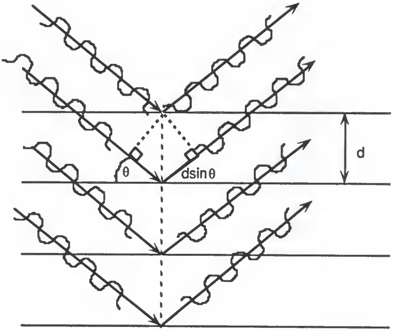

Figure 1-13. Principle of coherent scattering from a series of points equal distances apart.

All X-ray diffraction is dependent on the coherent scattering of light of a given energy by atoms or areas of high electron density which show some periodic structure. As shown in Figure 1-13, for incoming light of wavelength, $\lambda$, to constructively interfere with light reflected from the next periodic plane the difference in path length between the two reflected light waves, $2d\sin\theta$, must equal some integral multiple of the wavelength and is otherwise known as

$$n\lambda = 2d\sin\theta \qquad (1.8)$$

the Bragg condition. Peaks of light intensity reflected under this condition are referred to as Bragg peaks, and if $\lambda$ and $\theta$ are known will provide the periodic distance, d, or in the case of built up multilayers, layer spacing.[120]

SAXS of Langmuir-Blodgett multilayers. As mentioned previously, SAXS measurements have been used in the literature to prove an ordered multilayer structure in LB films. Additionally, X-ray diffraction can be used as a gauge to compare the order in comparable multilayer systems. The first X-ray diffraction patterns of LB films were published by Holley and Bernstein in 1936 and demonstrated the layer structure of fatty acid salt multilayers.[121] Since these early experiments, most X-ray diffraction studies of LB multilayer films have featured long chain fatty acids and their heavy metal salts. The spacing of the metal ions within the multilayers were actually used to determine layer spacing, since these large atoms have much greater diffracting power than the pure hydrocarbon molecules. With the advancement of equipment and

technology, the sensitivity and resolution of modern X-ray diffraction equipment has eliminated the need to include heavy metal atoms in determining the layer spacing and structure. Additionally, with synchrotron radiation sources available, even one monolayer can be detected under reasonable experimental conditions. With a more elaborate setup, the monolayer can be investigated while still on the water surface.[32,122-124]

Although most of the early X-ray analysis of LB multilayers involved simple fatty acids, salts and esters, recent literature features more complex systems such as polymers and biological materials, and mixtures of two or more components. Day and Lando investigated the layer structure of transferred polydiacetylene multilayers which were polymerized on the water surface.[125] Lvov et al. confirmed the structure of 4-n-octadecylphenol and barium behenate superlattices using X-ray diffraction experiments and determined the layers consisted of alternating bilayers of each component.[126] Matsuda[127] and Watanabe[128] used SAXS to describe changes in multilayer films of a particular polymer as another material was added. Systematic changes in the X-ray diffraction scattering with mixture composition have been used to gather information as to the interaction between the two compounds as transferred. Additionally, Chen et al. studied multilayers of electrically conductive Langmuir films of poly-3-thiophene and mixed films with stearic acid using SAXS, and monitored the thermal dependence of the multilayer structure containing various concentrations of stearic acid.[129]

In this body of work, emphasis will be placed on determining layer spacing of transferred multilayers. This data will be used to study the effect of varying dipping conditions and systematic changes in monolayer composition. The results will then be used to elucidate information on the molecular organization of the multilayers.

## Summary

The purpose of the research presented herein is to study the behavior of two side chain liquid crystalline polymers as monolayers at an air-water interface, and as defined thin films on solid substrates. Liquid crystalline materials of themselves are interesting in their self organizing abilities under certain conditions in the bulk. This research addresses the aspect of confining these naturally self-assembling molecules using the Langmuir-Blodgett technique, where they are inclined to orient with respect to an air-water interface. In addition to studying pure component films, blends with different materials were produced to manipulate film properties in a specific manner. Once stable films with the needed properties are obtained, they may be transferred to solid substrates in order to form highly ordered thin films of discrete thicknesses. It is expected that the behavior of these newly ordered films will differ from bulk or cast films, in the degree and control of ordering. The differences in molecular order and arrangement are expected to affect other physical features of the film.

In Chapter 2 details of the experimental apparatus and material synthesis will be documented in detail.

The monolayer and multilayer properties of a ferroelectric side chain liquid crystalline polymer will be discussed in Chapter 3.

The polymer formed very stable and fluid films, however, multilayers of the polymer tended to rearrange at room temperature. Additionally, blends of the polymer with corresponding side chain mesogen were made to manipulate the fluidity and lateral density of the monolayer and multilayer films. The blend monolayers' physical properties will be compared analogously with the pure components' and some conclusions will be drawn as to miscibility of the blend system and the optimization of blend composition.

In Chapter 4 the properties of another side chain liquid crystalline polymer will be discussed. This polymer contains a methacrylate backbone, is much more ordered than the polymer shown in Chapter 3, and contains no chiral mesogen. The stability of the monolayer films of this polymer were found to be less than adequate with respect to stability and deposition. Blends were made with stearic acid and poly(octadecylmethacrylate), both well documented monolayer forming materials, in order to improve the monolayer properties of the side chain liquid crystalline polymer. Blend monolayers were compared with pure components and miscibility of the blend system is discussed.

Chapter 5 contains a comparison and contrast of the two monolayer blend systems and LC polymers described in Chapters 3 and 4.

# CHAPTER 2

# EXPERIMENTAL

## Materials

### Poly(4-tetraetyleneoxide-4'-methoxybiphenyl methacrylate) (PM4)

The side chain liquid crystalline polymer denoted as PM4 was synthesized by Dr. Randy Duran and details of the synthesis and structural characterization have been published elsewhere.[130] The synthesis route is described in Figure 2-1. The polymer was synthesized free radically in THF solution and the tacticity of the polymer backbone was determined by 1H NMR (triad analysis) and was found to be 10.7% isotactic, 34.2% heterotactic and 55.1% syndiotactic. $M_n$ was determined by SEC to be 99,800 g/mol against a calibration curve of polystyrene and $M_w/M_n$ was determined as 2.7.

### Poly(octadecylmethacrylate) (PODMA)

The poly(octadecyl methacrylate) used in this research was synthesized radically in toluene solution, reprecipitated from toluene/methanol and had a $M_n$ of 196,500 g/mol ($M_w/M_n = 1.5$) against a polystyrene calibration curve. Tacticity of the poly(octadecyl methacrylate) was determined by 200 MHz $^1$H NMR and was found to be approximately 25% isotactic, 50% heterotactic and 25% syndiotactic triads respectively.

The stearic acid used in the blend studies with PM4 was purchased from TCI Chemical Co. and was used as received

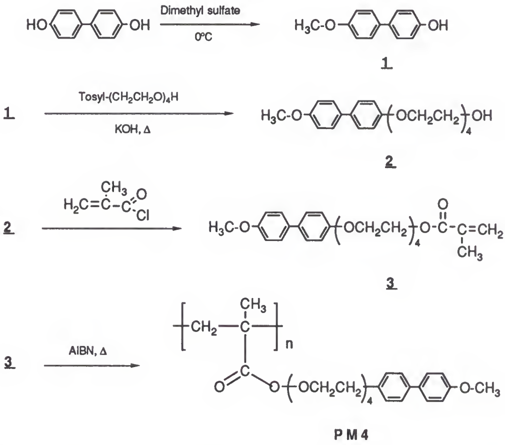

Figure 2-1. Scheme of synthesis of side chain liquid crystalline polymer, PM4.

### (R)-4'-(1-ethoxycarbonyl-1-ethoxy)phenyl-4-[4-(9-decenyloxy)-phenyl]benzoate (10PPB2)

(R)-4'-(1-ethoxycarbonyl-1-ethoxy)phenyl-4-[4-(9-decenyloxy)-phenyl]benzoate. The liquid crystalline mesogenic monomer, denoted as 10PPB2, was provided by Dr. Jawad Naciri and was synthesized as represented in the scheme shown in Figure 2-2, by the combination of compounds 4 and 5 in the presence of thionyl chloride and pyridine. Details of the synthesis procedure and synthesis of compounds 4 and 5 are published elsewhere.[117] The product was purified by silica gel chromatography and recrystallization from ethanol.

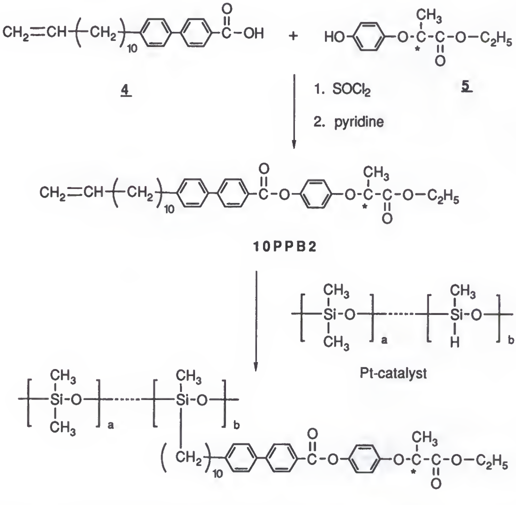

Figure 2-2. Synthesis scheme for 10PPB2 and 10PPB2-CO.

### 10PPB2-CO

The side chain liquid crystalline copolymer, denoted as 10PPB2-CO, was provided by Dr. Jawad Naciri and synthesized as shown in the remainder of the synthesis scheme in Figure 2-2. The backbone poly [(30-35%)methylhydrosiloxane-*co*-(65-70%) dimethylsiloxane] with a $M_n$ of 2000-2100 was purchased from a commercial source and used as received. The side chain mesogenic group was attached to the Si-H sites along the copolymer backbone by a classical hydrosilylation reaction[117,131] in the presence of a platinum catalyst. The polymer was purified by gel permeation chromatography eluted with toluene and precipitated from THF solution into methanol. The resulting polymer showed a $M_n$ of approximately 8000 gm/mol.

## Monolayers

### General Procedure and Equipment

Spreading solutions of the materials mentioned were prepared in spectro grade chloroform (Kodak or Fisher ACS) at 0.5-1.0 mg/mL concentrations. Blend solutions were prepared from stock solutions of the pure components and volumes delivered in a 1 or 5 mL Hamilton gas tight syringe (volume error ± 1$\mu$L) yielding a concentration error of approximately ± 1% neglecting error of initial solution and evaporation. Solutions were delivered using a Hamilton gas tight syringe (100 or 250 µLs) dropwise on the surface on the subphase surface.

Solutions were spread on ultra pure water (resistivity 18MΩ) subphase in all cases. Water was purified by deionization (Continental Water Systems), followed by polishing through a Millipore Milli-Q® Plus 5-bowl filtering system. Temperature of the subphase was controlled through circulation of water through channels below the trough well surface and circulating water temperature was controlled to ± 0.5°C with a Neslab refrigerating and heating circulating bath. Isotherms were performed at room temperature unless otherwise indicated.

All isotherms and various plots of $\Pi$, mean molecular area and time were collected on an LB5000 (KSV Instruments, Helsinki, Finland) computed controlled film balance and using the accompanying KSV software package (Version 4.4) for data acquisition. Monolayers were compressed at a speed of 2 $Å^2$/(molecule or repeat unit)*minute. This rate was determined to be below the range in which any of the isotherms showed measurable rate dependence. Mean molecular areas refer to the average surface area per molecule in the case of low molecular weight compounds (stearic acid and 10PPB2); and per side chain group or mesogen in the case of the side chain polymers (PODMA, PM4 and 10PPB2-CO) unless otherwise specified. All isotherms were run a minimum of two times, with a reproducibility error of less than 1.0 $Å^2$.

Integration of surface pressure versus surface area ($\Pi$-A) isotherms was accomplished using KSV analytical software provided with the film balance and instrumentation. The excess $\Delta G_{mix}$ values were obtained by graphical integration of isotherms. Integration limits were taken from a lower pressure limit of 0.3 mN/m in order to eliminate error caused by baseline fluctuations. Collapse pressures were determined by analyzing derivative isotherm curves ($d\Pi/dA$) which were smoothed by a 7-point smoothing routine and taking the minimum derivative value as the collapse surface area. Corresponding collapse pressures were then taken from the original isotherms.

Maximum standard deviations of isothermal analysis data is as follows: collapse pressure values - ± 2 mN/m; compressibility - ± 0.0009 mN/m; $\Delta A_{xs}$ - ± 1.2 %; and $\Delta G_{mix}^{xs}$ - ±1.9%.

### Brewster Angle Microscopy

The Brewster angle microscope used was a BAM1 from Nanofilm Technologie Gmbh (Göttingen, Germany). A He-Ne laser (p-polarized) was used as the light source. Schematic of the optical setup is shown in Figure 2-3. Angle of incidence was initially set to 53° and then adjusted to minimize the reflected intensity of the clean water surface prior to spreading of each film. All photos presented were taken with a rotatable analyzer set at 90° placed in between the reflected signal and CCD-camera. A frame grabbing program (Videopix, Sun Microsystems) was used to generate photos from video tape and convert them to a computer readable format. BAM intensity ratios were obtained by integrating the intensities over all pixels of the captured image for the clean water surface, $I_o$, and for the film as compressed, I. In the intensity versus surface area plots for the blends, all instrument settings including intensity gain were held constant, for the purpose of comparison.

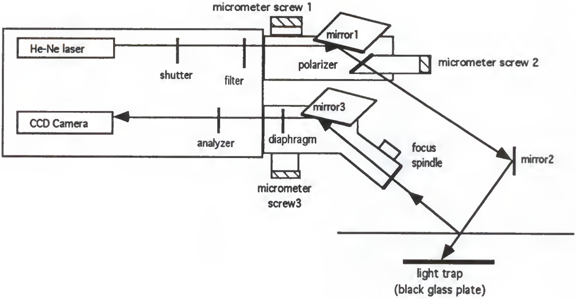

Figure 2-3. Schematic of the optics in the BAM1 Brewster angle microscope setup used. Micrometer screws adjust the angle of the corresponding mirrors. The filter adjust the level of the laser beam intensity.

## Multilayers

### General Procedure and Equipment

All multilayers were transferred to single crystal Si (100) wafers with a flatness of 3-10 Å . Silicon wafers were cleaned in a solution of concentrated $H_2SO_4$ and Nochromix® or concentrated sulfuric acid and 30% $H_2O_2$ heated on low for a few hours. After cleaning, wafers were rinsed at least 10 times with Milli-Q ultra pure water (>18 MΩ) and allowed to air dry.

All 10PPB2-CO and 10PPB2-CO/10PPB2 blend multilayers were transferred to hydrophobicized Si wafers (purchased from Semiconductor Processing, Inc., Boston, MA). Hydrophobization was achieved by chemiabsorption of a monolayer of octadecyltrichlorosilane (Aldrich) self assembled on the hydrophilic Si surface. Clean wafers were treated in an inert atmosphere with 2-5%(vol) octadecyltrichlorosilane (OTS) in anhydrous hexadecane (Aldrich) for 30 to 45 minutes with stirring to allow complete chemiabsorption. Wafers were removed from solution, while still under anhydrous conditions, and rinsed twice with distilled and degassed toluene to remove excess OTS from the region of the surface. Wafers were then rinsed with methanol followed by several rinses with Milli-Q® grade water to polymerize the surface monolayer.

Conventional vertical deposition (up and down through the film) was performed using a KSV LB5000 computer interfaced Langmuir-Blodgett trough and dual barrier drive system (compression from both ends towards the center) to ensure homogeneous deposition on both sides of the substrates. The dipping trough was a standard KSV teflon coated trough with dipping well in the center. A KSV alternate deposition trough, dipping arm, and dual control barrier system were used to produced the x-type deposited films of 10PPB2-CO and its blends with 10PPB2.

UV spectra and absorbence data used to confirm deposition of monolayer films were taken with a Perkin Elmer Lambda 9 instrument.

Dipping speeds and delay times varied with samples and are shown in Table 2-1.

Table 2-1. Multilayer samples and deposition conditions.

| Material | Dipping type* | Surface Pressure (∏, mN/m) | Temp. (°C) | Dipping Speed up | Dipping Speed down | Film type | Upper delay (s) |
|---|---|---|---|---|---|---|---|
| 10PPB2-CO | C | 25-27 | RT** | 10 | 10 | y | 30 |
| 10PPB2-CO | A | 25-27 | RT | n/a | 10 | x | 0 |
| 5% 10PPB2 | A | 25 | RT | n/a | 10 | x | 0 |
| 10% 10PPB2 | A | 25 | RT | n/a | 10 | x | 0 |
| 15% 10PPB2 | A | 25 | RT | n/a | 10 | x | 0 |
| 20% 10PPB2 | A | 25 | RT | n/a | 10 | x | 0 |
| 10% 10PPB2 | C | 25 | 31-32 | 6 | 8 | y | 30 |
| 20% 10PPB2 | C | 25 | 31-32 | 6 | 8 | y | 30 |
| 30% 10PPB2 | C | 25 | 31-32 | 6 | 8 | y | 30 |
| 50% 10PPB2 | C | 25 | 31-32 | 6 | 8 | y | 30 |
| PM4 | A | 5 | RT | 5 | n/a | z | 600 |
| 30% PODMA | A | 8 | RT | 5 | n/a | z | 600 |
| 50% PODMA | A | 10 | RT | 5 | n/a | z | 600 |
| 70% PODMA | A | 7 | RT | 5 | 5 | y | 600 |

* A-alternate; C-conventional.
**RT-room temperature (between 24-28°C)

X-Ray Measurements

Small angle X-ray measurements were performed in Washington, D.C. with the assistance of Dr. Bob Geer, a post doctoral assistant at Naval Research Laboratory. Two experimental setups were used to examine the order of the LB multilayers.

For the X-ray diffraction patterns and layer spacing data shown in Figures 3-7 and 3-8, X-ray diffraction measurements were performed on a Rigaku 2-circle diffractometer operating a 10kW and 1/6 mm slit width. The radiation was Cu K$\alpha$ from a Rigaku rotating anode source. A single crystal graphite analyzer and standard scintillation detector were used. The angular resolution of the scans was approximately 0.015° 2$\Theta$.

For the X-ray scans and data presented in Figures 3-24 - 3-26, 3-28, and 4-25, diffraction measurements were performed on a Rigaku RU-400 4-circle diffractometer using Cu Ka radiation from a rotating anode source. The X-ray beam was collimated by a 0.12° entrance and exit slits along with a Soller slit placed in front of the graphite analyzer. The diffracted intensity was measured using a scintillation detector.

### Differential Scanning Calorimetry

Bulk samples of PM4, PODMA and a 50% PODMA were prepared from dilute solutions of chloroform. Solvent was added and allowed to evaporate until a sample of 4-8 mg was obtained. Open pans were vacuum dried at room temperature for several hours to insure no residual solvent or excess moisture remained in the sample. DSC scans were run on a computer controlled Perkin Elmer DSC-7 with a TAC-7 Instrument Controller. Temperature ramp speeds for the scans shown are 20°/min with a two minute delay at the end of heating scans. Cooling scans were also obtained, but are not shown, and were run at the same 20°/min rate.

Thermal Stability Microscope Study of Multilayers

An attempt to compare the multilayer stability of 10PPB2-CO/10PPB2 blends was made by observing the dewetting of the films from the substrate while varying the temperature. Silicon wafers for the study were from the same batch purchased from Semiconductor Processing, Inc. Wafers were thoroughly cleaned by the method mentioned previously. Hydrophobization was achieved by OTS/hexadecane solution by the procedure mentioned previously and under dry box conditions. Thirty layer samples of 10PPB2-CO were produced by alternate deposition.

The samples were observed with a Nikon Diaphot optical microscope in a reflectance setup. The film was observed with a 10X objective and the eyepiece was removed during intensity measurements. Heating of the samples was accomplished with a Mettler FP82 stage controlled by Mettler FP80 Central Processor. Intensity was measured with a light intensity attachment controlled by the FP80 processor. Intensity values were recorded with an XY-chart recorder. Temperature heating rate was 5°C/minute (comparable to DSC rates used to determine transitions in the bulk).

Temperature values of dewetting ranged from approximately 125-180°C, and one sample remained intact at 200°C. Due to the erratic temperature values, no data is presented in the text. The different temperature values obtained from similar samples are believed to be caused by defects in the surface or minute contamination of the multilayers during deposition. Under routine experimental conditions, dust and other contaminants are present and normally do not effect the results. Apparently, the dewetting process is more sensitive to the presence of such contamination. These dust or other contaminants appear to act as nucleating agents, which open "holes" in the film that spread as the temperature is raised.

Based on the above observations, the sample which remained intact at 200°C most likely contained the least amount of contamination or defects in surface treatment. This result demonstrates the remarkable thermal stability possible in LB films of this material, considering that the isotropic melt temperature of this material is 150-162°C as determined by DSC.

# CHAPTER 3

# BLENDS OF A FERROELECTRIC SIDE CHAIN LIQUID CRYSTALLINE COPOLYMER WITH CORRESPONDING MESOGENIC MONOMER: MIXTURES FOR PRODUCING A MORE LATERALLY CONDENSED MONOLAYER

## Introduction

Some smectic liquid crystalline materials containing chiral moieties are known to exhibit a local spontaneous polarization due to a preferred molecular orientation within the layers. In such materials, although each layer has an effective polarization, bulk polarization can be observed only by untwisting the helical progression of the layer polarization vector as described in Chapter 1. It has been demonstrated[102,103,107] that this can be achieved by surface boundary effects.

The problems in forming these "surface stabilized"[102,103,107] ferroelectric films are that the films must be uniform and in the range of microns in thickness. However, for certain materials that spread on a water surface to form a monolayer, the Langmuir-Blodgett technique can be used to transfer these monomolecular films and build up organized multilayers of discrete thickness.[2,52]

The ferroelectric liquid crystalline copolymer, denoted as 10PPB2-CO, shown in Figure 3-1 was found to spread from a chloroform solution to form stable monolayer films. The corresponding liquid crystalline homopolymer and monomer film properties have been previously reported.[108] Despite containing identical mesogenic groups, the bulk and film properties of the copolymer are quite different from the homopolymer and monomer. The copolymer, 10PPB2-CO, appears to be relatively more stable and easily transferred.

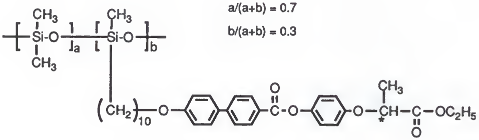

$$\text{Crystal} \xrightarrow{15^\circ\text{C}} S_C^{*} \xrightarrow{136^\circ\text{C}} S_A \xrightarrow{150\text{-}162^\circ\text{C}} \text{Isotropic}$$

Figure 3-1. Structure and bulk thermal properties of 10PPB2-CO.

In the research presented herein, multilayer films have been produced using conventional vertical deposition (up and down through a compressed film). Additionally, pure x-type deposition (substrate passes through monolayer film only on the downstroke) was achieved using an alternate LB deposition system. These films were compared by transfer data and small angle x-ray diffraction. In addition, some hybrid structures were produced to probe the different architectures that result when varying the transfer route. Based on the resulting data, it was concluded that rearrangement occurred in the transferred multilayer films. Mixtures of the copolymer with corresponding mesogenic monomer, denoted as 10PPB2 were made in an effort reduce the rearrangement after transfer, and at the same time improve the FELC properties of the multilayer films.

The monomer (10PPB2) was chosen as the best blending candidate to alter the 10PPB2-CO films for two reasons. First, the copolymer and the monomer have been shown to be completely miscible over all concentrations in the bulk,[90] therefore, miscibility in the monolayers is favorable. Secondly, 10PPB2 is crystalline in the bulk phase at room temperature and forms more closely-packed Langmuir films than the copolymer. Therefore, it appears to be a suitable mixing material to reduce mobility and surface area of the side chain groups in 10PPB2-CO monolayers.

Several methods were employed to determine miscibility in the monolayers. Conventional data analysis, such as compressibility and collapse pressure trends with blend composition, isobaric data of mean molecular area versus blend concentration, calculation of the excess free energy of mixing ($\Delta G_{mix}{}^{xs}$), and thermal dependence studies of blend isotherms are presented and discussed.[2,43,86-88,132-135] Investigations on the morphology of the blended monolayers are presented in the form of Brewster angle micrographs and reflected intensity studies.[118,119] Using a commercially available instrument, the blend films were recorded during compression and analyzed. Additionally, the use of a rotating analyzer placed in front of the camera allowed information concerning the orientational order of the molecules at the surface to be obtained.

Transfer of the blend films to solid substrates was also investigated. Both conventional and alternate deposition was used to transfer films up to 50% 10PPB2. Small angle X-ray diffraction analysis of the data will be used to obtain structural and layer order information for the multilayer samples. Based on these and monolayer results, a model for the organization of the mono- and multilayer blends will be put forth.

## Monolayers and Multilayers of the Pure Copolymer

### Monolayer Film behavior of 10PPB2-CO

Figure 3-2 shows a curve of film surface pressure versus mean molecular area/mesogenic unit for 10PPB2-CO. The film exhibits what can be described as a "reversible collapse";[30] and upon compression above collapse, followed by expansion, the film respreads to form a similar monolayer film. The second compression (Figure 3-2, curve 3) exhibits no hysteresis behavior and falls on top of the first compression curve. Since the copolymer is in a liquid crystalline phase (smectic C*) rather than crystalline phase in the bulk at this temperature, the backbone has considerable thermal energy and flexibility. This freedom of movement in the polymer backbone may prevent the mesogenic group crystallization; which is thought to cause the collapse irreversibility for the homopolymer and monomer. It may also account for the fluid film behavior demonstrated in Figure 3-2. Additionally, monolayers of 10PPB2-CO were found to be thermally stable over a wide range of temperatures. Characteristics of the films were investigated over a temperature range of 11-28°C with no significant change in isotherm appearance.

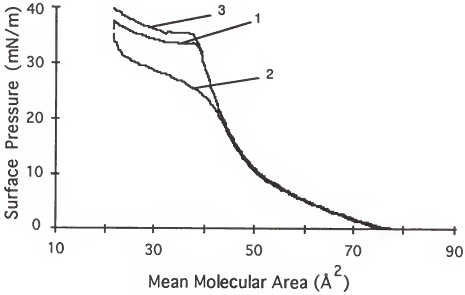

Figure 3-2. Compression (1), expansion (2) and recompression (3) of a 10PPB2-CO monolayer. The retracing of the first compression curve during the second compression demonstrates the fluid nature of the copolymer monolayer film.

### Deposition Behavior of 10PPB2-CO

In order to utilize the properties of a ferroelectric LC monolayer or any LB monolayer in general, the film must be transferred to a solid substrate. To produce films suitable for a SSFLC device, 50 to 100 layers must be built up, depending on the helical pitch of the FELC material. Therefore, deposition that is consistent and homogeneous up to large layer numbers is necessary for future applications of these compounds.

Deposition of 10PPB2-CO monolayers was possible on both hydrophilic and hydrophobic substrates. However, multilayers could only be achieved on hydrophobicized surfaces. The subsequent downstroke on hydrophilic substrates resulted in almost quantitative film redeposition onto the water surface.

In most multilayer films produced by standard (up and down through the compressed film) vertical deposition, initial y-type deposition would rapidly change to x-type in 5 or 6 cycles. Some samples were obtained with approximate y-type deposition, however the upstroke transfer ratio was not consistent and never greater than 0.8 (See Figure 3-4, top graph). Regardless of the conditions, downstroke transfer was always 1.0 (+/- 0.05) and was consistent up to 100 layers with no decay in transfer ratio.

Alternate deposition of 10PPB2-CO to produce x-type multilayers. Transfer ratios significantly less than 1.0 indicate a suboptimum transfer process. Since 10PPB2-CO upstroke layer ratios were considerably low and not consistent, these layers are most likely inhomogenous. All previous y-type deposition multilayer samples of 30 or more layers had visible "stripes" of varying colors indicating non uniform film thickness. If the downstroke transferred film adheres better to the substrate and to previously transferred layers, multilayers formed with only downstroke deposition should give films of more uniform thickness.

To construct films containing no upstroke transfer, an alternate deposition trough and specialized dipping arm were used. These types of LB deposition systems are most often used to produce multilayers with two different alternating monolayer films.

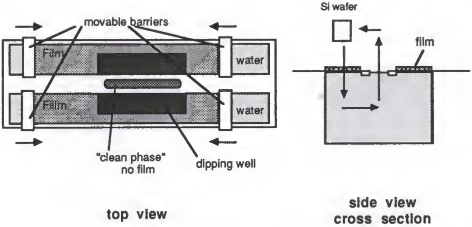

Figure 3-3. Schematic representation of alternate LB trough and x-deposition.

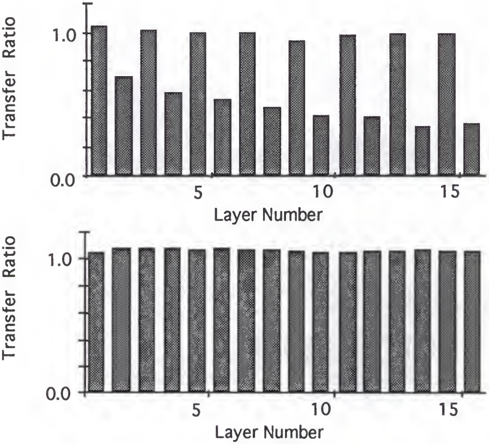

Figure 3-4. (Top) Transfer ratio data for a y-deposited film of 10PPB2-CO. Odd layers represent the downstroke and even layers represent upstroke transfer. (Bottom) A x-deposited film with all transfer on downstroke.

However, in this case, the system allowed the elimination of the upstroke component in 10PPB2-CO deposition as shown in Figure 3-3.

A sequence of sending the substrate down through the film and up through the clean phase produced pure x-type deposition in the FELC copolymer multilayers. Downstroke transfer ratios were consistently 1.0 ± 0.05 (See Figure 3-4, bottom graph), with no apparent decay of transfer up to 100 layers. It was discovered that when this deposition method was used, films of 30 or more layers were homogenous in color and texture indicating that the previous visible defects were absent in these films.

Alternate deposition of 10PPB2-CO to produce mixed film types. To probe the differences in layer structure resulting from x- and y-type copolymer deposition, an alternate deposition method was used to produce mixed 10PPB2-CO layers of various ratios of x-type and y-type deposition. Deposition sequences incorporating regularly space y-type "defect" layers into the x-type deposition were designed and utilized. Upstroke layers were introduced systematically with the ratios ranging from two downstrokes/one upstroke to 9 down/1 up. Transfer ratios were similar to the previously seen data, with downstrokes approximately 1.0 and consistent; and upstrokes ranging from 0.4 to 0.8 and erratic. As the ratio of defect layers over number of x-type layers decreased, the macroscopic defects and stripes in the films became less evident. However, as long as any upstroke layer was present in the film some heterogeneity was observed.

Two examples of mixed deposition films are shown schematically in Figure 3-5. In Figure 3-5(a) a multilayer with equal ratio of x-type monolayers and y-type bilayers, assuming no rearrangement after deposition, is shown; and in Figure 3-5(b) a similar multilayer is displayed with a 2:1 ratio of monolayer to bilayer buildup. From this theoretical architecture, an X-ray diffraction pattern of the layer spacing would display two sets of Bragg peaks corresponding to the monolayer (x-type) and bilayer (y-type) repeat layer spacing. Additionally, there would be a set of Bragg peaks corresponding to the superstructure of monolayer and

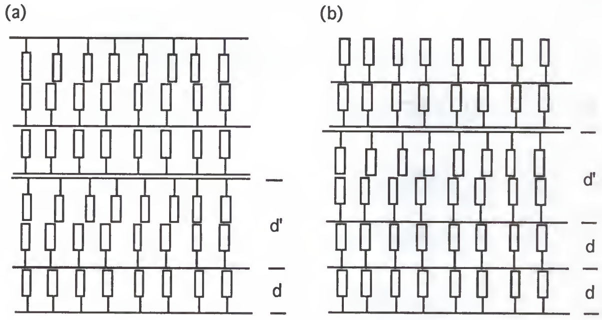

2 down, 1 up

3 down, 1 up

Figure 3-5. Schematical representation of 10PPB2-CO mixed type multilayers. Path through the film for the multilayer (a) is down, down, then up, and for (b) is down, down, down, then up, to achieve mixed x- and y-type deposition.

bilayer repeat sequence such as in Figure 3-5(a) of monolayer plus bilayer spacing (i.e., d + d'). Since there would be fewer repeating units of this superstructure and the spacing would be rather large, these peaks would probably be overshadowed by the former diffraction patterns.

Alternating multilayers of 10PPB2-CO and 6PPB2-CO. The copolymer 10PPB2-CO is one of a homologous series of copolymers with a variable side chain spacer length of 6, 8, or 10 methylene groups. The copolymer 6PPB2-CO with a six methylene unit spacer has also been studied as monolayers and multilayers.[82] The deposition of this polymer is similar to that of 10PPB2-CO in the general macroscopic morphological differences observed in x-type and y-type multilayer film deposition. However, the y-type transfer shows more consistent upstroke transfer ratios of 0.8 to 0.9, however, still less than the corresponding downstroke ratios. The x-type 6PPB2-CO deposition is analogous to 10PPB2-CO in that it is very consistent and produces visibly more homogenous films than conventional y-type of 6PPB2-CO.

The copolymer 6PPB2-CO was used with 10PPB2-CO to form alternating layers of each compound in two different buildup paths. The 10PPB2-CO monolayers were transferred always on the downstroke in both multilayer architectures, with the 6PPB2-CO monolayers transferred on the upstroke in one multilayer structure to form an asymmetric "y-type" buildup (barring rearrangement) as shown in Figure 3-6(a); and in the other architecture, the 6PPB2-CO monolayer was transferred on the downstroke to produce alternating "x-type" multilayers as depicted in Figure 3-6(b).

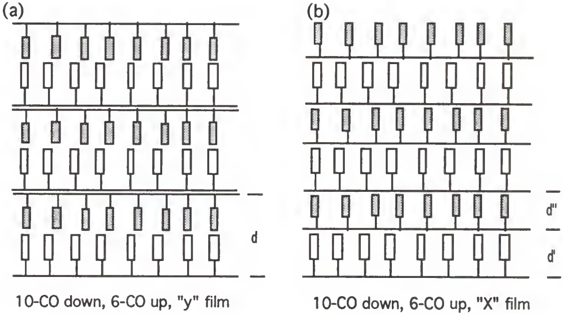

Figure 3-6. Schematical representation of a 10PPB2-CO and 6PPB2-CO alternating films. Shaded rectangles represent the 6PPB2-CO side chain mesogens, unshaded rectangles represent 10PPB2-CO mesogens. Film (a) represents an asymmetric "y-type" deposition. Film (b) represents an alternating "x-type" transfer.

## Small Angle X-ray Analysis.

Small angle X-ray diffraction was used to probe the structure of the multilayer films described above and to investigate the differences, if any, between different types of film transfer. Data was collected using the diffractometer described in the experimental section.

Shown in Figure 3-7 is diffraction data from a 30-layer film in which the transfer was x-type (down through the film). The peak in the scan at $(2\theta) = 1.90°$ corresponds to the layer spacing (46.5Å). The presence of the three higher harmonics indicates a well defined layer order; much more so than would be observed in bulk samples of the monomer which displays at most two orders of diffraction from smectic layering. The inset is from

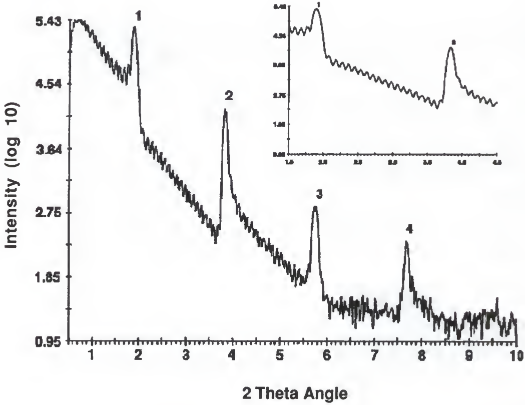

Figure 3-7. X-ray diffraction pattern for 30 layers 10PPB2-CO, x-type film, showing the high degree of organization within the layers. The numbered maxima correspond to d-spacings in Å as follows: 1 - 46.49, 2 - 23.00, 3 - 15.38, and 4 - 11.50. Inset shows subsidiary maxima occuring between the first and second Bragg peak.

the same film, showing greater detail of the structure present between the first and second harmonics. The presence of such interference maxima in the diffraction data unambiguously confirms a very uniform multilayer film, while the several orders of Bragg peaks indicate a well defined layer structure present within these films.[136] Similar data were obtained from a 30-layer film produced using y-type deposition. However, when the x-type and y-type layers were compared, it was discovered that the Bragg peaks corresponding to the interlayer spacings were identical within error. A diffraction pattern for an x-type and a y-type mulitlayer both of approximately 30 layers, are overlaid with Bragg peaks labeled is shown in Figure 3-8.

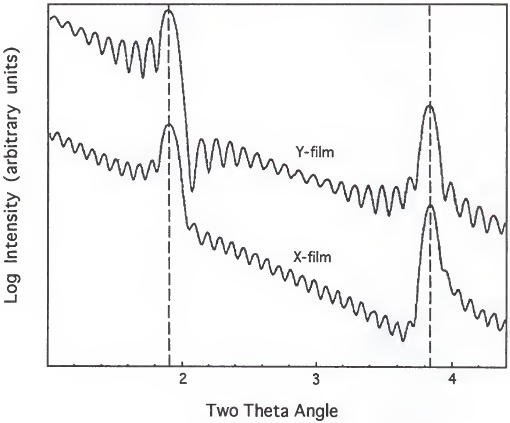

Figure 3-8. Overlay of X-ray diffraction patterns from a 30 layer multilayer x-type film and y-type deposited film. Dotted lines indicate the Bragg peak positions.

This data proved perplexing considering the dramatic difference in the 10PPB2-CO deposition behavior depending on which of the two methods was used. The monolayer is thought to be asymmetrical and oriented with respect to the water surface and differing downstroke versus upstroke transfer data substantiates this premise. However, it is known that multilayers may arrange after deposition,[45] especially if the molecules are transferred in an orientation that is not preferred. Upon further consideration, the possibility of rearrangement seems almost inevitable, since the monolayers are deposited at low densities (or large mean molecular areas) relative to close packing areas in the bulk; and the liquid nature of the polymer at room temperature gives the side chain groups significant energy and mobility.

Additional X-ray data confirms the rearrangement of the 10PPB2-CO multilayers and as alternating films with 6PPB2-CO. A summary of the X-ray layer spacing data is contained in Table 3-1. Within error, all mixed deposition multilayers of 10PPB2-CO showed no difference in layer spacing. Also, in the alternating layers of 10PPB2-CO and 6PPB2-CO no difference in layer spacing dependent on the sequence of layer build up (i.e. "x-type" or "y-type" alternating layers) was observed. Both the alternating films contained only one set of Bragg peaks corresponding to a single layer repeat sequence of approximately 42.6 Å, which was intermediate between the d-spacing of the pure component films. Based on the combination of the X-ray data, rearrangement of the side chain groups in the 10PPB2-CO and in the 6PPB2-CO multilayer films is evident.

The implication of this data is that the overall multilayer structure is not as would be theoretically expected with the transfer of isolated and immobile monolayers. There are two

Table 3-1. Summary of X-Ray layer spacing of various multilayers of 10PPB2-CO and alternate layers with 6PPB2-CO.

| Polymers | Film Type | d-spacing (Å) |
|---|---|---|
| 10PPB2-CO | Y | 47.2 |
| 10PPB2-CO | X | 46.9 ± 0.8 |
| 10PPB2-CO | mixed-2 down, 1up | 47.1 |
| 10PPB2-CO | mixed-3 down, 1 up | 46.6 |
| 10PPB2-CO/6PPB2-CO | "Y", 10-CO down, 6-CO up | 42.6 ± .2 |
| 10PPB2-CO/6PPB2-CO | "X", 10-CO down, 6-CO down | 42.5 |
| 6PPB2-CO | X | 35.6 |

general possibilities for rearrangement that would maintain the highly ordered layer structure seen in the X-ray diffraction patterns and account for the trend in layer spacings. The first possibile arrangement is that in the x-type deposition, every other monolayer flips completely over and forms a bilayer. This might be feasible since the calculated extended length of the side chain and backbone are only 42Å, while the observed layer spacing is approximately 47Å. However, this procedure seems unreasonable energetically and entropically. An alternative rearrangement is that of an interdigitated layer organization as shown schematically in Figure 3-9. This would involve some of the mesogens flipping over and interdigitation between the layers in both types of deposition. This is the most reasonable rearrangement scheme, since this is the most favored side chain ordering, as seen in the bulk copolymer. Other multilayer films of side chain polymers, such as PODMA, have also been shown to interdigitate after deposition; demonstrating a similar drive towards this rearrangement organization.

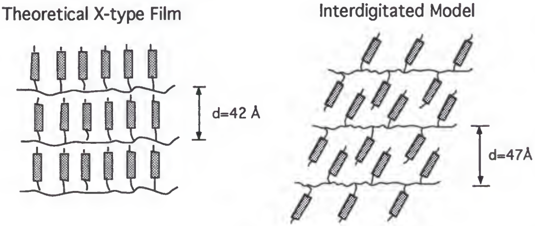

Figure 3-9. Schematic representation of an x-type film (left) of a side chain polymer with side chains extended and no tilt of the mesogens. The proposed interdigitated model (right) is also shown with the side chains tilted as they are in the bulk smectic layers of 10PPB2-CO.

## Monolayers and Multilayers of Copolymer/Mesogen Blends

The monolayer and multilayer behavior of the side-chain FE LC copolymer, denoted as 10PPB2-CO, has been previously investigated,[80] and is described in the previous sections of this chapter. In harnessing the ferroelectric LC properties of these materials, it is important to have films that are both thermally stable and ordered with respect to mesogen orientation. The goal of previous section was to produce such organized films of 10PPB2-CO by the Langmuir-Blodgett deposition technique since this copolymer forms stable monolayers on a water surface.[80] However, the transferred films were found to rearrange independent of deposition method or sequence. This rearrangement upon multilayer formation, thus limits control over the packing density and stacking sequences attainable in these films. Therefore, mixtures with side chain mesogenic group (Figure 3-10) were made in an attempt to reduce the rearrangement in the transferred films, and to increase the lateral density both in the monolayer and multilayers.

**10PPB2-CO**

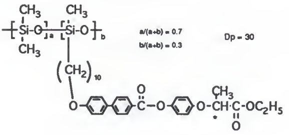

**10PPB2**

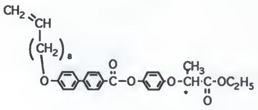

Figure 3-10. Structures of 10PPB2-CO and 10PPB2 (monomer).

### Bulk Properties of the Pure Components.

The copolymer and monomer studied in this work have been previously studied in the bulk state and at the air-water interface.[80,117,81,109,108] The thermotropic polymorphism for the bulk monomer and copolymer is shown in Figure 3-11. The 10PPB2-CO copolymer is in a liquid crystalline state at room temperature, unlike the monomer whose Sc* phase is at elevated temperatures. Both the copolymer and monomer contain a chiral center in the mesogenic group, show a chiral smectic C mesophase (Sc*) and exhibit ferroelectric liquid crystalline properties.[117]

10PPB2-CO:

$$\text{Crystal} \xrightarrow{15^{\circ}\text{C}} S_C^{*} \xrightarrow{136^{\circ}\text{C}} S_A \xrightarrow{150\text{-}162^{\circ}\text{C}} \text{Isotropic}$$

10PPB2:

$$\text{Crystal} \xrightarrow{67^{\circ}\text{C}} S_C^{*} \xrightarrow{95.4^{\circ}\text{C}} S_A \xrightarrow{125^{\circ}\text{C}} \text{Isotropic}$$

Figure 3-11. Thermal behavior of the copolymer and monomer.

## Monolayer Film Behavior of the Pure Components

Monolayer film behavior of the monomer, 10PPB2, has been documented in detail elsewhere.[109] Thermal dependence of the monomer is shown in Figure 3-12(a) and agrees with previous findings of Rettig and coworkers.[109] Based on Brewster angle microscopy and hysteresis experiments it was determined that the monomer exists as an ordered fluid phase below the transition region and exhibits birefringent behavior consistent with long-range orientational correlations between mesogens. Above the transition pressure, the monomer film is a highly incompressible solid film, and has a surface area consistent with close-packing of the mesogen.[137] It is apparent from the isotherms that small changes in temperature over the range of 20 - 30°C drastically affect the monolayer behavior in the transition region. However, the compressibility and surface area of the less condensed phase (before

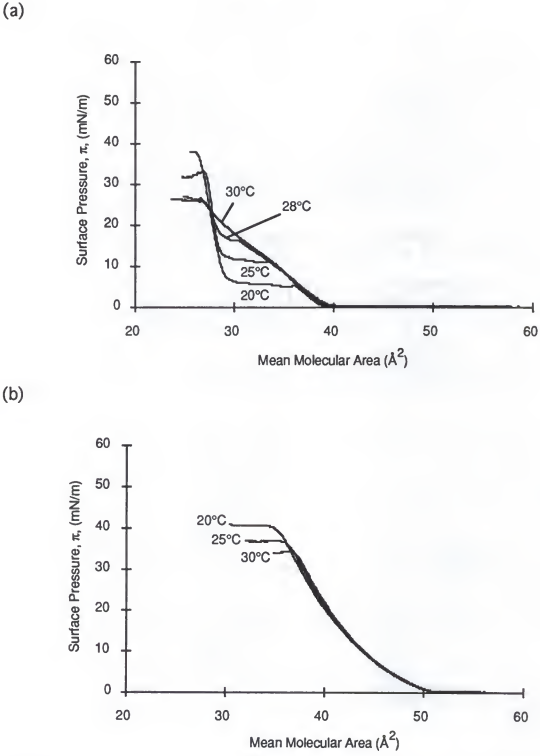

Figure 3-12. Isotherms of 10PPB2 (monomer) (a) and 10PPB2-CO (b) at various temperatures.

the transition plateau region) at a given pressure are not highly temperature dependent.

For comparison, the thermal dependence of the copolymer over the same temperature range is shown in Figure 3-12(b). Comparing the copolymer and monomer isotherms, the copolymer is in a significantly more expanded state. Since the copolymer collapse point is only slightly smaller than the monomer onset point, it can be asserted that the copolymer side chain groups are not close packed at collapse. Relative to the monomer, the copolymer is more stable over all pressures below collapse as shown in the plot of change in surface area versus time at constant pressure in Figure 3-13. It is also resistant to change with temperature over the range

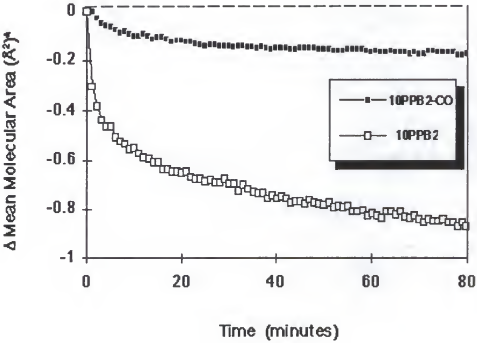

Figure 3-13. Isobaric creep of 10PPB2-CO and 10PPB2 monolayers at 10 mN/m.

shown (Figure 3-12(b)). Hysteresis curves, generated by compressing over collapse pressure with subsequent reexpansion and recompression, show reversible collapse[30] and fluid film behavior.[80,137] Previous work by Adams et al. demonstrated that the equilibrium "collapse" pressure, corresponding to the inflection point of the curve at high pressure, was a transition of liquid crystalline monolayer to bulk liquid crystalline material in equilibrium with the monolayer.[137]

## Monolayer Film Behavior of the Blends

Isotherms of 10PPB2/10PPB2-CO blends with monomer concentrations of 20, 30, 50 and 70 % (mol%) at different temperatures are shown in Figures 3-14(a-d). The influence of the monomer content in the form of a phase transition is more evident in the blends at lower temperatures and at a higher monomer concentration. There is no apparent transition region throughout the temperature range for the 20% concentration (mol %) 10PPB2 (Figure 3-14(a)). This may indicate that at these concentrations the polymer content is still effective in disrupting lateral ordering or crystallization of the monomer and copolymer side groups. At 30% 10PPB2 composition the isotherms look similar to those of the copolymer and 20% mixture; however, a shoulder appears in the 30% curve at 20°C. Under these conditions, the film could be compressed to pressures significantly above the calculated collapse point. Although the 50% and 70% monomer blends resemble the general shape of the monomer isotherm curves - they show an

(a)

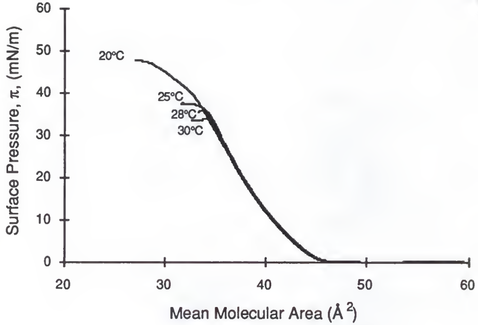

(b)

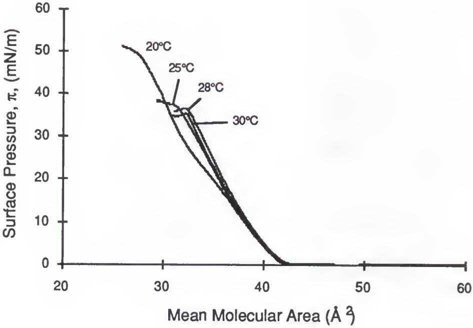

Figure 3-14. Isotherms of blend concentrations (a) 20% and (b) 30%10PPB2 at various temperatures.

(c)

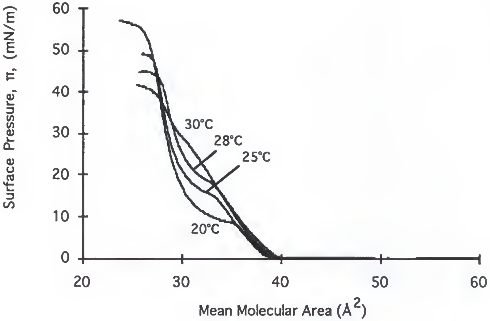

(d)

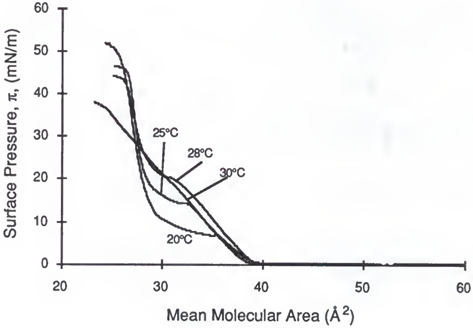

Figure 3-14 (continued). Isotherms of blend concentrations (c) 50% and (d) 70% 10PPB2 at various temperatures.

increase in pressure and decrease in transition region width with decreasing monomer content. In other words, the added copolymer causes the liquid analogous phase to persist at higher surface pressures much like increasing the temperature in the case of the pure monomer. The 50% and 70% compositions can also be overcompressed to pressures well above the collapse point, as was seen in the 30% film at 20°C. This phenomenon may be caused by the polymer side chain groups co-crystallizing with monomer under these conditions, and the underlying polymer backbone "rigidifying" the monolayer, thus inhibiting the collapse process.

Compressibility and collapse of the blend monolayers. The above observations indicate that the pure components may be miscible because the isotherm features are not additive of the pure component isotherms and vary continuously with composition. However, they are not necessarily conclusive and a more detailed analysis is necessary. According to Crisp[26] and Gaines,[138] a composition dependent decrease in compressibility from additive values is an indication of miscibility. The compressibility of a monolayer film, $C_s$, may be described as follows,

$$C_s = -1 / A \, (dA/d\Pi) \qquad (3.1)$$

where $dA/d\Pi$ is the inverse slope of the isotherm at surface area, A. Compressibility data were analyzed versus blend composition and some examples are shown in Figures 3-15(a)-(d). The results for pressures higher than 10 mN/m are not included due to anomolously high compressibilities obtained in the transition regions of the isotherms. The 10PPB2-CO/10PPB2 blend films show a decreased compressibility from additivity of the pure films at all temperatures shown in Figure 3-15. In the case of complete phase separation, monolayer compressibility should be additive of the compressibilities of the pure component domains. For truly miscible films, strong interactions between components should produce a more coherent film which would show lower compressibility than an

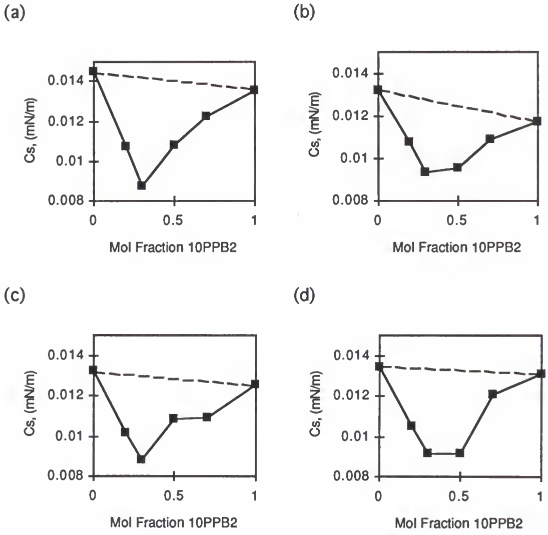

Figure 3-15. Compressibility, Cs, versus blend composition at 5 mN/m and a. 20°C, b. 25°C, c. 28°C, and d. 30°C.

ideal mixing value. The negative deviation of the 10PPB2-CO/10PPB2 compressibilities from an ideal mixing relation (shown as the dotted lines in Figure 3-15) indicates miscibility as well as attractive interactions between components.

According to Gaines,[138] in the case of total immiscibility, a mixed film will collapse at the pressure of the less stable component; while the collapse pressures ($\Pi c$) of miscible mixtures vary continuously with composition (often showing a positive or negative deviation from linearity). This is explained by application of the Phase Rule as put forth by Crisp.[26] In the case of an immiscible monolayer film with two coexisting phases at collapse, the degrees of freedom are reduced to zero, resulting in the invariance of collapse pressure with composition. If the system is miscible, i.e. one monolayer phase at collapse, the degree of freedom is one, and there will be a continuous variation of collapse pressure with concentration of one blend compound.

Although the collapse pressure is often equated with equilibrium spreading pressure (ESP), the processes are very different. Collapse may be dependent upon kinetic factors such as concentration and compression speed while equilibrium spreading pressure is independent of both. While an ESP has not been observed for either pure component, equilibrium values for the have been approached by reducing barrier speed and concentration until no further change in the isotherm is detected. However, monolayer overcompression (beyond ESP) is almost certain. The copolymer, on the other hand, shows a collapse very close to the theoretical ESP, but represents a transition from liquid crystalline monolayer to a bulk liquid crystalline phase.[137] Because of this behavior, reproducibility of monomer and blend isotherms, and the care in which collapse was determined, the data analysis is believed valid, though only qualitative interpretations can be drawn.

The actual collapse pressures of the monolayers are not necessarily evident from the isotherm curves. However, an accepted

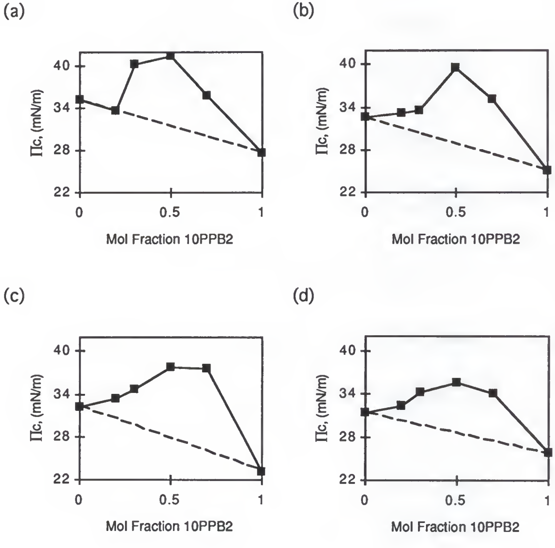

Figure 3-16. Collapse pressure, $\Pi_c$, versus blend composition at 20°C (a), 25°C (b), 28°C (c), and 30°C (d).

collapse point is taken as the minimum value of the isotherm derivative (d∏/dA) curve.[138] This method was employed to determine collapse pressures of all blend monolayers presented in Figure 3-16. In these plots of ∏c versus monomer concentration, ∏c varies continuously with blend composition, indicating a completely miscible system. However, the 20% concentration at 20°C appears to lie on the ideal mixing line while in all other instances there is a positive deviation from additivity. This would infer that this mixture at 20°C behaves as an ideal solution but still is a miscible blend composition. It also appears that the film collapse with 20% added monomer added is dominated by the packing and collapse of the polysiloxane backbone, due to the large area occupied by the copolymer monomer unit (approx. 40 $Å^2$) and the small interaction between mesogenic units under these conditions.

## Thermodynamics of mixing in the monolayer blends.

The qualitative analysis of the isotherm behavior presented above is a useful indication of miscibility but cannot describe the types of interactions, extent of interaction, or whether partial demixing occurs. Thermodynamic analysis of the isothermal data is often used[86-88,132,135] to evaluate quantitatively the ease of mixing or interactions between the components. When considering the thermodynamic behavior of monolayers, ∏-A isotherms may be viewed as the two-dimensional analog of a Pressure-Volume isotherm curve for a three-dimensional system. The obvious difference is that since a pressure is applied mechanically during compression, the experimental conditions are often not at equilibrium. However, at low compression rates, isotherms can be used to evaluate the extent of interaction and miscibility of the monolayer blend components. The compression rates in the isotherms shown was 2 $Å^2$/molecule(or repeat unit)*min and was found to be well below compression rates where speed dependence of the isotherms is observed.

The most commonly used method for miscibility determination is the analysis of isobaric surface area versus blend composition. An alternative area representation is that of excess surface area versus concentration of one blend component. The excess area values represent the difference in blend component packing efficiency over the additive mixing values. The excess area, $\Delta A_{xs}$ is given as follows,

$$\Delta A_{xs} = A - ( c_1A_1 + c_2A_2 ) \quad (3.2)$$

where, A is the blend surface area at a given surface pressure, $c_1$ and $c_2$ are the mol fractions of components 1 and 2, and $A_1$ and $A_2$ are the surface areas of components 1 and 2, respectively. It becomes clear that $\Delta A_{xs}$ is the difference in area of a particular blend composition as compared with the calculated ideal mixing area (contained in the terms within the parentheses). Plots of $\Delta A_{xs}$ for the 10PPB2-CO/10PPB2 blends at various temperatures are shown in Figure 3-17. When determining miscibility of a blend, a linear relationship at or around zero almost always indicates phase separation with large domain size. For a miscible system, negative excess area values are expected, while positive values are usually a clear sign of phase separation. Since a negative deviation is evident in all curves shown, intimate mixing is inferred.[2,29,133]

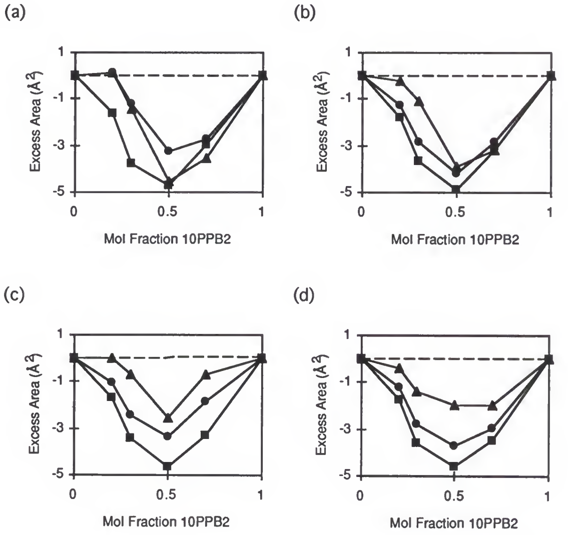

Figure 3-17. $\Delta A_{xs}$ versus blend concentration of 10PPB2 at a. 20°C, b. 25°C, c. 28°C, and d. 30°C. Surface pressures are 5 mN/m (■), 10mN/m (●), and 20 mN/m (▲).

To describe the extent of interaction between the blend materials, it is useful to look at the excess $\Delta G$ of mixing.[133,134] For a two-component blend system, this is described according to the Goodrich method[139] as applied by Bacon and Barnes[133] as follows,

$$\Delta G_{mix}^{xs,\pi} = {}_{0}\int^{\pi} (A - c_1A_1 - c_2A_2)\ d\pi \qquad (3.3)$$

The value in the parentheses is $\Delta A_{xs}$. $\Delta G_{mix}^{xs}$ for an ideal system is equal to zero where there is no interaction between the individual components. In the case of any miscibility of the system $\Delta G_{mix}^{xs}$ will have a negative value.

To calculate $\Delta G_{mix}^{xs}$ by the integration method of Goodrich, the path of the isotherm is assumed to be reversible. For the monomer and blend monolayers which show a transition region, isotherm reversibility was experimentally confirmed below the transition pressure. Therefore, $\Delta G_{mix}^{xs}$ data will be presented for pressures below the transition, which vary according to the composition and temperature being discussed. In the case of isotherms at 30°C, all compositions are in a fluid phase throughout the shown pressures.

In Figure 3-18, $\Delta G_{mix}^{xs}$ values vs. composition are plotted for several temperatures. While in the excess area plots from Figure 3-17 pressures up to 20 mN/m are shown, pressures for the $\Delta G_{mix}^{xs}$ values are limited to those below the transition region for all compositions under these conditions for the reasons state above. All values presented show a small but significant negative deviation from zero, and their magnitudes are similar with data reported on other miscible monolayer blend systems in the literature.[133]

A notable feature of the $\Delta A_{xs}$ values versus the corresponding $\Delta G_{mix}^{xs}$ is that the minimum of the curves is shifted right in the

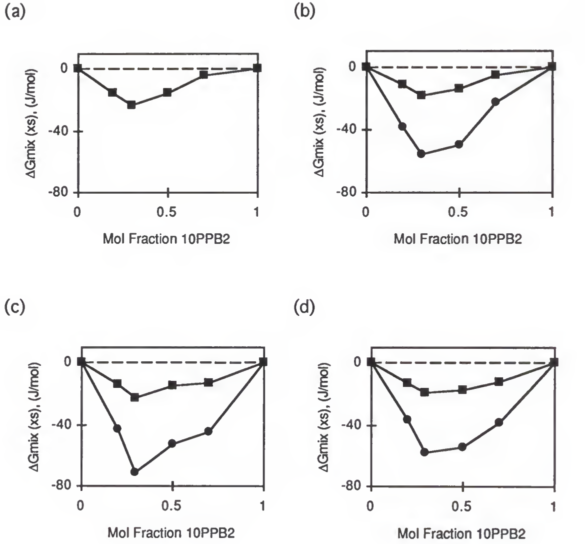

Figure 3-18. $\Delta G_{mix}{}^{xs}$ versus blend concentration of 10PPB2 at a. 20°C, b. 25°C, c. 28°C, and d. 30°C. Surface pressures are 5 mN/m (■) and 10mN/m (●).

$\Delta A_{xs}$ plots. Most of the $\Delta G_{mix}{}^{xs}$ curves appear to have minima somewhere close to 40% while the $\Delta A_{xs}$ plots are either centered at 50% or skewed to higher concentrations. This may be explained by the difference in origin of these values. The $\Delta A_{xs}$ data is taken at a given point on the isotherm curve and is a path independent value. It represents the final efficiency in packing of the two components at a given pressure. However, $\Delta G_{mix}$ values are integrated as the area under the isotherm and are highly dependent on the shape of the isothermal curve. These values represent the spontaneity or "ease" of mixing up to a given pressure value. The $\Delta G_{mix}{}^{xs}$ minima shifted left of the corresponding $\Delta A_{xs}$ values implies that although maximum mesogen group packing efficiency of packing the mesogenic groups occurs at approximately 50% 10PPB2, the mixing achieved with least effort (more spontaneous) is at slightly lower concentrations. It is clear from this analysis that blending the monomer and copolymer is an effective manner of increasing the surface mass density of mesogenic side chain groups (approximately 12% at 25°C and 5 mN/m) in the monolayers relative to the pure copolymer films. As alluded to in the introduction, this may provide a rational means of stabilizing the built up layer structure in monolayers transferred to solid substrates, and increase the LC interactions of the mesogens required for application in FELC fast switching devices.

It is also relevant to note here the similarity of the $\Delta A_{xs}$ curves for the two-dimensional monolayers of the blends with the thermodynamic phase boundaries obtained for bulk mixtures of the same components. It has been found[90] that the phase diagram of 10PPB2 and 10PPB2-CO has a pronounced minimum of the Smectic A-Smectic C* phase boundary, the location of the minimum occurring at about 50%. It is interesting that the minima of the $\Delta A_{xs}$ versus mole fraction for the blend monolayers also occur at the same concentration. These results indicate that the thermodynamics of the copolymer and monomer mixtures in their bulk and monolayer states may be similar.

Alternative analysis of thermodynamic data. It has been proposed in a previously published work[137] that the actual limiting copolymer packing area is more accurately represented by calculation of the repeat unit as per siloxane unit rather than per mesogenic unit as in the above mentioned data. This is explained by the premise that the siloxane backbone is at the water surface and determines isothermal behavior of the film. The rationalization was based on the observation that the copolymer isotherm shared more similarities with that of a pure poly(dimethylsiloxane) (PDMS) monolayer than with the monomer film. Based on the recalculated blend isotherms as compared to initial isotherm values, the true representation of the side chain copolymer backbone may be somewhere in between the original assumption of the backbone and comonomer units behaving as "spacers" between the mesogens; and an extended chain configuration of the siloxane backbone.

Recalculated $\Delta A_{xs}$ versus blend composition are shown in Figure 3-19(a). The negative deviation from linearity is still seen but the minimum is shifted to much smaller 10PPB2 concentrations and its magnitude is smaller. This new representation gives information on the excess area per siloxane unit rather than per mesogen, and indicates the largest allowable additional packing of monomer along the backbone is approximately 30%. Assuming there is no difference in attached or added mesogenic groups, this infers a maximum total substitution allowable along the backbone of roughly 60%.

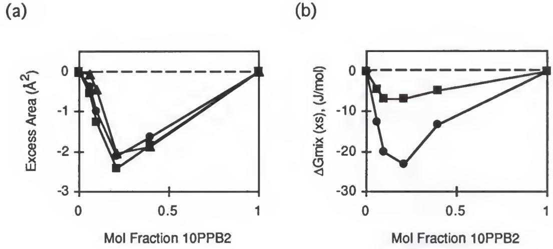

Figure 3-19. Recalculated plots of $\Delta A_{xs}$ (a) and $\Delta G_{mix}{}^{xs}$ (b) versus blend composition at 25°C. New calculated areas and free energies of mixing are based on a limiting repeat unit of a siloxane group for the 10PPB2-CO copolymer. Surface pressures are 5 mN/m (■), 10mN/m (●), and 20 mN/m (▲).

Recalculated $\Delta G_{mix}{}^{xs}$ versus blend composition at 25°C is shown in Figure 3-19(b). The shift and decrease in magnitude of the minimum is similar to that in the recalculated $\Delta A_{xs}$ plot described above. The minimum occurs at approximately 20% added monomer concentration and corresponds to the greatest ease of substitution along the backbone occurring at 50% total (attached and added) substitution of mesogen per backbone group.

Brewster Angle Microscopy (BAM).

Although the above methods provide an overall insight into degree of interactions and areas occupied by the molecules within the monolayer, they cannot relate any morphological features of the films, such as aggregation, crystallization, or local orientational order of the mesogenic groups due to their liquid crystalline nature. To visualize these features of the pure components as well as blend monolayer films, Brewster angle microscopy was employed to investigate film morphology at the air-water interface. For the BAM photos shown in Figure 3-20, an analyzer was placed in front of the CCD camera and set to 90° (analogous to cross polarizers in an optical microscope) so that the intensity changes reflect the extent of orientational order in the monolayer.

The photos of pure 10PPB2-CO are not shown because morphological features were unresolvable in the reflected image at this pressure. A uniform dark image, as was seen in 10PPB2-CO at low pressures, suggests the lack of birefringence and single phase behavior in the monolayers. As this film is compressed to much higher pressures, a faint granular texture appears which is similar to that seen in the BAM photos of 20% and 30% blends. These granular domains grow brighter as the film is compressed towards a second pressure increase (around 12 Å$^2$). A more extensive study of the collapse behavior of this and similar copolymers is published by Adams et al.,[137] and indicates a change in the tilt orientational order and concurrent build up of smectic layers occurs upon collapse. It is this build up of additional and more condensed layers that accounts for the sharp increase in brightness of this region.

In Figure 3-20, BAM photos of several blend concentrations (20-100 mol% 10PPB2) at 10 mN/m are shown. At this pressure and temperature the blends and pure components are in a similar fluid phase (or below any phase transition). The photos in Figures 3-20(a-e) show the progression of morphological features with increasing

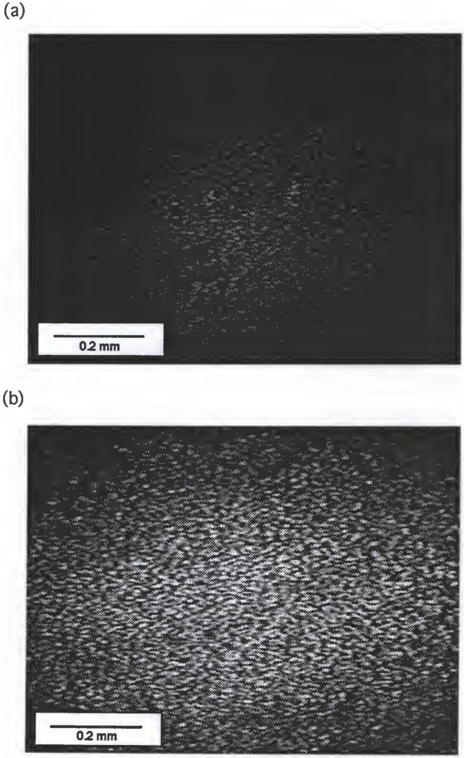

Figure 3-20. Brewster angle micrographs taken at 10mN/m and 25°C of 10PPB2/10PPB2-CO blend concentrations a) 20% and b) 30%.

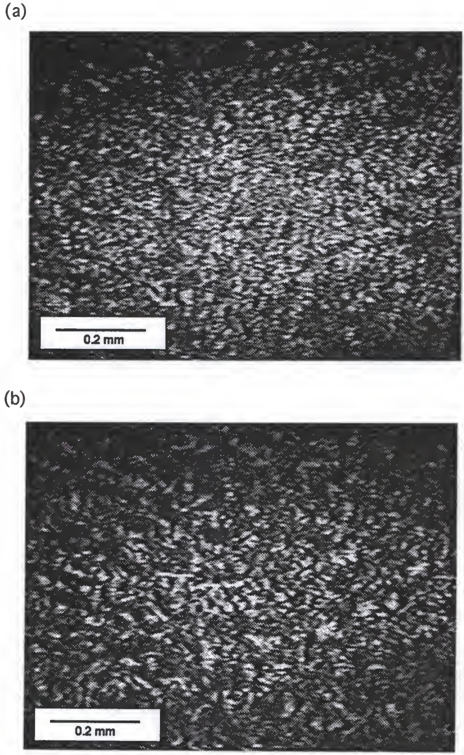

Figure 3-20 (continued). Brewster angle micrographs taken at 10mN/m and 25°C of 10PPB2/10PPB2-CO blend concentrations c) 40% and d) 50%.

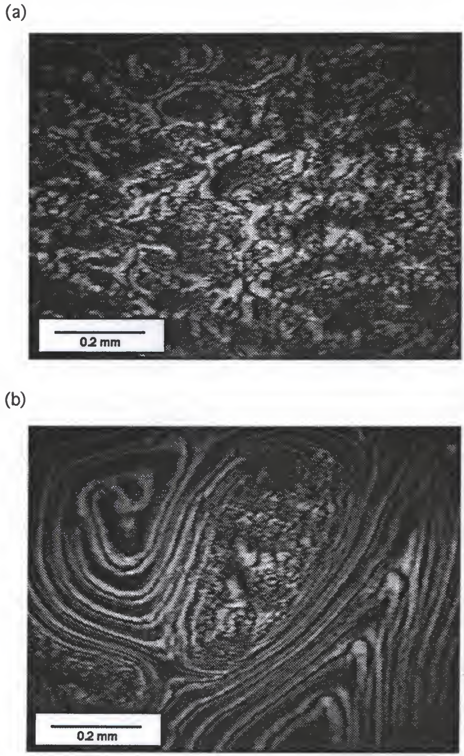

Figure 3-20 (continued). Brewster angle micrographs taken at 10mN/m and 25°C of 10PPB2/10PPB2-CO blend concentrations e) 70%, and f) 100%.

monomer concentration in the blend monolayers. Areas of similar brightness indicate areas with similar tilt orientational order. It has been proposed that the unusual striped textures of the monomer (Figure 3-20(f)) are due to defects caused by fluctuations of $\hat{n}$ , the projection of the mesogenic group tilt director on the layer plane,[82] as is seen in chiral smectic free standing films.[140] Smaller and less organized structures emerge in the 40% blend film photo. These textures are all in agreement with a single phase with variations in mesogen tilt degeneracy. Granular structures which constitute regions over which the tilt order is coupled, increase in size, and are evident in a type of a schlieren texture at 50% and 70%. Even at 70%, however, there are no large areas of the striped domains seen in the monomer.

The pure monomer monolayer film shows fluid birefringent domains separated by disordered or dark regions at high surface areas (observed up to 90 Å$^2$) which correspond to a liquid or liquid crystalline-gas coexistence region. The characteristic birefringent fluid striped texture as shown in Figure 3-20(f) appears from the surface pressure onset up to the liquid-condensed transition region. However, at room temperature the bulk monomer is crystalline. At the water surface, the hydration interaction and lowering of the water surface energy are thus sufficient to keep the monomer as an ordered liquid in the monolayer rather than a condensed crystalline phase seen in the bulk. This effect is sufficiently strong enough to disrupt the monomer-monomer cohesive forces to form the disordered isotropic phase seen in the copolymer as compared to the liquid crystalline bulk phase.

The above results show the polymer is homogeneously dispersed in the blends. More importantly, the results show the significant effect of the polymer disrupting long range tilt interactions in the monolayer. This is not surprising since the "meandering" path of the polymer backbone on the water surface would affect the local tilt directors of the side groups. As such, this may be an interesting example of a polymer used to plasticize a low molecular weight compound.

BAM annealing study. Since the size and shape of the striped texture seen in 10PPB2 is dependent upon compression speed (slower speeds yield smaller more extensive stripes), these features should require additional time to evolve in the presence of the disruptive force of the more viscous polymer. An annealing experiment was performed with the Brewster angle microscope on the 70% blend by compressing the film to 5 mN/m and holding the pressure constant. Micrographs at various times are shown in Figure 3-21. At time zero (Figure 3-21(a)), the disordered structure expected from Figure 3-20(e) is seen. However, after only 10 minutes (Figure 3-21(b)) a crude striped structure evolves. After 30 minutes (Figure 3-21(c)), large domains (on the order of 1-2 mm) of these textures are present. Three photos at 30 minutes are shown which were taken within approximately a 1-2 minute time frame. This was done to show the film fluidity at this pressure. This also confirms that the structures shown were not isolated or local phenomena.

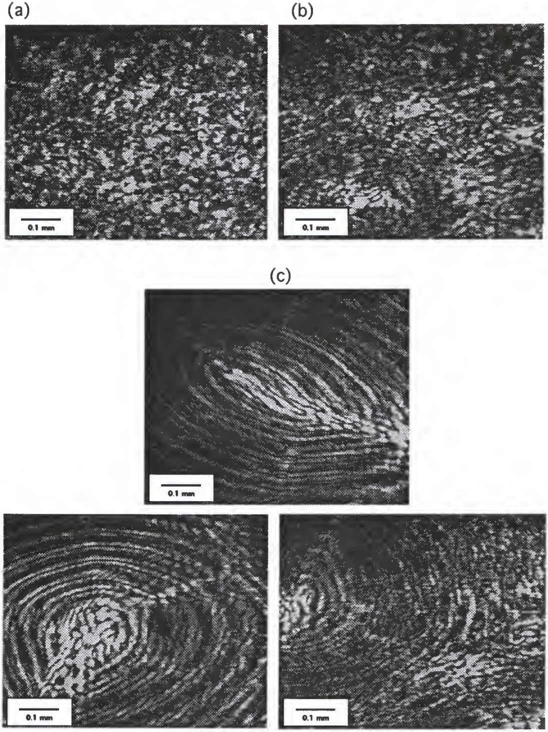

Figure 3-21. BAM annealing experiment of 70% 10PPB2 at 5 mN/m. Photos are shown at various times during the experiment with (a) at 0 minutes, (b) 10 minutes, and (c) 30 minutes. Time values are within 1 minute of the indicated value.

Although the emergence of monomer like structures indicate a similar order in the 70% blend film, it does not indicate phase separation. There is no domain formation evident in the pictures taken throughout monolayer compression, and overall reflected intensity from the monolayer is homogeneous. Remember also that the pure copolymer at this pressure would be evident as domains by dark patches, due to its lack of reflected intensity under these conditions. Additionally, the resulting structure in the 70% blend film, although similar to the monomer is more disordered and shows less contrast.

BAM intensity measurements. In the BAM experiments, the amount of light reflected while the analyzer is in place in front of the CCD camera is an indication of the orientational order or birefringence in the films. This is presented as the intensity ratio, the integrated intensity captured by the camera at a given pressure during monolayer compression (I) relative to that of a pure water surface (Io). Plots of the intensity ratio (I/Io) and surface pressure versus mean molecular area for various blend concentrations are shown in Figure 3-20. In the experiments, all settings including intensity gain were held identical, for the purpose of comparison.

Curve a shows the intensity plot for the pure copolymer. As was stated earlier the intensity does not significantly increase until elevated pressures, indicating a lack of long range orientational order until further smectic multilayer buildup. The combination of the lack of birefringent reflectance and the

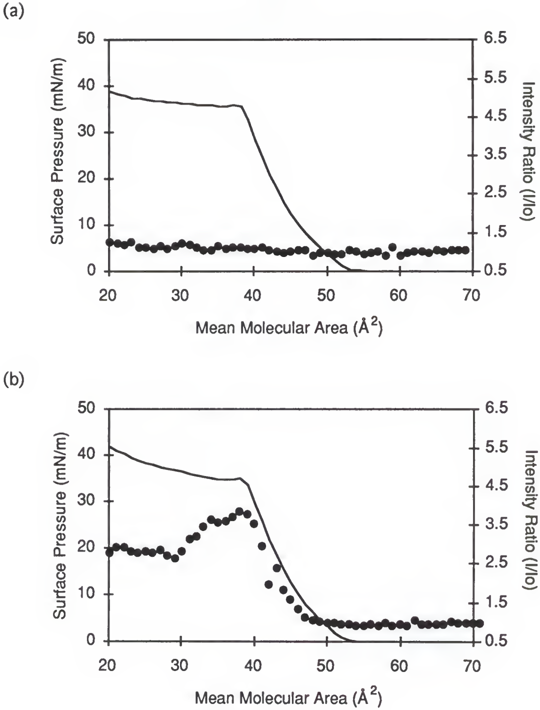

Figure 3-22. Intensity ratios (I/Io, where I=integrated intensity at a given area, and Io=integrated intensity of the clean water phase before spreading the film) and surface pressure versus mean molecular area for (a) 0% and (b) 10% 10PPB2.

(c)

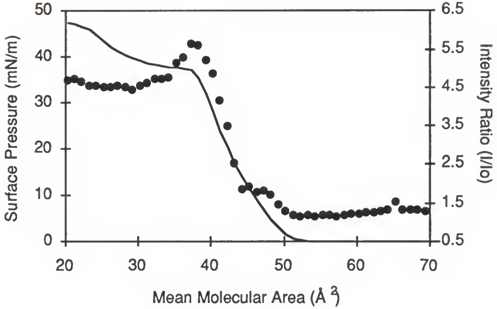

(d)

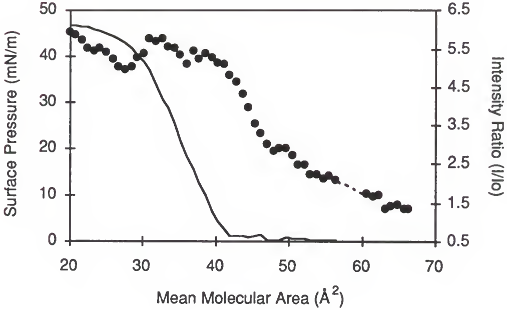

Figure 3-22 (continued). Intensity ratios (I/Io, where I=integrated intensity at a given area, and Io=integrated intensity of the clean water phase before spreading the film) and surface pressure versus mean molecular area for (c) 20% and (d) 30% 1OPPB2. Dotted line represents area where values are not shown due to dust which caused noise in the data.

significant pressure increase infers an isotropic liquid-like monolayer phase. As in the monomer film, this indicates that the monolayer film is one step further disordered than the corresponding bulk phase, which under these conditions for the copolymer is in a Smectic C* liquid crystalline phase. This is thought to be caused by the polysiloxane backbone interaction with the water surface resulting in two net effects. First, the hydration of the backbone in the water surface extends the chain and increases the distance between mesogenic groups sufficiently to prevent interaction. Secondly, the water surface acts as an external field, which coupled with the weak amphiphilic character of the copolymer causes all side groups to point away from the water surface. This tends to prevent the antiparallel mesogen packing necessary for the ordering observed in the bulk (See Figure 3-23). Compared to the monomer behavior both in the bulk and at the air-water interface, the addition of a polymer backbone acts to produce additional disorder among the liquid crystalline mesogens in the copolymer.

In Figure 3-22, curves b-d show intensity ratio plots for the blends The curves all show intensity increase at or before the onset of surface pressure increase. As shown in Figure 3-22(b), with only 10% addition of monomer, intensity increases in magnitude and onset mean molecular area. Although the shape of the 20% curve is similar to the 10%, the maximum intensity is greater - suggesting a greater concentration of molecules with the same orientational ordering. The onset area of the 20% curve is also shifted to somewhat higher values. A further intensity ratio increase is seen in the 30% concentration as well as an earlier onset surface area.

Plots of the 40% and higher concentrations were not shown due to a high noise level in the intensity ratio values due to aggregates floating in and out of the field of view at high mean molecular area.

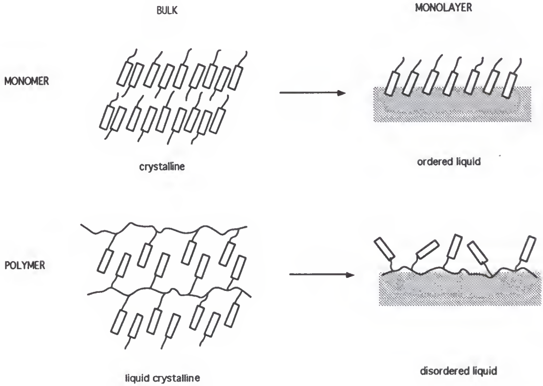

Figure 3-23. Differences in theoretical packing of mesogenic groups in the bulk and monolayer of 10PPB2 and 10PPB2-CO at room temperature.

The above results suggest that blending monomer with the copolymer has two effects. First, by adding monomer, a greater concentration of mesogenic units show long range orientational ordering. Second, by adding monomer, the onset of orientational ordering shifts to higher surface areas, surpassing the surface pressure onset point. This interpretation, in agreement with much of the previous data, indicates attractive interactions between monomer and copolymer mesogens, as well as more efficient packing of these side groups and mesogens.

### Deposition of Blend Monolayers of 10PPB2/10PPB2-CO

With blend miscibility established, transferring the blend monolayers to solid substrates was the next process to be investigated. Deposition of these ferroelectric liquid crystalline blends was of interest, in order to determine the feasibility of producing homogeneous and ordered thin films of discrete thickness as future SSFLC devices. The blend multilayers should have advantages over the pure copolymer films, in that additional monomer concentration would decrease ferroelectric switching times. The mixed LB films, if successfully deposited, would also have an advantage over the monomer, since no significant 10PPB2 deposition beyond one layer has been possible.

Blend monolayer deposition was facilitated under two conditions. At room temperature, on hydrophobic substrates, x-type film deposition was possible up to 20% 10PPB2. Transfer ratios under these conditions were constant, and similar to that of pure 10PPB2-CO. The resulting monolayers appeared homogeneous on a macroscopic scale. At elevated temperatures of 30-32°C, using hydrophobic Si wafers and conventional deposition, overall y-type transfer occurred in blend compositions up to 70% 10PPB2, but no transfer was possible in the pure 10PPB2 films. No x-type transfer was possible on blend concentrations greater than 20% monomer under reasonable conditions.

The purpose of blending 10PPB2 with the copolymer, 10PPB2-CO, was to increase the mesogen density in the layers relative to the pure copolymer at the water surface and in the transferred films; and, if possible, eliminate rearrangement of the layers after deposition. However, upon increasing the mesogen density, greater interactions between mesogens and a more viscous monolayer film results. This increased viscosity causes problems with deposition and transfer, as was seen in the 10PPB2 monolayer films. In fact, most often LB films must be deposited in a fluid phase in order for successful transfer to occur.[2,45,52] Such viscosity effects are seen in the deposition behavior with blend composition of the 10PPB2/10PPB2-CO monolayer films. At room temperature, only films up to 20% monomer mesogen can be transferred. In isotherms of the 20% blend, the monolayer appears to be similar to the copolymer and in a fluid phase at the transfer pressure of 25 mN/m. Films of concentration higher than 20% 10PPB2 are in a more condensed region of the isotherm under these conditions, and the monomer's film component influence is more visible. Under the second set of conditions, 30-32°C, all the blend monolayers are in a fluid phase, thus facilitating transfer. The transition to y-type deposition may be caused by the additional mesogenic group concentration, thus changing the surface energy of the monolayer. However, at elevated temperatures, the mesogens may have sufficient additional thermal energy to rearrange after transfer; while the films at or below 20% which do transfer at room temperature are most likely too fluid to prevent rearrangement. Thus, it appears that in the monolayers increased mesogen density required to eliminate rearrangement in transferred multilayer films, serves also to restrict the monolayer deposition due to the increased film viscosity.

## X-ray Diffraction of Blend Multilayers

In order to probe the resulting multilayer structure of those blend films that could be transferred to solid substrates, small angle X-ray diffraction was used. X-ray diffraction patterns of the 10PPB2/10PPB2-CO blend multilayers transferred at room temperature and using x-type transfer are shown in Figures 3-24 and 3-26. In Figure 3-24 results from 10 layers of blends ranging

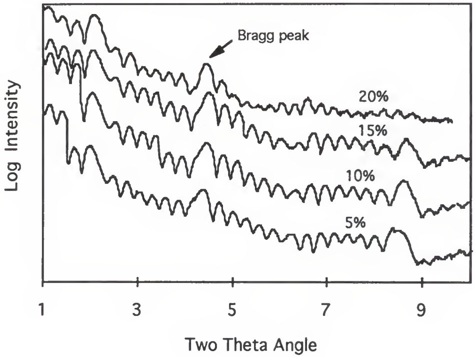

Figure 3-24. Small angle X-ray diffraction patterns from 10 layer films of 10PPB2/10PPB2-CO blend monolayers. Percent notations represent concentration 10PPB2 in multilayer film.

from 5-20% 10PPB2 are overlaid, and the second order Bragg peak position indicated. Even at such low layer numbers, Bragg peaks are evident indicating a highly ordered layer structure is present. Also, the subsidiary maxima between peaks is well defined, (although this decreases with additional monomer concentration) which indicates a well defined substrate surface and outer multilayer surface.

While a fourth order peak is evident at around 8.6°, the third order peak is missing or significantly reduced in all the curves. The 10PPB2-CO multilayer X-ray pattern shown previously in Figure 3-7 (as well as all other 10PPB2-CO films used in the initial studies), did have a significant third order Bragg peak corresponding to the layer spacing. However, the synthetic batch of copolymer used in the initial studies was slightly different from the copolymer used in the blend isotherm and multilayer experiments. Multilayer X-ray patterns of the 10PPB2-CO used in the blend studies resembled more closely the behavior of the bulk copolymer shown in Figure 3-25. The differences in the two batches of polymer are slight overall, but are believed to be due to a small difference in backbone substitution of the side chain mesogen. A greater percent substitution most likely occurs in the copolymer sample used in the blend studies. The third order harmonic peak seen in the first copolymer multilayer samples is believed, based on modeling studies,[141] to be due to a slightly less interdigitated layer structure. This theory additionally accounts for the increased layer spacing of films from this particular 10PPB2-CO sample.

The differences in the two 10PPB2-CO samples were undetectable with respect to bulk thermal properties, ferroelectric response (switching times), and only a minor change in monolayer isotherm was noticeable. The 10PPB2-CO monolayer film behavior for both copolymer samples was identical in the reversibility of collapse, fluidity, stability, and deposition behavior. Since the analogous experiments were performed from the same polymer batches, it is believed that the relative observations put forth are valid.

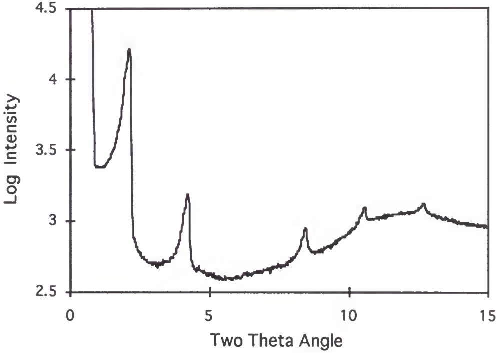

Figure 3-25. Powder X-ray diffraction pattern from a bulk sample of 10PPB2-CO (from the batch used in the blend experiments).

Figure 3-26 shows scattering curves of 30 layer blend films from 0 to 20% monomer content, deposited at room temperature and 25 mN/m. The presence of a well ordered layer structure is demonstrated in all films by the three orders of Bragg peaks shown. The 10PPB2-CO (0%) multilayer pattern has in additional a 5th and 6th order harmonic at higher angles than shown in Figure 3-26. Layer order in the blend films appears to decrease with increasing 10PPB2 concentration and is most prominently indicated in the 20% pattern. In the area of the diffraction pattern right of the (0,0,3) peak position, a broad hump is

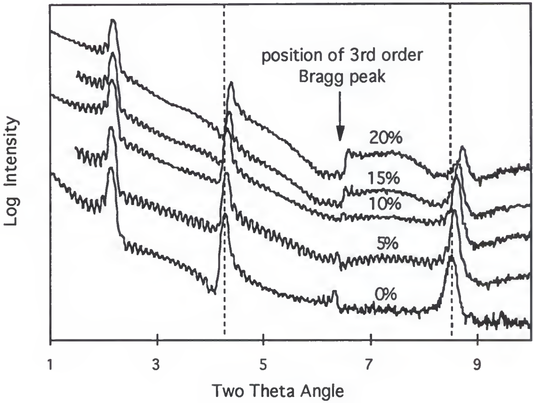

Figure 3-26. Small angle X-ray diffraction patterns of 30 layer 10PPB2/10PPB2-CO blend multilayers. Percentages indicate mol% 10PPB2 mesogens Arrow indicates the position where the 3rd order Bragg peak should occur. Dotted lines indicate the 2nd and 4th order Bragg peak positions of the pure 10PPB2-CO multilayer film. The lines are a visual aid to demonstrate the shift of the blend multilayer peaks.

present in the 20% 10PPB2 multilayer which indicates diffuse scattering and areas of disorder. There is also a detectable shift from right to left in the "dip" near the position of the third order Bragg peak of the blend multilayers. Based on modeling studies, this shift with increasing monomer content is believed to be caused by a decrease in the lateral polymer backbone confinement.

Table 3-2. Layer Spacing of 10PPB2/10PPB2-CO Blend Multilayers as Determined by Small Angle X-ray Scattering.

| Blend Composition (mol% 10PPB2) | Layer Spacing (Å)* | Standard Deviation ± (Å)** |
|---|---|---|
| 0 | 41.37 | 0.11 |
| 5 | 41.13 | 0.13 |
| 10 | 40.89 | 0.09 |
| 15 | 40.65 | 0.09 |
| 20 | 40.39 | 0.2 |

*taken as average of spacing from 1st, 2nd and 4th order peak position.
**standard deviation of 1st, 2nd and 4th order layer spacing values.

The dotted lines shown in the X-ray pattern of Figure 3-26 indicate the position of the pure copolymer layer spacing peaks, and demonstrate the Bragg peak shift with increasing 10PPB2 concentration. Layer spacings were determined by averaging the first, second, and fourth harmonic peaks, and are listed along with standard deviation values in Table 3-2. Although the change in layer spacing with concentration is small, the trend is consistent and linear as shown in the plot of d(Å) versus blend concentration in Figure 3-27.

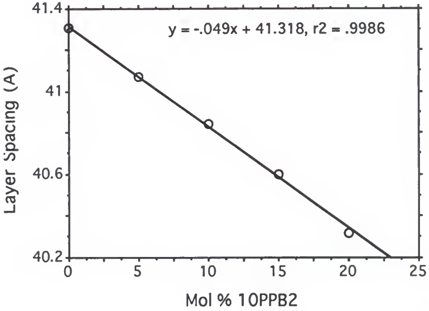

Figure 3-27. Plot of layer spacing as calculated from X-ray diffraction patterns, versus concentration (mol%) 10PPB2.

Based on the above observations and data, there is little change in the rearrangement process seen in the pure copolymer multilayer films, upon adding small amounts of mesogenic monomer. However, the detectable changes with concentration, indicate a stronger interaction of the LC mesogenic side groups. This enhanced mesogen attraction lowers the layer spacing slightly and pulls the polymer backbone from its confined layer area relative to the 10PPB2-CO films. The fluid nature of the blend films is apparently similar to the copolymer not only in the monolayer, but also upon transfer to a solid substrate. Despite rearrangement of the thin films, the increased mesogen interaction at lower blend concentrations may have a more pronounced effect on the ferroelectric response times and properties and will be investigated in future research.

Monolayer 10PPB2-CO/10PPB2 blends with concentrations greater than 20% 10PPB2 were successfully transferred to hydrophobic silicon wafers at 30-32°C, and by conventional y-type deposition. Ten and thirty layer samples were produced. In the latter, stripes in the dipping direction as noted with the y-type 10PPB2-CO films were evident. These macroscopic defects represent overall thickness inhomogeneity of the multilayer films.

A representative X-ray diffraction pattern from a thirty layer 50% 10PPB2 film is shown in Figure 3-28. This diffraction pattern is quite complicated, containing several peaks and bumps which are not easily identified as Bragg scattering, diffuse scattering, or some shorter range modulation in the film. The peaks identified as Bragg scattering from layer periodicity normal to the substrate surface are labeled in parentheses and correspond to a period length of 41.33 Å with three orders of diffraction shown. This is in the same spacing range as the other multilayer samples seen, but is much closer to the characteristic layer spacing seen in the bulk 10PPB2-CO samples. This layer structure is not as well defined as any other multilayers shown herein for two reasons: 1, the peak broadening especially in the second and third order harmonics, and 2, the presence of only three orders of diffraction. Additionally, the third order peak is not significantly dampened as in other samples, which may relate to less interdigitated side chains from this layer structure.

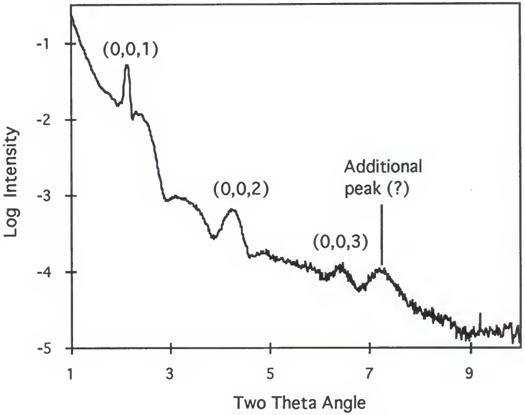

Figure 3-28. Small angle X-ray diffraction pattern for a 30 layer 50% 10PPB2 multilayer film transferred by y-type deposition and at a temperature of 30-32°C. Bragg scattering from a layer periodicity of 41.33Å are indicated by the corresponding indices. An additional scattering peak is labeled which corresponds to another periodic layer structure.

There are several other features of the pattern which are not as easily explained as the three Bragg peaks noted above, and most likely represent areas of the multilayer film containing more complicated layer architectures. The most easily identifiable additional peak is labeled in Figure 3-28; it falls to the right of the (0,0,3) Bragg peak and is located at 7.25 degrees, on a scale of $2\theta$.

No definite assignment can be made based on this diffraction pattern alone, but it can be concluded that the presence of this peak indicates an additional periodic structure within the layer film. Some possibilities exist for the source and assignment of this peak, assuming it is due to Bragg scattering. First, if it is due to a first order diffraction structure, the periodic length would be approximately 12.2Å. Although the possibility of this occurrence cannot be ruled out, it is unlikely that any periodic structure of this small length exists in the film. Second, the peak could correspond to a higher harmonic diffraction from a larger layer structure, namely, a bilayer as transferred in the y-type deposition used. For a bilayer structure, a layer d-spacing of 60 to 80 Å would be expected. By using this periodicity range, the two theta value of the peak, and by applying several n values in the relation in Equation (1.8) possible assignments are put forth. If the peak were to correspond to a (0,0,6) reflection the layer spacing would be approximately 73.1 Å. This would involve two layers of the side chain polymer/monomeric mesogen mixture with no interdigitation and a side chain tilt angle of 29 to 30 degrees from the layer normal. This is a reasonable structure for the side chains with respect to normal tilt angles. However, the presence of a sixth order reflection would infer an extensive and ordered bilayer structure which should additionally be evident with lower harmonic peaks of greater intensity. The calculated lower order peaks (in two theta degrees) corresponding to this model would be as follows: (1) 1.2, (2) 2.4, (3) 3.62, (4) 4.83, (5) 6.04. Excluding the first order peak (which theoretically should be strongest), most of the other peaks can be rationalized from the diffraction pattern in Figure 3-28. The second order peak of 2.4 degrees could be located in the hump to the right of the first Bragg peak of the 41.33 Å diffraction and the third order of 3.62 corresponding to the following bump. There appears to be an almost discernible peak around the area of the 4th harmonic of 4.83, but the 5th order occurs at a dip just before the (0,0,3) peak of the indexed layer spacing. The presence of two different coexisting periodicities in the film can cause complications of diffraction patterns in the form of extinction and modulation of various peaks. Although this could account for the missing or broadened peaks of the above scenario, no conclusive data or calculations are available to confirm it.

It can be concluded from the dipping and X-ray data that the higher concentration blends (greater than 20%) transferred in a y-type fashion are produce more disordered LB multilayer films relative to the pure 10PPB2-CO multilayers and lower concentration blend multilayers from 5-20% produced by x-type deposition. Although some rearrangement occurs, as evidenced by diffraction corresponding to the interdigitated layer periodicity seen in the previous multilayers, some alternate layer structure persists in the film which may correspond to bilayers "frozen" into the more viscous monolayer films.

## Summary

Conventional deposition methods are not the only way to produce monocomponent multilayer films. In fact, alternate deposition may be the best method for producing defect free films of materials whose deposition behavior tends towards x- or z-type films. Despite the rearrangement seen in the 10PPB2-CO multilayers, the alternate deposition of the monolayers produced more macroscopically homogeneous films. X-ray diffraction patterns of x- and y-type deposition methods showed no layer structural differences, but the variances in layer thickness visible in the films would have an effect on the film's FE response in a SSFLC device.

The rearrangement seen in the 10PPB2-CO copolymer multilayers is most likely due to the monolayer fluidity and low density as transferred, and results in the layer organization similar to the bulk copolymer. Although the alternate deposition method provides more homogeneous multilayers and the Langmuir-Blodgett method allows control over total film thickness, a greater deal of control over the multilayer organization is desired in these films.

In an effort to reduce the monolayer rearrangement in the multilayer films, mixtures of the copolymer with corresponding mesogenic monomer were studied at the air-water interface and as transferred to solid substrates. In order for the mixtures to be useful for the above purposes, the blend components must be miscible both at the air-water interface and in the multilayer films.

There are a number of methods to analyze miscibility in mixed monolayers at an air-water interface. Although most methods are not conclusive when viewed alone, several methods employed which yield similar results is very convincing. Additionally, the results from these analyses can give further information as to the type of interaction within the films and characteristics of the resulting blend films. The results for the 10PPB2-CO/10PPB2 blend monolayers may be summarized as follows:

i) Decreased blend film compressibility relative to the pure compounds indicated not only a miscible system but that there were attractive forces between two components to cause such a decrease.

ii) Increase in the collapse pressure indicates positive interaction between components creating a more coherent blend monolayer which is more resistant to collapse.

iii) Excess area values give maximum blend packing efficiency as 50% added monomer to copolymer mesogenic group, and in recalculated data 30% added monomer per siloxane unit in the copolymer.

iv) Excess free energy of mixing values show not only that the blends are miscible, but that the most spontaneous mixing occurs at approximately 40% added 10PPB2 to copolymer mesogen, and 20% added per siloxane unit in the copolymer.

Based on the above conclusions, the large mean molecular area occupied by the copolymer mesogens, as well as the lack of birefringent intensity seen in the copolymer isotherms, the packing of 10PPB2-CO and blend films at the air-water interface is proposed as shown in Figure 3-28. Recalculated thermodynamic isothermal data indicates that the backbone is far more crucial in the monolayer packing than was initially presumed. The extension of the siloxane backbone and its probable interaction with the water surface, prevent any extensive interaction between the side chain mesogenic groups in the pure copolymer films. Additionally, the lack of birefringence seen in 10PPB2-CO BAM intensity data confirms that there is little long range correlation between the side group mesogens such as that seen in the monomer. Due to the large area and the probable existence of gaps between the copolymer mesogens, the monomer mesogen may be accommodated within the packing confines of the copolymer up to a certain percent composition. However above this loading capacity the excess monomer would be squeezed out or initially excluded from the polymer packing area. Although evenly dispersed among the copolymer/monomer areas the excess monomer appear to organize on a small scale as they would in pure monomer film.

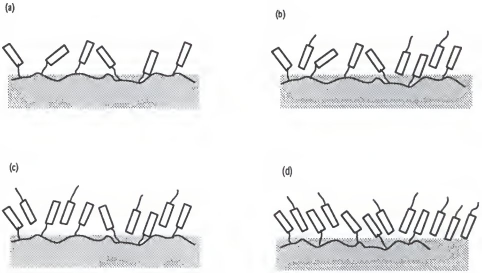

Figure 3-28. Proposed packing of mesogens in pure films and blends. (a) Pure copolymer monolayer, (b) low monomer concentration (5-20%), (c) moderate monomer concentration (25-50%), and (d) higher monomer concentration (55%+).

Regarding the transfer of the 10PPB2/10PPB2-CO blend monolayers to solid substrates and the resulting multilayer structures, two general conclusions can be drawn.

i) At concentrations of 20% 10PPB2 or lower, transfer of films is possible by x-type deposition, similar to that in pure 10PPB2-CO films. The resulting multilayers display similar rearrangement behavior as the pure copolymer films as well, but there is evidence of enhanced interaction between the side chains and some change in the multilayer organization occurs as a function of blend composition.

ii) At 10PPB2 concentrations higher than 20%, transfer is only possible at 30°C or greater and y-type deposition is preferred. The resulting multilayers are significantly less ordered with respect to defined layering. However, there is some evidence of an additional bilayer structure existing throughout the film. The presence of some areas of uninterdigitated layers, point to the restricted movement of the mesogens at higher local concentrations and the inability of the mixtures to freely rearrange.

# CHAPTER 4

# BLENDS OF A SIDE-CHAIN LIQUID CRYSTALLINE POLYMER WITH POLY(OCTADECYLMETHACRYLATE) AT THE AIR-WATER INTERFACE: MIXTURES FOR PRODUCING A MORE FLUID AND STABLE MONOLAYER

## Introduction

Liquid crystalline polymers are of interest due to their self ordering capabilities, with the added advantage over low molecular weight compounds of greater mechanical and thermal stability. It is interesting to consider the behavior of these compounds when they are confined to approximately two dimensions at an air/water interface. The side chain liquid crystalline polymers shown below (Figure 4-1) have previously been investigated and their individual bulk properties well documented.[142-146] The polymers were found to spread on a water surface and yield typical reproducible isotherms upon compression using a Langmuir-Blodgett (LB) trough. Not all polymers which spread on a water surface form stable monolayer films. Problems which arise in polymeric monolayers include incomplete spreading, long relaxation times and viscous behavior.[27] Using a hysteresis technique (compression of the film to a predetermined surface pressure, holding for a delay time, and then re-expansion of the film to zero pressure) it was discovered that most of the monolayer films of the polymers shown in Figure 4-1, were not stable for long time periods in a reasonable surface pressure range. The only exception was the polymer containing four ethylene oxide units ( x=4 in Figure 4-1, and denoted as PM4). This polymer was stable at large mean molecular areas and surface pressures no greater than 5 mN/m. Because it did exhibit stable film behavior in a measurable pressure range, the polymer PM4 was chosen as the best candidate for further investigation as a monolayer film and possibly as transferred to a solid substrate.

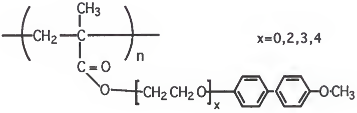

Figure 4-1. Structure of the side chain liquid crystalline polymers.

As a contrast to the blend system presented in Chapter 3, the monolayer film of PM4 was fluid only at low surface pressures (approximately 7 mN/m or less) where presumably the side chain groups are very far apart. At high pressures the PM4 film was highly viscous and unstable and did not exhibit the reversible collapse behavior as seen in the 10PPB2-CO films. It was the focus of the research presented in this chapter to increase the fluid and stable region of the isotherm, by breaking up interactions between the side chain groups. Previous work has shown that mixtures of film forming polymers with low molecular weight compounds and other polymers can enhance the film stability at the water surface.[60,147,148] A low molecular weight compound (stearic acid) and an analogous polymer poly(octadecylmethacrylate) shown in Figure 4-2, were each blended with the polymer PM4. Preliminary results indicated that the blends with PODMA increased stability of the films more dramatically than mixtures with stearic acid, and emphasis will be placed on the polymer-polymer blend system of PM4 and PODMA. This chapter will further discuss the behavior of these polymer mixtures confined as monolayers at a water surface, and pose possible explanations for the results.

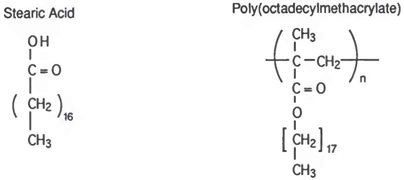
Stearic Acid

Poly(octadecylmethacrylate)

Figure 4-2. Compounds blended with LC polymer PM4.

Additionally, PM4 and PODMA blend monolayers were transferred to solid Si wafers as multilayer films. Deposition behavior and transfer are analyzed with respect to the blends. Also, small angle X-ray scattering is used to probe the molecular architecture of the built-up thin films, and to gain additional insight into the monolayer structure before transfer.

## Monolayers and Multilayers of the Pure LC Polymer

### Bulk Properties of PM4

The bulk and solution properties of the side chain liquid crystalline polymer, PM4 have been thoroughly discussed elsewhere.[142-146] The polymer is in a crystalline state at room temperature and exhibits a smectic E phase above 38°C. This smectic phase is highly ordered within the layers. The polymer PM4, as well as the other side chain LC polymers in this series, have an interesting packing behavior in the bulk. Most side chain LC polymers of this type pack with bulky side groups alternating on opposite sides of the polymer chain. However, the side chain groups of the polymers shown in Figure 4-2, pack on the same side of the polymer chain, due to the mostly syndiotactic nature of the PMMA backbone and its rigidity. This organization results in a ribbon-like

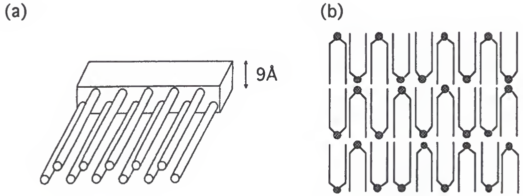

Figure 4-3. Ribbonlike structures of the PM4 polymer in the smectic layers. (a) Side chain polymer with pendant mesogenic groups on same side of the polymer backbone. (b) Packing of the polymer "ribbons". Open circles represent the polymer chains viewed end on and lines represent side chain groups.

structure of the polymer, and in the case of PM4, these ribbons pack within the smectic layers in an overall anti parallel fashion (Figure 4-3). The exact crystal structure has been elucidated by Duran et al. by thorough X-ray diffraction analyses.[142,144]

## Monolayer Properties of PM4

The film properties of PM4 were studied with respect to stability, reproducibility, deposition, and thermal dependence.[78] The isotherm, as shown in Figure 4-4, was reproducible to +/- 1 $Å^2$, and showed little dependence with small temperature fluctuations. Initially, it was thought that the monolayer curve represented a liquid condensed phase (Region II), a biphasic region (Region III) and a solid analogous region (Region IV) with a collapse at approximately 38.5-39.0 mN/m. However, were this the case, collapse would occur at 17.5 $Å^2$, whereas the closest packing area for the methoxybiphenyl side chain in the bulk is approximately 22 $Å^2$. If the LC polymer is forming the "ribbon" structure preferred in the bulk phase, this region of the isotherm could represent the close packing of these structures. The strong cohesive interactions expected between the ribbons (since the polymer crystallizes at room temperature) would account for the viscous nature of the monolayer at high pressure. The ability to attain areas smaller than in the bulk is most likely an overcompression phenomena; where the film "buckles" slightly to relieve pressure. Above collapse, the buckling is more severe and irreversible. The stiffness of the film at high pressures was evident in earlier experiments using a trough with a single barrier drive. During compression from one side of the trough, the Wilhelmy plate was distorted away from the barrier by the stiff polymer film at high pressures. Above collapse of the monolayer, the cohesion of the film was macroscopically visible as rigid sheets of film floating on the water surface.

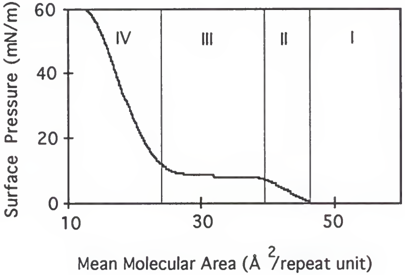

Figure 4-4. Surface pressure vs. mean molecular area isotherm for PM4. Numbered areas represent phases in the ∏-area curve: (I) liquid condensed-gas coexistence region, (II) homogeneous liquid condensed region, (III) liquid condensed-condensed (crystalline) coexistence or transition region, (IV) highly incompressible condensed film.

By compressing the monolayer film to various pressures along the isotherm and reexpanding it, information can be gathered as to the short term stability of the monolayer at each point, based on the hysteresis of the compression/expansion cycle. This type of isothermal analysis is usually referred to as a hysteresis experiment, and several cycles are shown in Figure 4-5 for the polymer PM4 at 26°C. In the first compression curve, the barrier was stopped at 5 mN/m, which is in the liquid condensed region of the isotherm. The barrier was held for two minutes, and the film reexpanded to approximately 60 $Å^2$. There is no visible hysteresis effect in this cycle, indicating that the film is stable (little or no pressure decrease with the barrier stopped) at this pressure. The second cycle (Figure 4-5, curve 2) was taken to a pressure above the transition region but below the indicated collapse of 35 mN/m. There is a sharp drop in pressure once the barrier is stopped, and a dramatic hysteresis effect is seen in the gap between the corresponding compression and expansion curves. The next compression shows a shifted curve in region II of the isotherm, but the transition pressure and pressure curve above the transition remain the same. This indicates that some aggregation or crystallization of the film occurs at high pressure, and is maintained after expansion of the monolayer. However, there is not necessarily any collapse beyond a monolayer, since collapse would involve a breakdown of the original monolayer, and would be evident in a shifting of the isotherm curve to smaller areas. This shift is seen when the monolayer is compressed above the determined collapse pressure, as in hysteresis cycles 3 and 4 of Figure 4-5. The irreversibility of the isotherm in this and at higher pressures indicates that the film is not in equilibrium within the reasonable time frame of the experiments. This is further substantiated by previous stability measurements which showed a constant decay of mean area per monomer unit at pressures above the transition region.[78]

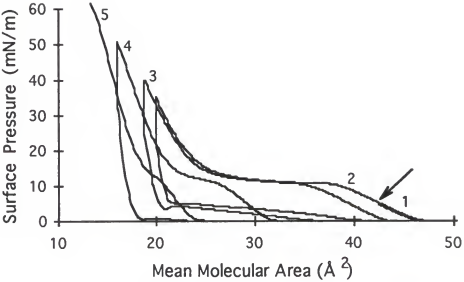

Figure 4-5. Hysteresis effect of compression/expansion cycles on PM4 monolayer film. Wait time between compression and expansion curves for all cycles was 2 minutes. Numbers indicate compression/expansion cycles, 1, first hysteresis cycle up to 10 mN/m (indicated by arrow), 2, second cycle to 35 mN/m, 3, third cycle up to 40 mN/m, 4, fourth cycle up to 50 mN/m, and 5, last compression.

The thermal behavior of PM4 monolayers over the range of 26 to 35°C are shown in Figure 4-6. There is little effect seen in the liquid condensed region of the isotherm caused by these temperature variations. However, the condensed region (IV) exhibits a dramatic change over this temperature range. This is not surprising since the previous results indicated that the monolayer is not in equilibrium above the plateau region of the isotherm. Processes such as collapse and kinetic dependent processes should be facilitated at lower pressures if the temperature (and hence kinetic energy) is raised, which is the trend seen in the condensed region of the PM4

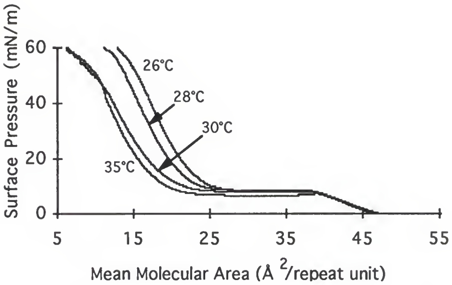

Figure 4-6. Thermal behavior of PM4 monolayers. There is little effect of changing temperature over the range shown in the fluid region and even in the transition region. However, the more condensed phase region appears much more sensitive to small temperature variations.

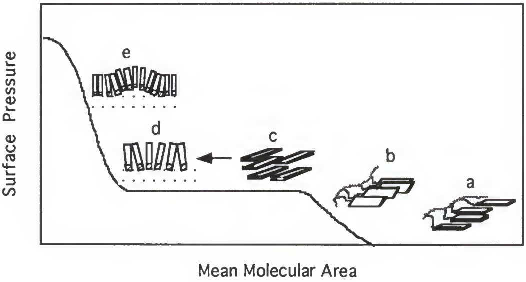

Figure 4-7. Proposed organization of LC polymer, PM4 monolayer. (a) Liquid-gas coexistence region, mesogens flat on the water surface, (b) liquid condensed region, mesogens begin to tilt, (c) polymer chains organize in "ribbons", which begin to orient vertically as in (d), overcompression of the monolayer (e) and low mean areas obtained by buckling of the film.

isotherms. Additionally, the lowering of the plateau pressure with increasing temperature, confirms that this is not a true phase coexistence region. According to the Clausius-Clapeyron equation a phase transition pressure would increase with increasing pressure. Therefore, this flat pressure transition must represent some rearrangement in the monolayer to relieve pressure, as opposed to a condensation process.

Deposition of PM4 monolayers

The side chain LC polymer transferred to a hydrophilic substrate to form Z-type multilayer films up to 50 layers, with transfer ratios exceeding 0.9 (Figure 4-8 shows five layers). UV data shows an approximately linear relationship of absorbance

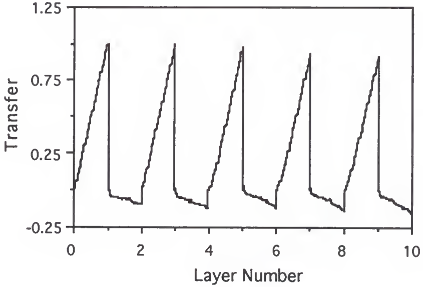

Figure 4-8. Transfer versus layer number for PM4 at 5 mN/m and 25°C. Even number layers are the transfer from air to below the water surface. Odd number layers represent the upward transfer out of the water.

versus number of layers. In the UV spectra taken of the same film the next day, no noticeable change in absorbance is observed, illustrating the transferred multilayer film's stability for short periods of time. However, transfer conditions are at 5 mN/m and approximately 40 angstroms squared per monomer repeat unit. In the bulk, the closest packing area of the biphenyl group is 22 Å$^2$. Therefore, the side chains are far from being closely packed, and large gaps must be present in the film.

## Monolayers and Multilayers of PM4/PODMA Blends

Mixtures were made of PM4 with PODMA and stearic acid to enhance the SCLC polymer film's properties and optimize packing at the air-water interface. Substances with long alkyl chains were considered the best candidates for two reasons. First, the long alkyl chains would plasticize the LC side chains which are rigid due to the strong interactions between mesogenic groups. Secondly, the hydrocarbon chains would add a more defined hydrophobic region to the film in order to "anchor" it out of the water phase.

### PODMA Monolayer Behavior

The primary mixing compound used in blends with PM4 is a polymeric analog of a fatty acid, poly(octadecylmethacrylate) (PODMA) (Figure 4-2). It has been previously studied thoroughly in the bulk and at the air-water interface.[49,77,149,150] Some slight discrepancies were found with respect to the deposition and isotherm shapes in this study and those referenced from previous studies. These may be due to the differences in backbone tacticity of the polymer samples. The referenced studies were of isotactic or syndiotactic polymer samples, whereas the polymer sample used in this study was atactic (see details in Chapter 2).

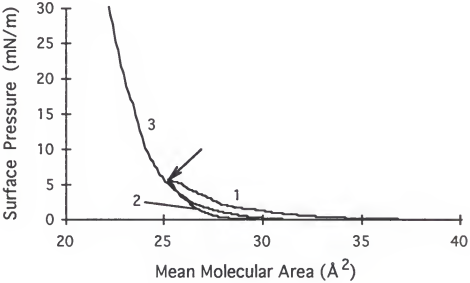

Figure 4-9. Hysteresis cycle of PODMA monolayer. Curve 1 is the first compression up to 5 mN/m (indicated by arrow), curve 2 is the reexpansion to zero pressure, and curve 3 is the second compression to collapse. The delay time at the end of each compression and expansion curve was 2 minutes.

In Figure 4-9 a hysteresis cycle up to 5 mN/m is shown along with the subsequent recompression to collapse. Even at this low pressure, the PODMA film shows significant hysteresis and the second compression is slightly shifted to lower areas. This along with the stability data cited in the previous paragraph, indicates that the poly(octadecylmethacrylate) monolayer film is not in an equilibrium state under reasonable experimental conditions.

Crisp[27] categorized PODMA as a monolayer film of the coherent and semi-crystalline type. This category includes polymers that do spread completely to form monolayers on a water surface, but possess greater cohesion forces than fluid polymer films (such as those of 10PPB2-CO seen in Chapter 3). According to Crisp,[27] PODMA monolayer "gel" or begin to aggregate to solid form at zero pressure, and is a solid film at 5 mN/m. Monolayer films in such solid-like states are known to exhibit hysteresis behavior due to increased relaxation times.

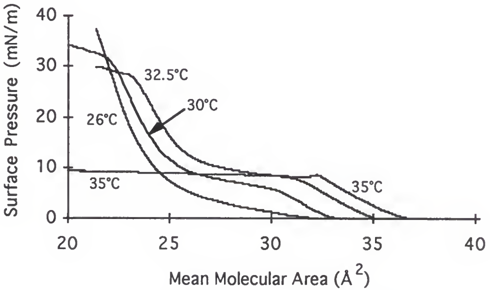

Figure 4-10. Isotherms of PODMA at various temperatures.

Isotherms at various temperatures within a range of 26°C to 35°C are shown in Figure 4-10. This is the same temperature range over which isotherms of PM4 was shown in Figure 4-6. It is evident that the PODMA is far more temperature sensitive than the PM4 monolayer films under these conditions. This temperature dependent behavior will be a sensitive gauge to blend monolayer characterization. In the case of complete phase separation, a proportionate portion of the film containing PODMA would behave similarly to the pure component monolayer film.

### Monolayer Film Behavior of the Blends

Plots of isothermal data from monolayer films can give a great deal information as to the physical state of the molecules in the layer. Additionally, when mixing two or more components in a monolayer film, isotherms of the mixtures yield some insight to the phase miscibility or physical state of the blends. In the following figures, isotherms of various PM4 and PODMA concentrations are shown at 26°C and at 35 °C. Due to the complexity of the curves and the number of isotherms, the concentration ranges have been separated and enlargements of transitions regions shown for clarity.

In Figure 4-11 (a) complete isotherm curves are shown for blend concentrations from 0 to 50% PODMA and a PODMA curve as well. In the high pressure region all of the blend curves fall at much small mean molecular areas than either of the pure components. Considering the close-packed nature of the pure isotherm films in this region, it is not likely that the blends are packing more efficiently in the monolayer to account for this large decrease in mean molecular area. The 15 and 25% isotherms are almost identical to the pure PM4 curve, but are shifted to lower areas. However, at 40 and most notably at 50% the isotherms are different in the shape and exhibit an increase in collapse pressure. This difference is clearer in the inset plot Figure 4-11(b), where the 50% transition region is significantly increased over that of PM4. Since no transition region is present in the pure PODMA film at this temperature, this feature is characteristic only of this blend. For the higher concentration PODMA blends of 60 to 85%, the isotherm behavior is markedly different from that of the lower concentrations especially in the larger area transition regions. In the higher pressure regions again all blend concentrations in the range fall below the areas of either pure component films. However, in the lower pressure regions additional transitions appear in the isothermal curves. The 60% film has three identifiable transitions occurring shortly after significant pressure increase, approximately 10-11 mN/m, and the most prominent at approximately 13 to 13.5 mN/m. The latter transition is the most obvious and is most likely analogous to the transitions seen in the lower blend concentrations. The 75% and 85% have only two discernible transitions which are more gradual and subtle than the transitions of the 50% and lower percent PODMA isotherms. It is interesting that the lowest pressure transition seen in the 60, 75 and 85% blend monolayers resembles the fluid phase region of the PODMA isotherms at slightly higher temperatures (28-30°C) and may reflect the inability of the hydrocarbon side chains to aggregate in these mixtures due to the presence of the side chain LC polymer.

Overall the lack of additivity in the shape of the isotherms of the blends of PM4 and PODMA at this temperature indicates

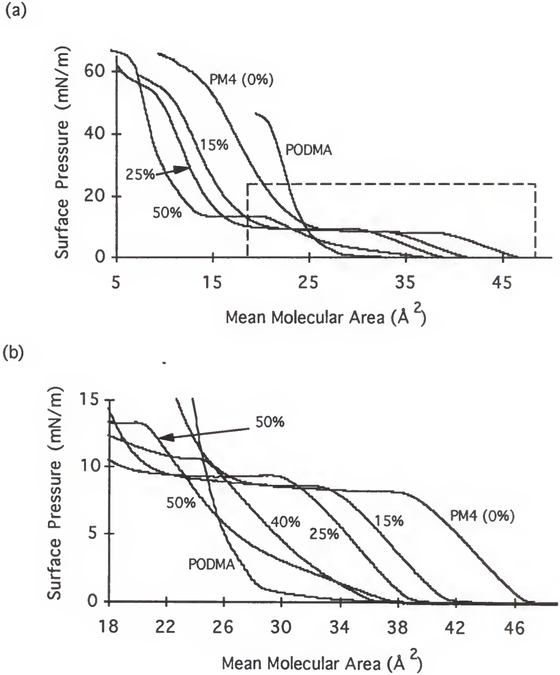

Figure 4-11. (a) Isotherms of 0 to 50% PODMA (mol % monomer repeat unit) and PODMA at 26°C. Dotted line encloses the isotherm region which is enlarged for clarity of the transition region in (b).

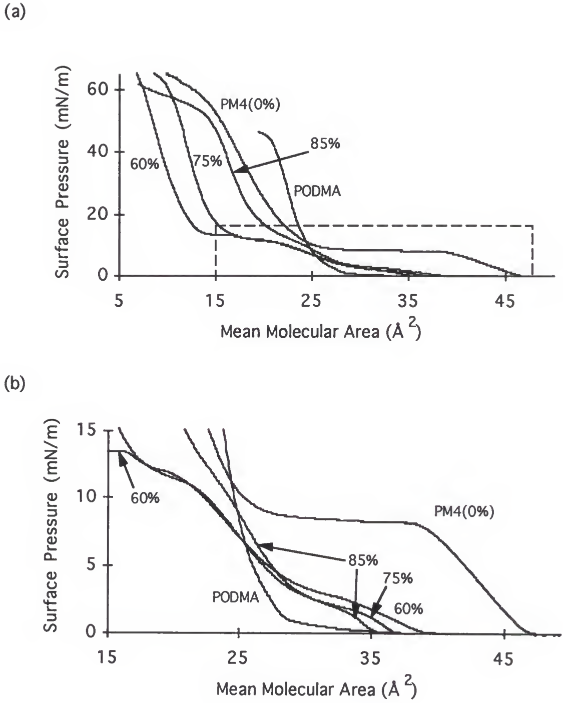

Figure 4-12. (a) Isotherms of 60 to 85% PODMA (mol monomer %) and PM4 at 26°C. Dotted line encloses the isotherm region which is enlarged for clarity of the transition region in (b).

significant, if not complete miscibility in the blends. The lower concentrations, 15 and 25%, show almost no change in isothermal behavior from that of PM4 which may be caused by the large area and gaps present in the PM4 films accommodated by the alkyl chains of the PODMA. However, at higher percent PODMA, the increased transition pressure and increased compressibility indicate that the alkyl chains are intimately mixing with the PM4 side chains. The mixing changes isothermal behavior of the blend monolayers by breaking up interactions between side groups, as well as preventing aggregation of the alkyl groups themselves.

Isotherms of some PM4/PODMA blend concentrations at 35°C are shown in Figures 4-13 and 4-14. At low PODMA concentrations, the isotherms plotted in Figure 4-13(a) and (b), show little change from those at 26°C except in the lowering of the collapse pressure. The most dramatic change in the isothermal behavior is in the melting of the PODMA monolayer to a fluid film. At the elevated temperature of 35°C the PODMA monolayer reaches a critical surface pressure at approximately 33 $Å^2$. This is significantly larger than the condensed PODMA monolayer which collapses at 22 $Å^2$. Were the temperature raised a few degrees, the small pressure increase which occurs around 8 $Å^2$ would disappear altogether. It's appearance here indicates that a small portion of the film is not completely fluid. The extended flat region of the isotherm at this temperature is characteristic of a fluid monolayer in equilibrium with bulk material. In this case, the critical pressure before the

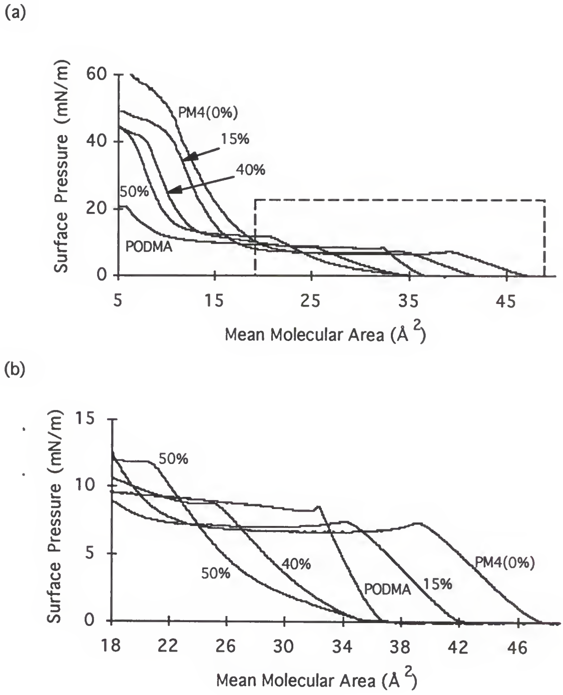

Figure 4-13. (a) Isotherms of 0 to 50% PODMA (mol monomer %) and PODMA at 35°C. Dotted line encloses the isotherm region which is enlarged for clarity of the transition region in (b).

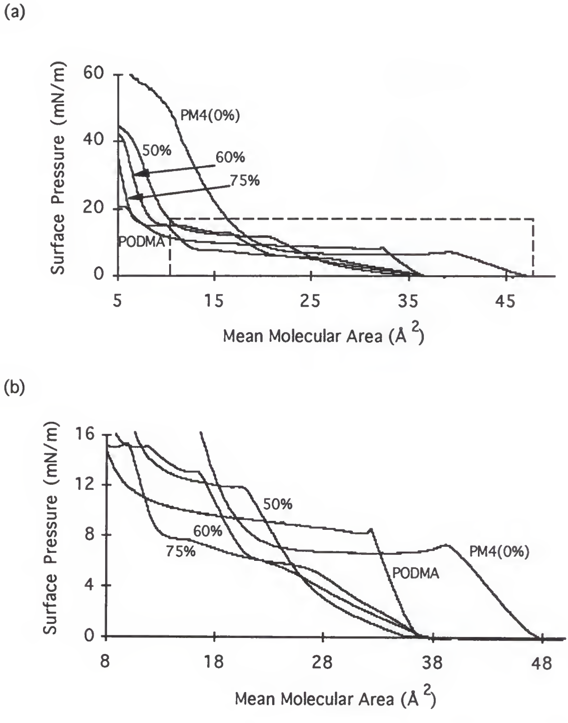

Figure 4-14. (a) Isotherms 50 to 75% PODMA (mol monomer %) and PODMA at 35°C. Dotted line encloses the isotherm region which is enlarged for clarity of the transition region in (b).

plateau region would be a true equilibrium spreading pressure as described in Chapter 3.

Despite the melting of a pure PODMA monolayer at this temperature, the mixtures up to 50% appear relatively unaffected in the transition region. And although the isotherms indicate intimate mixing, the films resist the extreme fluidification seen in the pure PODMA films. In the enlarged transition region Figure 4-13(b), the increasing transition pressure trend is still evident, although the PODMA curve is now more prominent.

At higher PODMA concentrations and 35°C, the isotherms in Figure 4-14(a) show a more pronounced temperature dependence than those seen in 26°C for the same compositions. Although the blend curves at higher pressures now fall in between the pure component curves, similar to the lower concentration blend monolayers, there is a reversal in area position of the 60 and 75% isotherms relative to the 26°C analogous isotherms. It is apparent from the isothermal behavior that the PODMA component of these films has a greater influence on the physical state of these blend monolayers.

Hysteresis Curve of 50% PODMA. To ensure that the fluid region of the blends was stable as in the PM4 isotherm, a hysteresis curve of a 50% PODMA monolayer film was obtained and is plotted in Figure 4-15. The first compression/expansion cycle was to 10 mN/m, which is 5 mN/m higher than the first cycle used in the PM4 experiment, and is in a region where the pure PM4 isotherm is relatively unstable. However, for this 50% PODMA blend isotherm, no hysteresis effect was seen in this first compression/expansion curve, and the second compression (curve 3, Figure 4-15) is identical to the first compression up to 10 mN/m. This experiment demonstrates the enhanced stability of this particular blend and implies similar properties in the other blend concentrations that could not be accounted for in the case of gross phase separation or immiscibility.

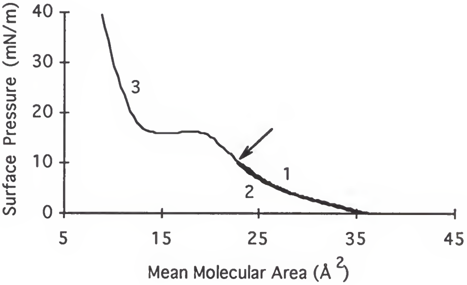

Figure 4-15. Hysteresis curve of 50% PODMA. Arrow indicates stopping point of the first compression.

Monolayer Film Stability of PM4/PODMA Blends. In order to deposit monolayer films on a solid substrate by the conventional vertical dipping method, films must exhibit reasonable stability at the desired transfer pressure. To monitor this, films were compressed to a particular surface pressure and held at this pressure while monitoring the change in the mean molecular area versus time. Figure 4-16 shows the isobaric stability of several

PM4/PODMA blend concentrations and the pure components at 5 mN/m. The curve shows only the higher blend concentrations, however, the lower mol% blends (15, 25, 40 and 50%) showed similar behavior to PM4 and were left out for clarity. The enhancement of the blend stability from an additive relationship is apparent, with the 60% curve falling on top of the pure PM4 component and the 75% PODMA curve only slightly less stable (within 15 to 20 minutes relatively little change in MMA is seen).

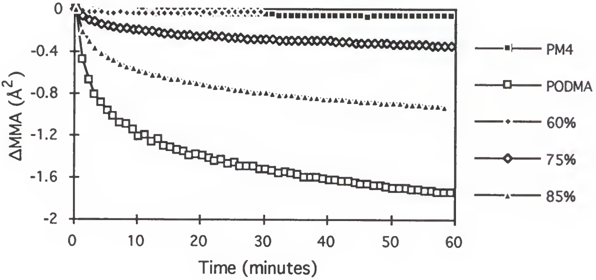

Figure 4-16. The above graph shows the change in mean molecular area (ΔMMA) with time at a constant applied film pressure of 5 mN/m and at 26°C.

Although it would be expected that the 85% PODMA blend would closely mirror the properties of the PODMA monolayer behavior, the stability after one hour at 10 mN/m shows a change of approximately 0.9 Å$^2$ per monomer unit in the 85% blend versus 1.8

Å$^2$ per monomer shown in the PODMA monolayer within the same time interval.

Collapse Pressure of PM4/PODMA Monolayer Blends. As described in Chapter 3, Crisp's application of the phase rule to monolayer blend system can be used to analyze miscibility of mixtures at the air-water interface by analyzing collapse pressure as a function of blend composition. The collapse pressure (more accurately equilibrium spreading pressure) should vary continuously with blend composition in the case of miscibility, and be invariant with composition in the case of immiscibility due to the additional loss of a degree of freedom. In Figure 4-17 plots of collapse pressure versus mol fraction PODMA are shown for temperatures from 26°C to 35°C. In the curve from 26°C (Figures 4-17(a)) the blend values vary with composition and are, within error, significantly higher than the collapse pressure of the less stable component (in both cases, PODMA). However, at 30 and 32.5°C, the value of the 85% PODMA collapse is within the error value range of the PODMA collapse pressure. At 35°C no value is available for the 85% PODMA monolayer, however, due to the trend of the previous two plots it would likely fall near the PODMA collapse. This indicates at higher temperatures, there is a demixing in the monolayer blends of 85% and higher, most likely due to the melting and increased kinetic energy of the alkyl side chains in the PODMA.

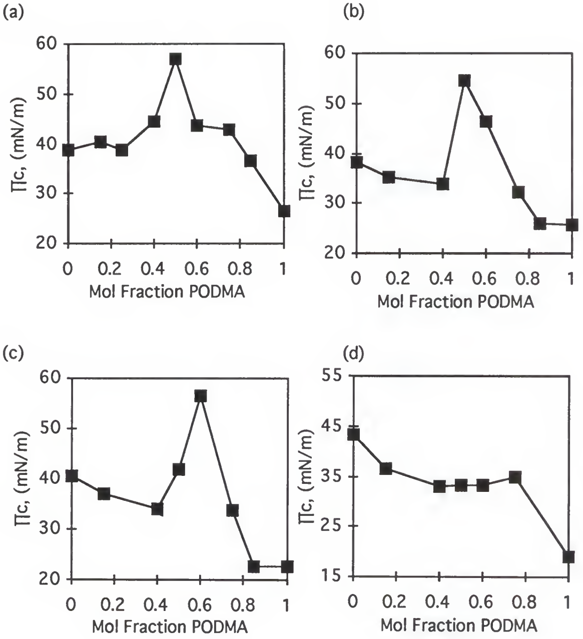

Figure 4-17. Plots of collapse pressure, ∏c versus mol fraction PODMA for monolayer blends of PM4 and PODMA. Curves are shown for various temperatures a) 26°C, (b) 30°C, (c) 32.5°C, and (d) 35°C . Collapse pressures were determined as the maximum value of the d∏/dA curve.

## Thermodynamics of Mixing in the Monolayer Blends

As mentioned in Chapter 3, excess areas of mixing have been used extensively in the literature as a method for determining the miscibility and extent of interaction of monolayer blend components. When used in combination with isothermal analysis, plots of excess area versus blend composition can be quite informative in visualizing the changes that occur at the water surface when blending compounds in monolayers. In Figure 4-18 plots of excess area, $\Delta A_{xs}$, are plotted versus blend concentration at various surface pressures and temperatures. Figure 4-18(a) and (b) are plots taken from data at 26 and 30°C respectively, and show only large negative deviations from an ideal mixing relationship. At 35°C (Figure 4-18(c)), the higher pressure values are only slightly negative or positive. These are within error values of the ideal mixing line at zero. The melting of PODMA and the increased energy of the components apparently does not allow the closer or more efficient packing of the blend monolayers seen in the lower temperatures, however, at 5 mN/m the excess area values are still significantly negative. Since the area of most interest in this study is below the transition region where the films are relatively in an equilibrium state and stable as monolayers, from this data it appears that the blends are miscible over all concentrations and over the temperature range shown.

Isothermal data can also be analyzed by calculation of excess thermodynamic parameters, and in particular, $\Delta G_{mix}{}^{xs}$. Often, it is assumed that the $\Delta A_{xs}$ values will agree with the

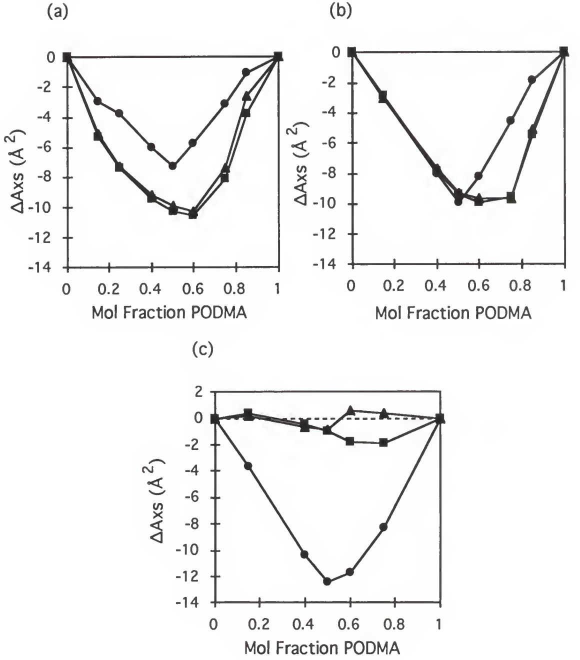

Figure 4-18. Plots of $\Delta A_{xs}$ for PM4/PODMA monolayer isotherms versus mol fraction PODMA. Data was taken at (a) 26°C, (b) 30°C, and (c) 35°C. Curves correspond to surface pressures: (-●-) 5 mN/m, (-▲-) 15 mN/m, and (-■-) 20 mN/m.

$\Delta G_{mix}^{xs}$ plotted against composition, although the origins of the values are different. Although $\Delta A_{xs}$ values indicate the change in area occupied by the blend components, they do not reflect the energy or work done to get the components to this packing density, as does $\Delta G_{mix}^{xs}$. There are cases in the literature[135] that show conflicting $\Delta A_{xs}$ and $\Delta G_{mix}^{xs}$ data and in such cases, careful analysis of the data is required. In Figure 4-19 plots of $\Delta A_{xs}$ and $\Delta G_{mix}^{xs}$ versus PODMA mol fraction at 5 mN/m; plots of several temperatures are included in each graph. The implications from each graph are almost opposite in reference to miscibility of the blends at this pressure. While the $\Delta A_{xs}$ values are significantly negative for each temperature, the $\Delta G_{mix}^{xs}$ plot infers that the blends spontaneously mix only at 26°C and up to 25% PODMA.

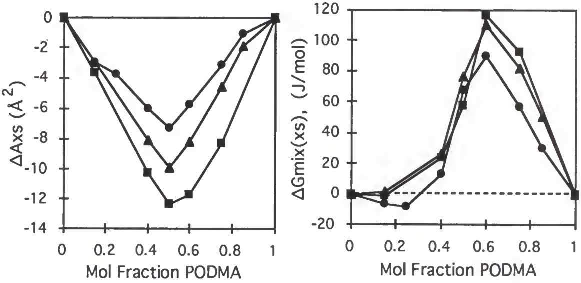

Figure 4-19. Excess area (left) and excess free energy of mixing (right) for PM4/PODMA monolayer blends versus PODMA concentration, taken at 5 mN/m. Different curves correspond to various temperatures as follows: (-●-) 26°C, (-▲-) 30°C, and (-■-) 35°C.

Since isotherms from various temperatures were obtained, the temperature dependence of the $\Delta G_{mix}^{xs}$ values allows the free energy to be separated into $\Delta S_{mix}^{xs}$ and $\Delta H_{mix}^{xs}$ terms. It is useful in determining the origin of mixing, to analyze whether mixing is dominated by packing constraints, $\Delta S_{mix}^{xs}$, or by attractive (or repulsive) forces, $\Delta H_{mix}^{xs}$.

The excess entropy of mixing can be calculated by plotting $\Delta G_{mix}^{xs}$ versus temperature and using the slope, $(d\Delta G_{mix}^{xs}/dT)_{\Pi}$, in the following relationship, as put forth by Goodrich[139] and applied by Bacon and Barnes,[133]

$$\Delta S_{mix}^{xs} = -(d\Delta G_{mix}^{xs}/dT)_{\Pi} - \Delta A_{xs}(d\gamma/dT) \qquad (4.1)$$

where $\gamma$ is the surface tension of a pure water surface and $d\gamma/dT$ is the temperature dependence of the surface tension taken as the referenced value of -0.148 mN/m°C.[51] The excess enthalpy of mixing, $\Delta H_{mix}^{xs}$, can then be deduced from the relation,

$$\Delta G_{mix}^{xs} = \Delta H_{mix}^{xs} - T\Delta S_{mix}^{xs} \qquad (4.2)$$

where T is the temperature in Kelvin.[133]

In the PM4/PODMA blends, the above parameters were determined from the isotherms at 30° to 35°C where the PODMA was in the same fluid state as the PM4; and at 5 mN/m, since this pressure was believed to be below any obvious phase transition to avoid including the energy of a phase change in the values. Additionally, at 5 mN/m the pure components are both in a similarly fluid monolayer phase. Figure 4-20 shows the excess free energy, entropy, and enthalpy of mixing for the PM4/PODMA monolayer blends at 30°C and 5 mN/m. On this scale, the $\Delta G_{mix}^{xs}$ value is comparatively small relative to the values of $T\Delta S_{mix}^{xs}$ and $\Delta H_{mix}^{xs}$. This further shows that although the free energy values may be positive they are not excessively large. Because of this the enthalpic and entropic terms are quite close in values, with only a slightly more negative entropic term for 40% and higher blend compositions. The 15% PODMA values of $T\Delta S_{mix}^{xs}$ and $\Delta H_{mix}^{xs}$ are almost identical and the resulting $\Delta G_{mix}^{xs}$ is within error of the ideal mixing value of zero.

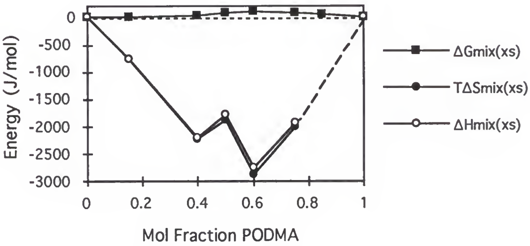

Figure 4-20. Excess thermodynamic values for mixing of the PM4/PODMA monolayer blends at 30°C. The dotted line is located at zero or the ideal mixing curve. The dashed line indicates the ambiguity of the values in this area due to the absence of ΔH and ΔS values for the 85% blend.

The large but equal values of $\Delta H_{mix}^{xs}$ and $T\Delta S_{mix}^{xs}$ represent the balance between two opposing forces. One, the very strong attractive forces between the PMMA backbones, has been well established by Crisp[27] who further demonstrated that pure PMMA molecules gel in a monolayer film at little or no applied film pressure. This attractive interaction is countered by the initial mixing of the side chains which disrupts the attractive forces that exist in the pure polymer monolayer films and prevents some interactions between the backbones of the two different polymers. Whether the side chains are immiscible, independent of the backbone, is not clear; and it is useful to look at some other examples of blend behavior to analyze these blends further.

### Other Monolayer Blend Examples

The side chain LC polymer, PM4, was blended with stearic acid in several concentrations. The stearic acid component is similar to a monomeric version of the PODMA polymer and may represent a version of the side chain of PODMA minus the backbone (where backbone refers only to the hydrocarbon polymer chain). The analysis of this blend should give insight into the isolated interaction (although the PMMA backbone is still present in the PM4) of the liquid crystalline side chain with the alkyl chains without the additional attractive forces between the two different PMMA backbones.

If no significant repulsive or attractive interactions were occurring between the polymer side chains and the long alkyl chains, a linear mixing relationship of the excess area values would be expected. Within experimental error, the mixing behavior of the PM4/stearic acid blends depicted in a $\Delta A_{xs}$ versus concentration plot appears linear (Figure 4-22). This indicates no net interaction between the components or complete phase separation and large domain formation. The ideal mixing relation of the $\Delta A_{xs}$ plot is expected in an immiscible mixture where at least one component is a small molecule. This arises from the high mobility of the small molecule which in an immiscible mixture forms large domains to decrease interaction with the other component.

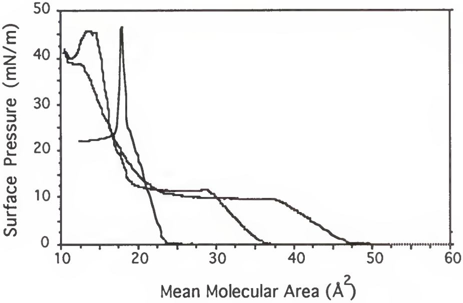

Figure 4-21. Isotherms of PM4, stearic acid, and a 1:1 blend.

Based on these results, it may be inferred that any miscibility in the PM4/PODMA monolayer blends is due to attractive interactions and miscibility of the identical backbones alone and not due to attractive forces between the side chain groups.

As a contrast, results from an immiscible (in bulk and at air-water interface) polymer/polymer blend study were analyzed and isobaric concentration versus area data are shown in Figure 4-23.

For this polymer mixture there is only a positive deviation from a linear curve indicating incompatibility. The positive deviation

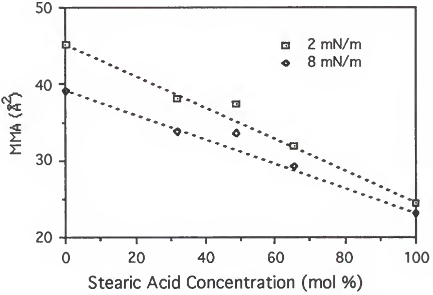

Figure 4-22. Mean molecular area vs. component concentration for PM4/stearic acid blends. The dotted lines represent a theoretical linear mixing relationship

would not be expected if the polymer mixture were in equilibrium. In equilibrium, the polymers would phase separate, and the observed surface areas would be simply the weighted average of the pure components similar to that seen in the PM4/stearic acid case. The behavior observed in this incompatible mixture is believed to result primarily from the decreased mobility of polymer chains constrained to a free surface. Upon compression the chains do not have time to phase separate and are constrained in conformations that they would normally not assume. It would be expected then, if the PM4/PODMA blends were truly immiscible, the $\Delta A_{XS}$ values would reflect this due to the inability for these high molecular weight molecules confined to a surface to phase separate easily.

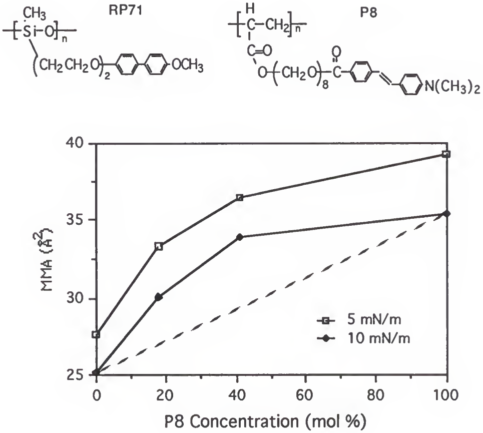

Figure 4-23. Immiscible polymer blend. Mean molecular area versus concentration data of the polymer mixture whose components are shown above the graph.

## Bulk Thermal Behavior of PM4/PODMA Blends

To determine miscibility of PM4/PODMA blends in the bulk phase, differential scanning calorimetry was used. Several scans of PM4, PODMA, and a 50% PODMA sample are shown in Figure 4-24. Usually in polymer blend analysis of DSC scans, glass transition temperatures are used as the criterion for miscibility. In the case

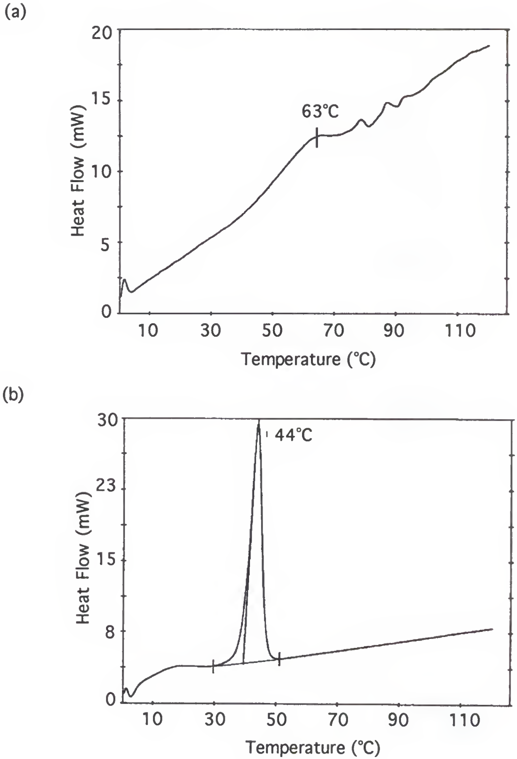

Figure 4-24. DSC scans for (a) PM4 and (b) PODMA blend sample. Temperature ramp speed was 20°C/min.

(c)

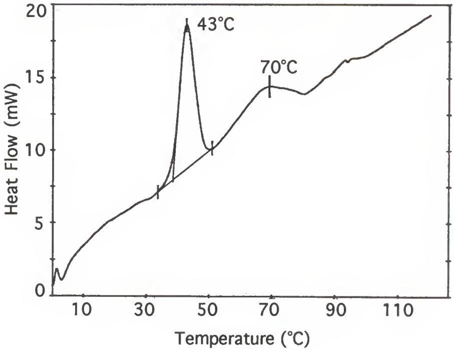

Figure 4-24 (continued). DSC scans for (c) 50% PODMA blend sample. Temperature ramp speed was 20°C/min.

of a miscible blend only one Tg, intermediate between the Tg values for the pure components, is seen. In an immiscible system, two Tg transitions are evident and occur at the temperatures seen in the individual polymers. In the case of PM4 and PODMA, this analysis was infeasible. First, the Tg of PODMA is -100°C and out of the range of the instrument used. Secondly, the Tg of PM4 is approximately 38°C and the melting of PODMA is approximately 36°C. Due to the broadness of the peaks, the melting of PODMA masked the Tg of PM4. Additionally, the sensitivity of the calorimeter used was not great enough to unambiguously detect the glass transition of the pure PM4 sample. Because of these factors, the trends of melting were observed to indicate miscibility.

Figures 4-24 (a) and (b) show DSC scans for the polymer components PM4 and PODMA, respectively. The DSC scan in Figure 4-21(c) is the first heating curve of a 50% PODMA blend sample. The blend heating scan appears to be an additive curve of the pure components. The middle peak corresponding to the PM4 component of the blend sample, is shifted to slightly higher temperature in the 50% PODMA scan. However, the broadness of this peak makes it difficult to determine temperature accurately. The lack of significant shifts in any heating phenomena in the regions studied indicates that the two components behave thermally independent of the other component. This leads to the conclusion that the polymers PM4 and PODMA are not thermodynamically miscible in the bulk phase.

### Deposition of PM4/PODMA Blend Monolayers

Although other work cited has shown that poly(octadecylmethacrylate) transfers to hydrophilic substrates, we were unable to build up more than one monolayer, even in the liquid region at elevated temperatures. Deposition was attempted at 32°C at a dipping speed of 5 mm/min and an upper delay of at least 20 minutes. Transfer occurred on the upstrokes and appeared to quantitatively redeposit upon the water surface during subsequent downstrokes.

Considering the deposition behavior of PM4 monolayers shown in Figure 4-8, which shows the tendency to Z-type layering, pure Z-type layers were produced using an alternate layer trough. Hydrophilic Si wafers were used to produce multilayers containing

50 transferred monolayer films of PM4, 30% PODMA, and 50% PODMA in a z-type deposition. Only approximately 24 layers could be obtained of the 75% PODMA films due to a gross decay in transfer ratios. While the PM4 monolayers were transferred at 5 mN/m (which was previously determined as an upper limit suitable for deposition), 30% PODMA monolayers were transferred successfully at 8 mN/m and 50% at 10 mN/m under the same conditions and with similar constant transfer ratios. No significant PODMA monolayer could be transferred beyond a monolayer under these conditions.

### X-ray of Blend Multilayers

In order to analyze the multilayer structure transferred by deposition of LB monolayer, small angle X-ray scattering was employed. Usually, the diffraction patterns from a well ordered multilayer film will show Bragg peaks corresponding to the layer spacing relative to the z-direction normal to the substrate surface. However, in the patterns shown in Figure 4-25, the PM4 (bottom) and 30, 50% and 75% blends (above PM4 curve, bottom to top respectively) show no distinct Bragg peaks. This absence infers a lack of defined layering in the multilayer structure. Considering the large areas at which the monolayers are transferred and the fluid disordered state in which they exist during transfer, this is not too surprising.

An obvious feature of the PM4 and reasonably evident in the 75% PODMA films is the subsidiary maxima that usually fall in between the Bragg peaks. These were seen consistently in Chapter 3 in the multilayer films of the copolymer and several blend films, however, Bragg peaks were also evident in these samples. The sharpness of the peaks corresponds to the smoothness of the two interfacial surfaces of the whole multilayer films, i.e., the substrate/multilayer interface and the outer surface of the multilayer film. Since there are no intense or evident Bragg peaks in the diffraction patterns from which to determine layer thickness, the subsidiary maxima can be used indirectly.

Interference subsidiary maxima or Kiessig fringes. In Langmuir-Blodgett films of small layers (usually 20 or less) secondary maxima and minima appear between the Bragg peaks which correspond to layer periodicity. These secondary maxima were first seen by Kiessig[151] in metal films and later noted in Langmuir-Blodgett films by Bisset and Iball.[152]. Parratt[153] was the first to derive a set of equations to describe these secondary interference patterns, also referred to as Kiessig fringes, which are analogous to Fresnel equations in optics. These films have also been compared as analogous to an optical diffraction grating with N slits, with N corresponding to layer number in a multilayer film. The interference which results in these patterns are reflections from the upper and lower surface of the multilayer. Therefore, their presence will indicate both a smooth substrate surface and smooth outer surface of the multilayer film.[154]

The position of each subsidiary maxima may be described by the following equation,

$$1/2\,(2m + 1)\,\lambda = 2d\,(\phi_m^2 - \phi_c^2)^{1/2} \qquad (4.3)$$

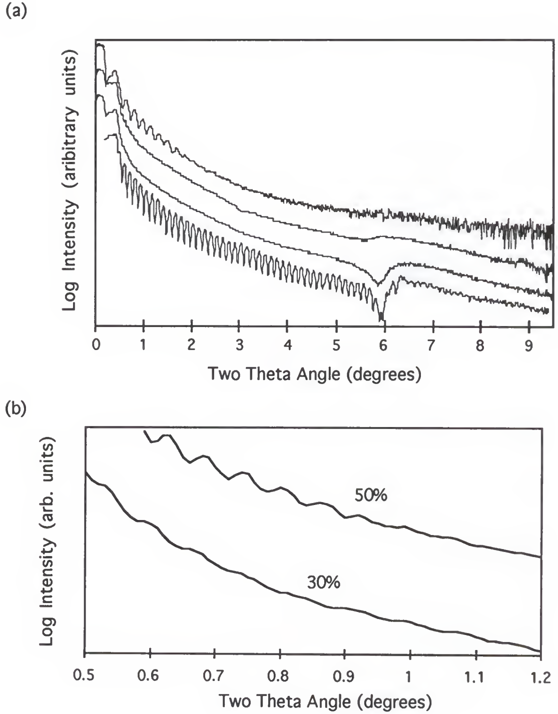

Figure 4-25. Small angle X-ray scattering patterns of PM4 and PM4/PODMA LB multilayers. (a) Scans are from bottom to top, PM4, 30% PODMA, 50% PODMA, and 75% PODMA. (b) Enlargement of the 30 and 50% PODMA multilayers to show the presence of Kiessig fringes in these films.

where m is an integer, $\lambda$ is the wavelength of the X-rays (in these experiments CuK$\alpha$ = 1.504 Å), d is the total multilayer thickness, $\phi_m$ is the angular position of the mth subsidiary maxima, and $\phi_c$ is the angular position of the critical angle for total reflection. By taking the difference in two adjacent interference peak positions, total layer thickness can be determined.[155] The values in Table 4-2 are averaged from several peaks, depending on the number discernible in the diffraction pattern.

Although in the subsidiary peaks in the 30 and 50% diffraction patterns and more subtle and less defined as in the PM4 or 75% PODMA blend multilayers, the distance between peaks was measurable. Based on this information combined with known number of layers deposited, an average layer spacing could be estimated. Table 4-1 shows a summary of this data. According to these results, the layer spacing of the blends increases as PODMA is added up to 50%, and decreases slightly at the higher concentration of 75% PODMA. Overall thickness increase could be seen macroscopically in the multilayer films with the same number of layers by color phase transitions. These color variations were seen before in multilayer samples of 10PPB2-CO and are analogous of the optical thickness gauge developed by Katherine Blodgett to determine thin film layer dimensions. From PM4, 30%, and 50% PODMA colors were reddish-brown, royal-purplish blue, and light sky blue, respectively. This corresponds to overall increasing multilayer thickness with added PODMA, further substantiating the thickness trends determined from the secondary maxima peaks.

Table 4-1. X-ray Diffraction Data for PM4/PODMA Multilayers

| Monolayer Composition | Total Film Thickness (Å) | Number of layers deposited | Average Layer Thickness (Å) |
|---|---|---|---|
| PM4 | 735 | 50 | 15 |
| 30% PODMA | 1260 | 50 | 25 |
| 50% PODMA | 1470 | 50 | 29 |
| 75% PODMA | 504 | 24 | 21 |

Considering the large area and lower surface pressure at which the polymer is transferred, the PM4 side chains in the multilayers must be more horizontal relative to the substrate plane than vertical. This is further substantiated by the relative small average layer spacing of the multilayers determined by X-ray diffraction. Referring to Figure 4-3, the close-packed crystal dimensions of a similar polymer had a width for polymer backbone and side chain of only 9 Å,[142] while the X-ray diffraction determination was approximately 13.5 to 15 Å. Since there is a measurable pressure increase at the point of transfer, for a layered structure to form the side chains would have to be tilted to some degree (Figure 4-7 (b)). The lack of distinct Bragg scattering expected from a defined layer structure however, is a strong indication that the backbones and side chains form an amorphous mixture within the monolayer with no defined order. Bragg coherent scattering from the multilayer would indicate a periodic electron density fluctuation along the normal axis of the substrate. With the side chains mostly horizontal to the layer plane, this would result in a mostly constant electron density along the layer z-axis.

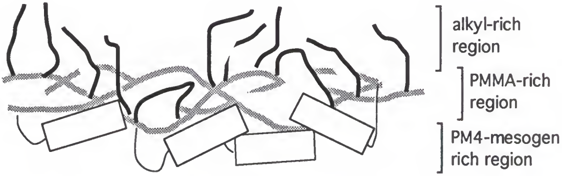

Figure 4-26. Proposed organization of PM4/PODMA blend monolayer and multilayers. Alkyl chains, polymer backbones, and PM4 side chains aggregate in regions of the monolayer, but each region remains disordered. Since the film components are crystalline or semi-crystalline at room temperature, no significant rearrangement occurs after transfer and this disorder is transferred to the multilayer.

It is this fluid disordered nature which makes the monolayer stable and easily transferred, but hampers the ability to produce close packed, ordered multilayers. By adding PODMA the layer thickness is increased. This increase may more reasonably be explained by the molecular phase separation of the alkyl chains out of the water and the segregation of the PM4 side chains on the other side of the PMMA domain of the monolayer as shown in Figure 4-26. However, since the pressure of transfer is increased in these blends the LC side chains may be closer packed than in the pure films. The lack of defined subsidiary maxima does not indicate that the blend multilayers are less ordered than the pure PM4 multilayers, but indicates that one of the interfaces of the multilayer, most likely the outer surface is rougher. This would infer that a less "soupy" and fluid structure exists in the blend monolayer, and that the segregation of different side chains induces a small increase in monolayer order. Segregation on a molecular scale would explain the maximum packing efficiency seen in the $\Delta A_{xs}$ values that occur around 50 to 60% PODMA. The equal mol ratio of side chains should make this local separation most stable, as is seen in the increased pressure stability in the fluid phase of these blend concentrations. The increase in layer spacing and overall film thickness corresponds with this model as well.

## Summary

The stability of polymer monolayer films can be enhanced by mixing with low molecular weight and polymeric compounds of suitable structure. It is well known that the miscibility of a polymer blend is not entropically favorable. In most cases, enthalpic interactions are required to ensure miscibility. However, when polymers are confined to a semi two-dimensional interface such as the air-water interface used in this study, phase separation as seen in the bulk is not as energetically feasible. Under the confined, and oriented conditions of a monolayer, the side chain polymers, PM4 and poly(octadecylmethacrylate) were miscible under the conditions studied with a few minor exceptions at higher temperatures. Due to the incompatible chemical nature of the LC side chain and hydrophilic spacer, with the PODMA alkyl hydrocarbon chain, the miscibility must be due to the strong attractive interactions of the poly(methylmethacrylate) backbones. To facilitate the close proximity of the backbones at higher pressures, the side chains must segregate to some extent on either side of a PMMA region. The alkyl chains would preferentially orient out of the water, while the slightly polar mesogen and hydrophilic ethylene oxide space would preferentially orient towards the water phase. This is the only possible physical packing design which could account for the extremely low area values seen at high pressures in the blend monolayers. The segregation starts at some extent, even in the fluid phase to account for the small areas seen in some blend concentrations, most notably around 50% just before the plateau region of the isotherms.

The term segregation however, does not imply domain formation or immiscibility. The mixing of the PMMA backbones, and the presence of a more defined hydrophobic region relative to the pure PM4 monolayer, provides additional pressure stability in the fluid region of the blend isotherms and additional resistance to collapse at higher pressures.

It is clear that the complexities introduced by side chain polymers in monolayer blends causes some discrepancies in the usual analysis of mixed monolayer isotherms, especially with respect to $\Delta G_{mix}{}^{xs}$. Although all other analyses indicated an overall miscible system, the values of $\Delta G_{mix}{}^{xs}$ would have indicated an phase separated system above 25% PODMA. In the case of negative $\Delta G_{mix}{}^{xs}$, miscibility can be assumed, but, positive values of the excess free energies of mixing should be analyzed further and supported or discounted with other accepted means of determining miscibility in monolayer blend systems.

# CHAPTER 5

# CONTRAST OF THE TWO BLEND MONOLAYER SYSTEMS

Two liquid crystalline polymers were studied as monolayers and as mixed with other materials at the air-water interface. Additionally, multilayers of blends and pure components were produced and studied. Although both polymers exhibit a thermotropic liquid crystalline phase, their behavior in the bulk phase and at the water surface were extremely different. Blend motivation and choice of mixing compounds were also quite dissimilar. Overall, the data presented represent extreme examples, with respect to monolayer blend behavior and multilayer structure.

## Bulk and Monolayer Behavior of the Liquid Crystalline Polymers

The differences in monolayer film behavior of the two LC side chain polymers can be partially attributed to their physical properties in the bulk phase. The FELC copolymer, 10PPB2-CO exhibited fluid and reversible film behavior at the air-water interface, and similarly, is in a fluid LC phase (Sc*) in the bulk. Consequently, since the LC polymer, PM4, is crystalline at room temperature in the bulk phase, and at elevated temperatures (>36°C) exists in a ordered LC phase ($S_E$), the monolayer behavior is mostly rigid and irreversible.

Since the presence of the air-water interface will affect the polymers on a molecular level, bulk behavior alone cannot account for the specific monolayer compression characteristics of the films. Comparing the structure of the side chain LC polymers gives some insight to the individual monolayer features. The polymers can be divided into three regions with different physical and chemical natures - backbone, flexible side chain spacer, and mesogen.

The backbone of the polymers significantly influences the overall behavior both in the bulk and monolayer. The presence of the siloxane polymer chain in the copolymer 10PPB2-CO affects its bulk properties; and accounts for the lowering of the liquid crystalline phase to room temperature from that of the pure side chain mesogen. Additionally, the fluid and stable monolayer character of the 10PPB2-CO films can be almost completely attributed to the flexible PDMS backbone. Considering that the side chain spacer and mesogen which comprises the 10PPB2 molecule, lend little fluidity or stability to the monomer films, it can be asssumed that the same is true in the copolymer. The poly(methylmethacrylate) (PMMA) backbone in the PM4 LC polymer, as Crisp[27] describes, forms a film of the "coherent type". PMMA monolayer films are stiff and "gel" or form aggregates, at low surface pressures. The backbone in the PM4 sample is mostly syndiotactic and extended, rather than forming a helical coil. This feature leads to the packing of the side chains on the same side of the polymer backbone in the ribbon structure shown in Figure 4-3. It would be expected that the mesogens are also on the same side of the backbone in the monolayers, and attempt to form this ribbon structure on the water surface at high areas. It would be interesting to observe the differences in PM4 monolayer behavior with different polymer tacticity.

Another important feature of the side chain liquid crystalline polymers is the flexible spacers which connect the mesogens to the backbone. The nature of these spacers is highly dissimilar in the two LC polymers. In amphiphilic side chain LC polymers, the spacer is usually comprised of methylene units, as in the FELC copolymer, or more recently fluorinated carbon chains. In both cases the spacer is usually hydrophobic in nature and would be expected to orient away from the water during film compression. Assuming that the side chains are flat relative to the water surface at high areas, this means that during compression as the side chains orient perpendicular to the surface the spacer is also oriented out of the water. This would be expected to be energetically favorable. However, in PM4, the spacer unit is ethylene oxide, and is of sufficient length to be considered hydrophilic relative to an analogous hydrocarbon chain. While at large areas the side chains are mostly horizontal to the water surface, during compression to high pressure, the side chains must be oriented to some extent out of the water. The dehydrating of the ethylene oxide spacer during this process would not likely be favorable. This may partially account for the instability of the monolayer in the region where the spacer is out of the water.

Finally, the mesogenic unit, while crucial in the liquid crystalline behavior in the bulk, cannot be significantly attributed to any particular monolayer characteristic of the films in the stable regions. The siloxane backbone of the 10PPB2-CO is obviously the most significant feature of the material with respect to monolayer behavior. In the stable region of the PM4 isotherm, the side chains are far apart and there is probably a stronger interaction between the water and the hydrophilic spacer and methacrylate polymer chain. However, at higher pressures, the close proximity of the mesogens and some crystallization of these groups, may account for the brittle, stiff films that result in this area of the PM4 isotherms.

## Monolayer Behavior and Structure of the Blend Systems

The motivation for blending the polymers in the research presented herein, are almost opposite in objective. The 10PPB2-CO monolayers were so fluid that no orientational order, as seen in the monomer films (Figure 3-21), was evident in the copolymer. Additionally, transfer of the fluid films to solid plates led to rearrangement of the layer organization. To manipulate these features in the monolayer, blends were made with the corresponding mesogenic monomer in order to increase mesogen lateral concentration and interaction. In other words, to make the monolayers less fluid. On the other hand, PM4 formed monolayers were so stiff and unstable at high pressures, that no transfer could be accomplished in the close packed film. Although, there was a stable film region at large mean surface area and low surface pressure, the films were far from being close packed or organized. To increase the fluid and stable region of the films, materials which form monolayers and which could serve to break up the strong interactions between the mesogens were chosen. Additionally, it was reasoned that since there was no well defined hydrophobic area in the PM4 polymer, materials such as PODMA, with long alkyl chains could serve to "anchor" the monolayer out of the water and stabilize the monolayer upon dehydration of the ethylene oxide spacers.

Although motivation and blending materials were dissimilar, the bulk of evidence points to miscible systems. Considering the different environment at the air-water interface, miscibility should be clarified. Here, miscibility, infers no large domain formation within the plane of the monolayer, or no repulsive interactions (which would be evidenced in positive excess area values). Under this criterion, both systems appear miscible with the possible exception of high PODMA (85%) concentration above 28°C (based on $\Pi c$ data). In the bulk and in the monolayer, the 10PPB2-CO/10PPB2 blend films were completely miscible. All data points to the mesogens of both the copolymer and monomer in this system, mixing intimately in the same horizontal plane of the monolayer film. Data from the PM4/PODMA film, however, points to miscibility within the plane of the monolayer, but somewhat phase separated normal to the surface of the water. Based on bulk blend data and a blend system with a comparable low molecular weight amphiphile, there is no indication that the side chains would coexist in the same plane of the film. However, the negative excess area values or the increase in the stable region of the isotherm indicate some interaction between the two polymers and gives no evidence for domain formation. The objective of "anchoring" the film out of the water with the long hydrocarbon chains may actually been achieved, however, well ordered monolayers were not, as seen in the transferred film data.

## Multilayer Structure of the Polymers and Blends

The multilayer films of the two side chain LC polymers and blends were just as different as their monolayer counterparts. While the 10PPB2-CO films displayed an unusually high degree of order for a polymeric LB film, the PM4 film showed almost no layer order at all in a 50 layer film. The differences in the layer order of the multilayer can be traced to two features - 1) the fluidity of the 10PPB2-CO monolayer and the rigidity of the PM4 film (in the absence of the water surface) and 2) at transfer pressure, the 10PPB2-CO side chains are mostly vertical to the water surface and oriented, while the PM4 side chains are mostly horizontal with respect to the surface and lack any significant orientation (normal to the surface). The last point leads to the stacking of PM4 layers with little variance in electron density normal to the layer planes. This density variance is the source of the Bragg peaks seen in the 10PPB2-CO multilayers, but absent from the PM4 and blend scans. Blending in both cases involves adding a less stable monolayers component (with respect to the pressure at transfer), and in both blend multilayers layer order is reduced, or not significantly enhanced. For the 10PPB2-CO/10PPB2 blend system, one objective was to increase the lateral density of the layers, while maintaining a well ordered multilayer film structure. Although rearrangement occurs, the films up to 15% are more dense at transfer, show greater interaction of the mesogens in the monolayer as demonstrated in the BAM photos (Figure 3-21 (a), relative to the copolymer which shows no reflected intensity) and BAM Intensity data (Figure 3-23), and remain well ordered based on X-ray diffraction patterns. The PM4/PODMA blend multilayers rather than increasing density within the plane, are, based on layer thickness determined by X-ray, simply producing thicker monolayers.

It is interesting here to mention some modeling work and other X-ray analysis done by Geer[156] and Lambooy[157] which can be compared with the multilayer films shown in this work. Geer analyzed an extensive set of multilayer samples of 10PPB2-CO with respect to layer roughness and the persistence of roughness from the substrate surface to the outer monolayer. Based on his results, it appears that the fluid copolymer films match any surface modulations of the substrate and perpetuate these features throughout the multilayer. As a contrast to this, X-ray patterns obtained by Lambooy of free standing LC films, showed similar features to those of the PM4 multilayers and some similarities to the 30% PODMA film. Based on modeling studies, Lambooy[157] put forth that these features were caused by smectic decay of the layer structure, from the substrate surface to the outer layers of film. This modeling method was used by Geer[156] who applied it to the PM4 films, and produced scattering patterns and electron density profiles[158] which support this analysis (Figure 5-1). Based on this, it appears that the rigidity of the PM4 films, cannot accommodate roughness or defects, and because of this a breakdown of layer structure occurs with increasing layer number.

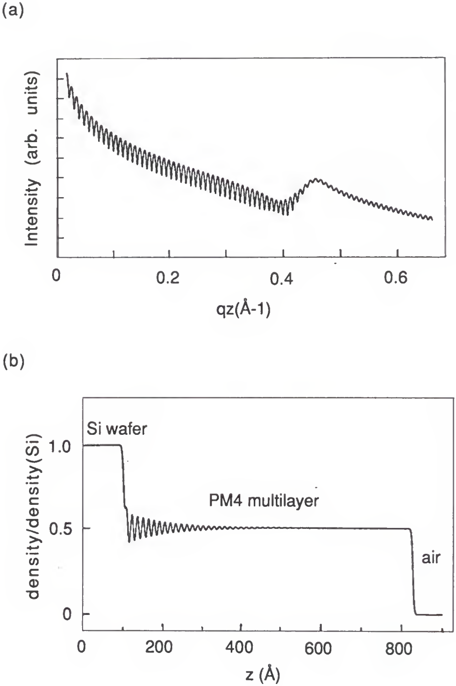

Figure 5-1. Modeling study based on smectic decay of the multilayer structure. (a) Theoretical reflectivity pattern for the PM4 multilayer structure of 50 layers (compare with Figure 4-22) (b) Density profile of the multilayer in (a).

## A Final Word

The research presented herein represents two contrasting examples of mixed monolayers and transferred multilayer films. However, each system has produced some data unique to these types of systems. While the literature has shown films which rearrange after and during transfer, there is not, to my knowledge, any account of this rearrangment producing such highly ordered layer structures, independent of deposition type as seen in 10PPB2-CO. Also, although there have been reports of mixed monolayers where one component is squeezed out; and others were there is binding of a second component from beneath the water surface, I have come across no accounts of the molecular phase separation of mixed polymers thought to occur in the PM4/PODMA blends.

## REFERENCES

[1] Abbott, E.A., *Flatland*, 6th ed., Dover Publications, Inc.: New York (1952).

[2] Gaines, G.L., *Insoluble Monolayers at Liquid-Gas Interfaces* John Wiley & Sons: New York(1966).

[3] Franklin, B., *Philos. Trans. R. Soc. London*, **64**, 445 (1774).

[4] Rayleigh, L., *Proc. R. Soc. London*, **47**, 364 (1890).

[5] Pockels, A., *Nature (London)*, **43**, 437 (1891).

[6] Pockels, A., *Nature (London)*, **46**, 418 (1892).

[7] Pockels, A., *Nature (London)*, **48**, 152 (1893).

[8] Langmuir, I., *J. Am. Chem. Soc.*, **39**, 1848 (1917).

[9] Langmuir, I., *Trans. Faraday Soc.*, **15**, 62 (1920).

[10] Blodgett, K., *J. Am. Chem. Soc.*, **57**, 1007 (1935).

[11] Blodgett, K., *Phys. Rev.*, **51**, 964 (1937).

[12] Blodgett, K.B., *J. Am. Chem. Soc.*, **56**, 495 (1934).

[13] Blodgett, K.B., *Film structure and method of preparation,* U. S. Patent 2,220,861, (1940), .

[14] Harkins, W.D.; Young, T.F.; and Boyd, E., *J. Chem. Phys.*, **8**, 954 (1940).

[15] Harkins, W.D. and Fischer, E.K., *J. Chem. Phys.*, **1**, 852 (1933).

[16] Harkins, W.D. and Meyers, R.J., *J. Phys. Chem.*, **40**, 959 (1936).

[17] Harkins, W.D. and Kirkwood, J.G., *J. Chem. Phys.*, **6**, 53 (1938).

[18] Harkins, W.D., *The Physical Chemistry of Surface Films* Rheinhold: New York (1952).

[19] Adam, N.K., *The Physics and Chemistry of Surfaces*, 3rd ed., Oxford University Press: London (1941).

[20] Adam, N.K. and Miller, J.G.F., *Proc. Royal Soc. (London)*, **142**, 401 (1933).

[21] Adam, N.K., *Proc. Royal Soc. (London)*, **A101**, 516 (1922).

[22] Rideal, E.K. and Marsden, J., *J. Chem. Soc.*, 1163 (1938).

[23] Rideal, E.K., *J. Chem. Soc.*, 423 (1945).

[24] Davies, J.T. and Rideal, E.K., *Proc. Royal Soc. (London)*, **A194**, 417 (1948).

[25] Rideal, E.K. and Tadayon, J., *Proc. Roy. Soc. (London)*, **A225**, 346 (1954).

[26] Crisp, D.J., *Research (London), Suppl.*, **23**,.

[27] Crisp, D.J., *J. Colloid Sci.*, **1**, 161 (1946).

[28] Crisp, D.J., *Surface Chemistry* Butterworths: London (1949).

[29] George L. Gaines, J., *J. Chem. Phys.*, **69**, 924 (1978).

[30] George L. Gaines, J., *Langmuir*, **7**, 834 (1991).

[31] Vogel, V. and Möbius, D., *Thin Solid Films*, **159**, 73 (1988).

[32] Möhwald, H., *Thin Solid Films*, **159**, 1 (1988).

[33] Möhwald, H., *J. Mol. Elec.*, **4**, 47 (1988).

[34] Duschl, C.; Kemper, D.; Frey, W.; Meller, P.; and Ringsdorf, H., *Journal of Physical Chemistry*, **93**, 4587 (1989).

[35] Penner, T.L.; Schildkraut, J.S.; Ringsdorf, H.; and Schuster, A., *Macromolecules*, **24**, 1041 (1991).

[36] Grainger, D.W.; Reichert, A.; Ringsdorf, H.; and Salesse, C., *FEBS Letters*, **252**, 73 (1989).

[37] Blankenburg, R.; Meller, P.; Ringsdorf, H.; and Salesse, C., *Biochemistry*, **28**, 8214 (1989).

[38] Ringsdorf, H. and Schupp, H., *J. Macromol. Sci., Chem.*, **A15**, 1015 (1981).

[39] Hupfer, B.; Ringsdorf, H.; and Schupp, H., *Makromol. Chem.*, **182**, 247 (1981).

[40] Bader, H.; Dorn, K.; Hupfer, B.; and Ringsdorf, H., *Adv. Polym. Sci.*, **64**, 1 (1985).

[41] Finkelmann, H.; Happ, M.; Portugall, M.; and Ringsdorf, H., *Makromol. Chem.*, **179**, 2541 (1978).

[42] Finkelmann, H.; Ringsdorf, H.; Siol, W.; and Wendorff, J.H., *Mesomorphic Order in Polymers and Polymerization in Liquid Crystalline Media*, vol. 74, ACS Symp. Ser. American Chemical Society: Washington, D. C. (1978).

[43] Büschl, R.; Hupfer, B.; and Ringsdorf, H., *Makromol. Chem., Rapid Commun.*, **3**, 589 (1982).

[44] Embs, F.; Funhoff, D.; Laschewsky, A.; Licht, U.; Ohst, H.; Prass, W.; Ringsdorf, H.; Wegner, G.; and Wehrmann, R., *Advanced Materials*, **3**, 25 (1991).

[45] Ulman, A., *An Introduction to Ultrthin Organic Films: From Langmuir-Blodgett to Self-Assembly* Academic Press: San Diego, CA (1991).

[46] Orthmann, E. and Wegner, G., *Angew. Chem.*, **98**, 1114 (1986).

[47] Kalachev, A.A.; Litvinow, V.M.; and Wegner, G., *Makromoleculare Chemie, Macromolecular Symposium*, **46**, 365 (1991).

[48] Arndt, T.; Schouten, A.J.; Schmidt, G.F.; and Wegner, G., *Makromol. Chem.*, **192**, 2215 (1991).

[49] Duda, G.; Shouten, A.J.; Arndt, T.; Lieser, G.; Schmidt, G.F.; Bubeck, C.; and Wegner, G., *Thin Solid Films*, **159**, 221 (1988).

[50] Hickel, W.; Dudan, G.; Wegner, G.; and Knoll, W., *Makromol. Chem. Rapid Commun.*, **10**, 353 (1989).

[51] Adamson, A.W., *Physical Chemistry of Surfaces*, 4th ed., John Wiley & Sons, Inc.: New York (1982).

[52] Roberts, G., *Langmuir-Blodgett Films* Plenum Press: New York (1990).

[53] Sagiv, J., *J. Amer. Chem. Soc.*, **102**, 92 (1980).

[54] Langmuir, I. and Schaefer, V.J., *J. Amer. Chem. Soc.*, **60**, 1351 (1938).

[55] Puterman, M.; T. Fort, J.; and Lando, J.B., *J. Colloid Interface Sci.*, **47**, 705 (1974).

[56] Holcroft, B.; Pety, M.C.; Roberts, G.G.; and Russell, G.J., *Thin Solid Films*, **134**, 83 (1985).

[57] Katz, J.R. and Samwell, P.J.P., *Naturwissenschaften*, **16**, 592 (1928).

[58] Takahashi, A.; Yoshida, A.; and Kawaguchi, M., *Macromolecules*, **15**, 1196 (1982).

[59] Kawaguchi, M.; Yoshida, A.; and Takahashi, A., *Macromolecules*, **16**, 956 (1983).

[60] Gabrielli, G.; Puggelli, M.; and Baglioni, P., *J. Colloid Interface Sci.*, **86**, 485 (1982).

[61] Gabrielli, G.; Baglioni, P.; and Ferroni, E., *Colloid Polym. Sci.*, **257**, 121 (1979).

[62] Ferroni, E.; Gabrielli, G.; and Puggelli, M., *Chim. Ind. (Milan)*, **42**, 147 (1967).

[63] G. L. Gaines, J., *Adv. Chem. Ser.*, **144**, 338 (1975).

[64] Noll, W.; Steinbach, H.; and Sucker, C., *Journal of Polymer Science: Part C*, **34**, 123 (1971).

[65] Zhou, H.; Stern, R.; Batich, C.; and Duran, R.S., *Makromol. Chem., Rapid Commun.*, **11**, 409 (1990).

[66] Zhou, H. and Duran, R.S., *Thin Solid Films*, **210/211**, 356 (1992).

[67] Duran, R.S. and Zhou, H.C., *Polymer*, **33**, 4019 (1992).

[68] Cemel, A.; T. Fort, J.; and Lando, J.B., *J. Polym. Sci.*, **10**, 2061 (1972).

[69] Fariss, G.; Lando, J.; and Rickert, S., *Thin Solid Films*, **99**, 305 (1983).

[70] Laschewsky, A.; Ringsdor, H.; and Schmidt, G., *Thin Solid Films*, **134**, 153 (1985).

[71] Kajzar, F. and Messier, J., *Thin Solid Films*, **99**, 109 (1983).

[72] Sigmund, W.M. and Duran, R.S., *Macromolecules*, **26**, 2616 (1993).

[73] Bodalia, R.; Manzanares, J.; Reiss, H.; and Duran, R.S., Macromolecules, to be submitted (1993).

[74] Sigmund, W.; Zhou, H.C.; Elsabee, M.; Reuhe, J.; Wegner, G.; and Duran, R.S., Langmuir to be submitted (1993).

[75] Elbert, R.; Laschewsky, A.; and Ringsdorf, H., *JACS*, **107**, 4134 (1985).

[76] Mumby, S.J.; Rabolt, J.F.; and Swalen, J.D., *Thin Solid Films*, **133**, 161 (1985).

[77] Mumby, S.J.; Rabolt, J.F.; and Swalen, J.D., *Macromolecules*, **19**, 1054 (1986).

[78] Thibodeaux, A.F.; Duran, R.S.; Ringsdorf, H.; Schuster, A.; Skoulios, A.; Gramain, P.; and Ford, W., "Blends of Side-Chain Liquid-Crystalline Polymers at the Air-Water Interface," in *Macromolecular Assemblies in Polymeric Systems,* vol. 493Stroeve, P. and Balazs, A.C., American Chemical Society, Washington, D.C., (1992), pp. 20.

[79] Bautista, M.O.; Duran, R.S.; and Ford, W.T., *Macromolecules*, **26**, 659 (1993).

[80] Thibodeaux, A.F.; Geer, R.; Qadri, S.; Naciri, J.; S., R.S.; and Duran, R.S., *Polymer Preprints*, **33**, 1220 (1992).

[81] Adams, J.; Thibodeaux, A.; Naciri, J.; Shashidhar, R.; and Duran, R.S., *ACS Polymer Preprints*, **33**, 1164 (1992).

[82] Adams, J.; Rettig, W.; Duran, R.S.; Naciri, J.; and Shashidhar, R., *Journal of Physical Chemistry*, **97**, 2021 (1993).

[83] Collet, P., *J. Phys. Radium*, **3**, 128 (1922).

[84] Leathes, J.B., *Lancet*, **1925**, 853 (1925).

[85] H. E. Ries, J. and Walker, D.C., *J. Colloid Sci.*, **16**, 361 (1961).

[86] Baglioni, P.; Dei, L.; Gabrielli, G.; Innocenti, F.M.; and Niccolai, A., *Colloid Poly. Sci.*, **266**, 783 (1988).

[87] Caminati, G.; Gabrielli, G.; Puggelli, M.; and Ferroni, E., *Colloid Poly. Sci.*, **267**, 237 (1989).

[88] Puggelli, M. and Gabrielli, G., *Colloid Polym. Sci.*, **261**, 166 (1983).

[89] , *Liquid-Crystalline Polymers*, ACS Symp. Ser. American Chemical Society: (1989).

[90] Ruth, J.; Naciri, J.; and Shashidhar, R., Liquid Crystals, in press (1993).

[91] Thibodeaux, A.F.; Rädler, U.; Shashidhar, R.; Naciri, J.; and Duran, R.S., *Macromolecules*, .

[92] Reinitzer, F., *Monatsh. Chem.*, **9**, 421 (1888).

[93] Lehmann, O.Z., *Kristallogr. Kristallgem. Kristallphys. Kristallchem.*, **18**, 464 (1890).

[94] Bawden, F.C. and Pirie, N.W., *Proc. R. Soc., Ser. B*, **123**, 1274 (1937).

[95] Elliot, A. and Ambrose, E.J., *Discuss. Faraday Soc.*, **9**, 246 (1950).

[96] Onsager, L., *N.Y. Acad. Sci.*, **51**, 627 (1949).

[97] Flory, P.J. and Abe, A., *Macromolecules*, **11**, 119 (1978).

[98] Flory, P.J., *Macromolecules*, **11**, 1138 (1978).

[99] McArdle, C.B., *Side Chain Liquid Crystal Polymers* Chapman and Hall: New York (1989).

[100] Allcock, H.R. and Lampe, F.W., *Contemporary Polymer Chemistry*, 2nd ed., Prentice Hall: Englewood Cliffs, NJ (1990).

[101] Xu, Y., *Ferroelectric Materials and Their Applications* North-Holland: Amsterdam (1991).

[102] Clark, N. and Lagerwall, S., *Appl. Phys. Lett.*, **36**, 899 (1980).

[103] Clark, N. and Lagerwall, S., *Ferroelectrics*, **59**, 25 (1984).

[104] Hiltrop, K. and Stegemeyer, H., *Ber. Bunsenges. Phys. Chem.*, **82**, 884 (1978).

[105] Staromylnska, J.; Saunder, F.C.; and Smith, G.W., *Mol. Cryst. Liq. Cryst.*, **109**, 233 (1984).

[106] Laschewsky, A., *Angew. Chem. Int. Ed. Engl. Adv. Mater.*, **28**, 1574 (1989).

[107] Clark, N. and Lagerwall, S., *Surface stabilized ferroelectric liquid crystal display device,* U. S. Patent 4,367,924, (1980), .

[108] Rettig, W.; Naciri, J.; Shashidhar, R.; and Duran, R.S., *Macromolecules*, **24**, 6539 (1991).

[109] Rettig, W.; Naciri, J.; Shashidhar, R.; and Duran, R.S., *Thin Solid Films*, **210**, 114 (1992).

[110] Hedestrand, G., *J. Phys. Chem.* , **28**, 1244 (1924).

[111] Blodgett, K.B., *Reduction of surface reflection,* U. S. Patent 2,220,861, (1940), .

[112] Blodgett, K.B., *Low-reflectance glass,* U. S. Patent 2,220,862, (1940), .

[113] Langmuir, I., *Method of substance detection,* U. S. Patent 2,232,539, (1941), .

[114] Blodgett, K.B., *Step guage for measuring thickness by means of interference,* U. S. Patent 2,587,282, .

[115] Schonhorn, H. and Gregor, H.P., *J. Amer. Chem. Soc.*, **83**, 3576 (1961).

[116] Henke, B.L., *X-Ray Anal.*, **7**, 460 (1964).

[117] Naciri, J.; Pfeiffer, S.; and Shashidhar, R., *Liquid Crystals*, **10**, 585 (1991).

[118] Hénon, S. and Meunier, J., *Rev. Sci. Instrum.*, **62**, 936 (1991).

[119] Hönig, D. and Möbius, D., *J. Phys. Chem.*, **95**, 4590 (1991).

[120] Wood, E.A., *Crystals and Light: An Introduction to Optical Crystallography*, 2nd rev. ed., Dover Publications, Inc.: London (1977).

[121] Holley, C. and Bernstein, S., *Phys. Rev.*, **49**, 403 (1936).

[122] Lin, B.; Peng, J.B.; Ketterson, J.B.; and Dutta, P., *Thin Solid Films*, **159**, 111 (1988).

[123] Grundy, M.J.; Richardson, R.M.; Roser, S.J.; and Penfold, J., *Thin Solid Films*, **159**, 43 (1988).

[124] Buhaenko, M.R.; Grundy, M.J.; Richardson, R.M.; and Roser, S.J., *Thin Solid Films*, **159**, 253 (1988).

[125] Day, D. and Lando, J.B., *Macromolecules*, **13**, 1478 (1980).

[126] M.Lvov, Y.; Troitsky, V.I.; and Feigin, L.A., *Mol. Cryst. Liq. Cryst.*, **172**, 89 (1989).

[127] Murakata, T.; Miyashita, T.; and Matsuda, M., *Macromolecules*, **22**, 2706 (1989).

[128] Watanabe, I.; Hong, K.; and Rubner, M.F., *Langmuir*, **6**, 1164-1172 (1990).

[129] Chen, J.M.; Yang, X.Q.; Chapman, D.; Nelson, M.; Skotheim, T.A.; Ehrlich, S.N.; Rosner, R.B.; and Rubner, M.F., *Mol. Crystl. Liq. Cryst.*, **190**, 145 (1990).

[130] Duran, R. and Gramain, P. , *Makromol. Chem.*, **188**, 2001 (1987).

[131] Naciri, J.; Mery, S.; Pfeiffer, S.; and Shashidhar, R., J. Amer. Chem. Soc., submitted (1993).

[132] Matsumoto, M.; Miyasaka, H.; Sekiguchi, T.; Tanaka, M.; Tachibana, H.; Nakamura, T.; Manda, E.; and Kawabata, Y., *Thin Solid Films*, **178**, 367 (1989).

[133] Bacon, K.J. and Barnes, G.T., *J. Colloid Interface Sci.*, **67**, 70 (1978).

[134] Ruiz, M.J.G. and Vilchez, M.A.C., *Colloid Poly. Sci.*, **269**, 77 (1991).

[135] Petrov, J.G.; Möbius, D.; and Angelova, A., *Langmuir*, **8**, 201 (1992).

[136] Geer, R.; Qadri, S.; and Shashidhar, R., Phys. Rev. A, submitted (1993).

[137] Adams, J.; Buske, A.; and Duran, R.S., Macromolecules, in press. (1992).

[138] G. L. Gaines, J.; Bellamy, W.D.; and Tweet, A.G., *J. Chem. Phys.*, **41**, 538 (1964).

[139] Goodrich, F.C., *Proceedings 2nd International Congress Surface Activity,* Vol. 1 (1957), .

[140] Takanishi, Y.; Takezoe, H.; and Fukuda, A., *Physical Review B,* **45**, 7684 (1992).

[141] Based on modeling and calculations performed by Dr. Bob Geer, at NRL Washington, D. C., and conversations Dr. Geer regarding the results., .

[142] Duran, R.; Guillon, D.; Gramain, P.; and Skoulios, A., *Makromol. Chem., Rapid Commun.*, **8**, 321 (1987).

[143] Duran, R. and Strazielle, C., *Macromolecules*, **20**, 2853 (1987).

[144] Duran, R.; Guillon, D.; Gramain, P.; and Skoulios, A., *J. Physique*, **48**, 2043 (1987).

[145] Duran, R.; Guillon, D.; Gramain, P.; and Skoulios, A., *J. Phys. France*, **49**, 121 (1988).

[146] Duran, R.; Guillon, D.; Gramain, P.; and Skoulios, A., *J. Phys. France*, **49**, 1455 (1988).

[147] Gabrielli, G.; Puggelli, M.; and Ferroni, E., *J. Colloid Interface Sci.*, **47**, 145 (1974).

[148] Gabrielli, G. and Baglioni, P., *J. Colloid Interface Sci.*, **73**, 582 (1980).

[149] Plate, N.A.; Shibaev, V.P.; Petrtukhin, B.S.; Zubov, Y.; and Kargin, V.A., *J. Poly. Sci: Part A-1*, **9**, 2291 (1971).

[150] Hsieh, H.W.S.; Post, B.; and Morawetz, H., *J. Poly. Sci.: Phys. Ed.*, **14**, 1241 (1976).

[151] Kiessig, H., *Ann. Phys. (Leipzig)*, **10**, 769 (1931).

[152] Bisset, D.C. and Iball, J., *Proc. Phys. Soc.*, **67A**, 315 (1954).

[153] Parratt, L.G., *Phys. Rev.*, **95**, 359 (1954).

[154] Pomerantz, M. and Segmüller, A., *Thin Solid Films*, **68**, 33 (1980).

[155] Kapp, D.S. and Wainfan, N., *Phys. Rev.*, **138**, A1490 (1965).

[156] Modeling and calculations performed by Dr. Bob Geer at NRL, Washington, D. C. Observations based on preliminary results and phone discussions of the data with Dr. Geer., .

[157] Lambooy, P., "Order and disorder in thin films of liquid crystals and polymers.," Ph.D. thesis, College van Hoogleraren, Amsterdam, Netherlands, December (1992).

[158] The film density profile in Figure 5-1 (b) is taken as

$$\rho(z)=\frac{\rho_{Si}}{2}\left\{1-\mathrm{erf}\left(\frac{z}{\sqrt{2}\sigma_1}\right)\right\}+\frac{\rho_{film}}{2}\left\{1-A_s e^{-\alpha_s}\cos(q_1 z)\left[\mathrm{erf}\left(\frac{z}{\sqrt{2}\sigma_1}\right)-\mathrm{erf}\left(\frac{z-D}{\sqrt{2}\sigma_A}\right)\right]\right\}$$

where $\rho_{Si}$ is the substrate density, $\rho_{film}$ is the mean density of the film, $A_s$ is the layering amplitude for layer spacing $2\pi/q1$, and decay length $1/\gamma$, was taken as double the first periodicty. The notation erf(z) is the standard error function.

# BIOGRAPHICAL SKETCH

The author was born in Lafayette, Louisiana in the heart of "Cajun Country", on the 12th day of December 1963. After moving to various cities in the South, the author's family settled in Birmingham, Alabama. After graduating from high school, she began studying art at the University of Montevallo, but soon discovered she did not have the perseverance to be a "starving artist."

She returned to Birmingham, and attended the University of Alabama at Birmingham, remained undecided, and began working as a biological technician at Southern Research Institute (SRI) in 1985. It was while working at SRI that she caught the "science" bug, and decided upon a major in chemistry. After graduating from UAB with an ACS certified B.S. degree, she returned to work at SRI, but this time as an assistant chemist. It was at SRI that she met her future husband, and after a year of work, they both decided to return to school to obtain advanced degrees.

The author entered graduate school in chemistry at the University of Florida in the fall of 1988. After five years of studying and research under the direction of Dr. Randy Duran, she finally defended her dissertation research and graduated officially December 1993. After graduation, the author will relocate to Spartanburg, South Carolina to work for Milliken Research Center.

I certify that I have read this study and that in my opinion it conforms to acceptable standards of scholarly presentation and is fully adequate, in scope and quality, as a dissertation for the degree of Doctor of Philosophy.

Randolph Duran

Randolph S. Duran, Chairman
Assistant Professor of Chemistry

I certify that I have read this study and that in my opinion it conforms to acceptable standards of scholarly presentation and is fully adequate, in scope and quality, as a dissertation for the degree of Doctor of Philosophy.

John Reynolds, Co-Chairman
Associate Professor of Chemistry

I certify that I have read this study and that in my opinion it conforms to acceptable standards of scholarly presentation and is fully adequate, in scope and quality, as a dissertation for the degree of Doctor of Philosophy.

Martin T. Vala

Martin T. Vala
Professor of Chemistry

I certify that I have read this study and that in my opinion it conforms to acceptable standards of scholarly presentation and is fully adequate, in scope and quality, as a dissertation for the degree of Doctor of Philosophy.

William Weltner Jr.

William Weltner, Jr.
Professor of Chemistry

I certify that I have read this study and that in my opinion it conforms to acceptable standards of scholarly presentation and is fully adequate, in scope and quality, as a dissertation for the degree of Doctor of Philosophy.

Kenneth B Wagener

Kenneth B. Wagener
Professor of Chemistry

I certify that I have read this study and that in my opinion it conforms to acceptable standards of scholarly presentation and is fully adequate, in scope and quality, as a dissertation for the degree of Doctor of Philosophy.

Chris Batich

Christopher D. Batich
Professor of Materials Science
and Engineering

This dissertation was submitted to the Graduate Faculty of the Department of Chemistry in the College of Liberal Arts and Sciences and to the Graduate School and was accepted as partial fulfillment of the requirements for the degree of Doctor of Philosophy.

December, 1993

Dean, Graduate School